Fall 2019

Structural Studies on the Mechanism of Argyrin B and the L12 – L11 Ribosomal Protein Interface

Christopher Swanson
Western Washington University, swansoc9@wwu.edu

Structural Studies on the Mechanism of Argyrin B and the L12 - L11 Ribosomal Protein Interface

By

Christopher Swanson

Accepted in Partial Completion
of the Requirements for the Degree
Master of Science

ADVISORY COMMITTEE

Dr. P. Clint Spiegel, Chair

Dr. Jeanine Amacher

Dr. John Antos

GRADUATE SCHOOL

David L Patrick, Interim Dean of the Graduate School

Master's Thesis

In presenting this thesis in partial fulfillment of the requirements for a master's degree at Western Washington University, I grant to Western Washington University the non-exclusive royalty-free right to archive, reproduce, distribute, and display the thesis in any and all forms, including electronic format, via any digital library mechanisms maintained by WWU.

I represent and warrant this is my original work and does not infringe or violate any rights of others. I warrant that I have obtained written permissions from the owner of any third party copyrighted material included in these files.

I acknowledge that I retain ownership rights to the copyright of this work, including but not limited to the right to use all or part of this work in future works, such as articles or books.

Library users are granted permission for individual, research and non-commercial reproduction of this work for educational purposes only. Any further digital posting of this document requires specific permission from the author.

Any copying or publication of this thesis for commercial purposes, or for financial gain, is not allowed without my written permission.

Christopher Swanson

11/21/2019

Structural Studies on the Mechanism of Argyrin B and the L12 – L11 Ribosomal Protein Interface

A Thesis
Presented to
The Faculty of
Western Washington University

In Partial Fulfillment
Of the Requirements for the Degree
Master of Science

by
Christopher Swanson
November 2019

Abstract

The mechanism of action of argyrin B and the molecular interactions of L11 and L12 has been undetermined and underrepresented in the research of bacterial translation. This work seeks to examine the mechanism of action of argyrin B by performing *in vitro* structural studies of its interaction with its specific target protein elongation factor-G. We demonstrate that argyrin B inhibits translation, and allows GTPase activity to proceed, contrary to assumptions made in prior research. We determine that ribosome recycling is the likely step through which argyrin B acts as an antibiotic, since translocation is unaffected by argyrin B and association with post-termination complexes are increased in the presence of argyrin B. We propose that the mechanism of action involves the ratcheting of EF-G 45 ° from a normal binding conformation with the ribosome, which sterically hinders the positioning of loop II of domain IV of EF-G and the cooperativity of EF-G and RRF in interrupting Bridge 2a, the largest intersubunit bridge on the ribosome. Furthermore, we provide preliminary insight on the molecular interactions present between L11 and the L12 C Terminal Domain by performing alanine scanning mutations on select glutamic acid and aspartic acid residues around an electronegatively charged pocket. These mutations while not effecting L11 binding in a tangible way, strongly influenced select GTPase activity.

Acknowledgements

The extension of gratitude or thanks to Dr. Clint Spiegel fails to capture the scope of how I have grown as a person and student under his tutelage. He allowed me to enter his lab without prior biochemical research experience and trusted me to perform complex experiments with only a summer of basic training in the techniques. His expertise helped guide my experimental conclusions and encouraged me to think independently as a scientist. There are few mentors in my life who have been more constructive, practical, and direct as Clint.

I thank Amanda Weis for her tolerance of my interruptions in her thesis writing the summer she trained me in all the necessary experiments for my Master's education. Her support and insights even after her departure from the lab was invaluable to my research and education as a biochemist.

I could not have asked for a better partner and significant other throughout graduate school than Emily Schneider, she was loving voice of reason and endless supportive. I love you.

My parents proved an invisible but essential part of my graduate career, without their help and encouragement this would have been impossible.

Shortly after I joined the Spiegel Lab, Riley Roberts joined the GTPase/Ribosome project with a similar lack of biochemical research experience. Our initial experiences, likened to the blind leading the blind, provided the foundation of a friendship I would not trade for all the high ribosome growth yields in the world.

Ian Smith, Kenny Childers, and Shaun Peters were invaluable consultants whenever my confidence in my procedures wavered, and all provided guidance on my journey through graduate school.

Lastly, I extend profound appreciation to all members of the Spiegel Lab past, present, and future for the blood, cytosine, and GTP they poured into their projects during their time at WWU.

List of Tables and Figures

Table of Abbreviations

Abbreviation	Full Name	Function
A site	Aminoacyl site	Binding site for aa-tRNAs on the ribosome
aa-tRNA	Aminoacyl transfer ribonucleic acid	tRNA bound to an amino acid; chaperones amino acid during protein synthesis until elongation occurs.
AEC	Anion exchange chromatography	Technique used to purify proteins based on their isoelectric point
ArgB	Argyrin B	Antibiotic with unknown mechanism; targets EF-G at allosteric binding site
ASL	Anticodon stem loop	Portion of a tRNA molecule that is complementary to the mRNA codon
Au	Absorbance Unit	Measurement of the amount of light that a substance absorbs via the $\log_{10}$(percentage of transmittance)
B2a	Intersubunit Bridge 2a	Largest of 13 intersubunit bridges present in the ribosome
BLI	Bio Layer Interferometry	Method for measuring binding via light scattering by change in mass bound to relevant antibody
Cryo EM	Cryo-electron microscopy	Technique used to study protein structure
CTD	Carboxy or C- Terminal Domain	The domain of a protein that harbors the terminal carboxyl group
CV	Column Volume	Volume of packed resin
DHFR	Dihydrofolate reductase	Enzymatic protein responsible for reducing dihydrofolic acid.
DMSO	Dimethyl sulfoxide	Organic solvent
DNA	Deoxyribonucleic acid	Storage medium for genes used by all prokaryotes and eukaryotes
E. coli	*Escherichia coli*	Gram-negative bacteria, common protein expression vector and model organism
EF-G	Elongation Factor G	GTPase; involved in translocation process of elongation and ribosome recycling
E site	Exit site	Site of deacylated tRNA binding before exiting the ribosome
EF-Tu	Elongation Factor Thermo-unstable	GTPase; involved in decoding process of elongation
fMet-tRNA^{fMet}	N-formyl methionine bound to transfer ribonucleic acid	Translation initiation signaling tRNA; chaperones first amino acid in all prokaryotic proteins

GAP	GTPase Activating Protein	Proteins involved in activation of GTPases
GDP	Guanosine 5'-diphosphate	Product of GTP cleavage
GDPNP	Guanosine 5'-[β,γ-imido]triphosphate	Uncleavable analogue of GTP
GTP	Guanosine 5'-triphosphate	Hydrolyzable molecule to that provides energy for GTPase function, catalysis, and regulation
GTPase	Guanosine 5'- triphosphate hydrolase	Enzymatic proteins that hydrolyze GTP, catalyze and regulate many cellular processes
h44	Small subunit helix 44	30S RNA helix involved in intersubunit Bridge 2a
H69	Large subunit helix 69	50S RNA helix involved in intersubunit Bridge 2a
IF1	Initiation Factor 1	Involved in translation initiation
IF2	Initiation Factor 2	GTPase; involved in translation initiation
IF3	Initiation Factor 3	Involved in translation initiation and ribosome recycling
IMAC	Immobilized metal affinity chromatography	Protein purification method
IPTG	Isopropyl β-D-1-thiogalactopyranoside	Lactose mimic, induces overexpression of proteins in bacterial vectors
LB	Lysogeny Broth	Media for bacterial cell growth
mRNA	Messenger RNA	Molecules that convey genetic information from DNA to the ribosome; dictate amino acid sequence of translated proteins
MW	Molecular Weight	Mass of one mole of a substance
MWCO	Molecular Weight Cut Off	The lowest molecular weight (in Daltons) in which 90% of the protein is retained by the membrane
Native PAGE	Native Polyacrylamide gel electrophoresis	Non denaturing method of separating proteins based on molecular weight
Ni-IDA	Nickel-iminodiacetic acid	IMAC substrate; binds $His_{(6)}$-tags
Ni-NTA	Nickel-nitrilotriacetic acid	IMAC substrate; binds $His_{(6)}$-tags
NTD	Amino- or N-Terminal Domain	The domain of a protein that contains the terminal α-amino group
PC	polycarbonate	Common plastic polymer
PDBid	Protein data bank identification number	Unique code for identifying protein structural models deposited into www.rcsb.org
Phe	Phenylalanine	Hydrophobic amino acid
PMSF	Phenylmethylsulfonyl fluoride	Serine protease inhibitor, prevents degradation of overexpressed protein during purification
PoTC	Post-Termination Ribosomal Complex	Ribosomal Complex formed after termination occurs in translation

POST	Post-Translocation Ribosomal Complex	Ribosomal Complex formed after translocation occurs in translation
PRE	Pre-Translocation Ribosomal Complex	Ribosomal Complex formed before translocation occurs in translation
P. aeruginosa	*Pseudomonas aeruginosa*	Gram-negative bacteria
PTC	Peptidyl-Transferase Center	Forms peptide bonds between the elongating peptide on the P-site tRNA and the amino acid on the A site tRNA
RF1	Release factor 1	Involved in translation termination, releases synthesized protein via UAG stop codons
RF2	Release factor 2	Involved in translation termination, releases synthesized protein via UGA stop codons
RF3	Release factor 3	GTPase; involved in translation termination and proofreading of final protein
RNA	Ribonucleic acid	Nucleic acid present in all living cells; varied cellular functions
RRF	Ribosome Recycling Factor	Protein involved in ribosome recycling; has key interactions with EF-G
rRNA	Ribosomal ribonucleic acid	Ribosomal Structural component
S	Svedberg unit	Sedimentation coefficient that reflects the rate at which a molecules sediment in a given solvent
SD	Shine Dalgarno Sequence	Codon sequence of mRNA that signals initiation of translation to the ribosome
SDM	Site-directed mutagenesis	Method to incorporate mutations into a gene of interest
SDS-PAGE	Sodium dodecyl sulfate polyacrylamide gel electrophoresis	Denaturing method of separating proteins based on molecular weight
SEC	Size exclusion chromatography	Chromatographic method to purify proteins based on molecular weight and size
SRL	Sarcin Ricin Loop	Portion of the 23S rRNA essential for GTP hydrolysis catalyzed steps in translation
TEV	Tobacco Etch Virus Protease	Protease that identifies and cleaves $His_{(6)}$-tag sequences
tRNA	Transfer ribonucleic acid	Binds, chaperones amino acids and associates with the ribosome
T. thermophilus	*Thermus thermophilus*	Gram-negative bacteria
UV/Vis spectroscopy	Ultraviolet-visible spectroscopy	Technique for quantification of ribosomes and proteins
WT	Wild-type	Descriptor for endogenously expressed protein
β-ME	2-β-mercaptoethanol	Reagent used to reduce disulfide bonds

Introduction

Chapter 1. Bacterial Translation

Translation is the fundamental process of protein synthesis, after DNA has been transcribed into mRNA, the mRNA is decoded by the ribosome which produces a long polymer chain made up of amino acids. These polymer chains fold into secondary protein structures which can then form more complex tertiary globular structures. Globular protein structure enables proteins to function as enzymatic catalysts for many biological chemical reactions. This process of protein production is fundamentally conserved across all known forms of Life and contains a myriad of sub-processes and cycles that ensure the continuity of life. This thesis will narrow its scope of focus to the translational systems of the kingdom prokaryota. With the advent of microbiology occurring only recently during human history, there is still a wealth of knowledge to be learned from the study of bacteria, notwithstanding the urgency of need for such information given the threat posed by antibiotic resistant strains of pathogenic bacteria. The pertinent basic information and summary of the major stages and structural aspects of bacterial translation will be communicated forthcoming.

Prokaryotic Ribosomes

The prokaryotic ribosome has two major subunits, the 50 Svedberg (50S) and 30 Svedberg (30S) subunit (Figure 1-1). These two massive complexes of RNA and protein stabilized by 13 inter-subunit bridging interactions to form a full 70S ribosome (Liu and Fredrick, 2016). Both subunits contain many key catalytic sites for successful protein synthesis: the 30S subunit binds the

mRNA which serve as the blueprints for the peptide strand, and the 50S subunit holds the "tunnel" that the new protein will extend out of. Post mRNA binding, the 70S ribosome has 3 distinct sites(Figure 1-1); the Aminoacyl- (A site), Peptidyl- (P site), and the Exit site (E site). (Rheinberger, Sternbach and Nierhaus, 1981). Each of these sites have a corresponding loop in the 50S subunit. The A-site is where aminoacylated-tRNA (aa-tRNA) is matched to its corresponding codon on the mRNA by the required translation factors. The P-site is where new amide bonds are formed, and a peptide strand grows through the channel of the 50S subunit. The E-site is where deacylated-tRNA leaves the ribosome. It is important to note that translation is a dynamic process; therefore, hybrid binding states of A/P and P/E exist as ribosomal conformations and/or binding partner interactions change(Schmeing and Ramakrishnan, 2009; Zhou *et al.*, 2014; Rodnina, 2018). The ribosome undergoes major conformational changes as the protein backbone is constructed and the four major stages of translation proceed.

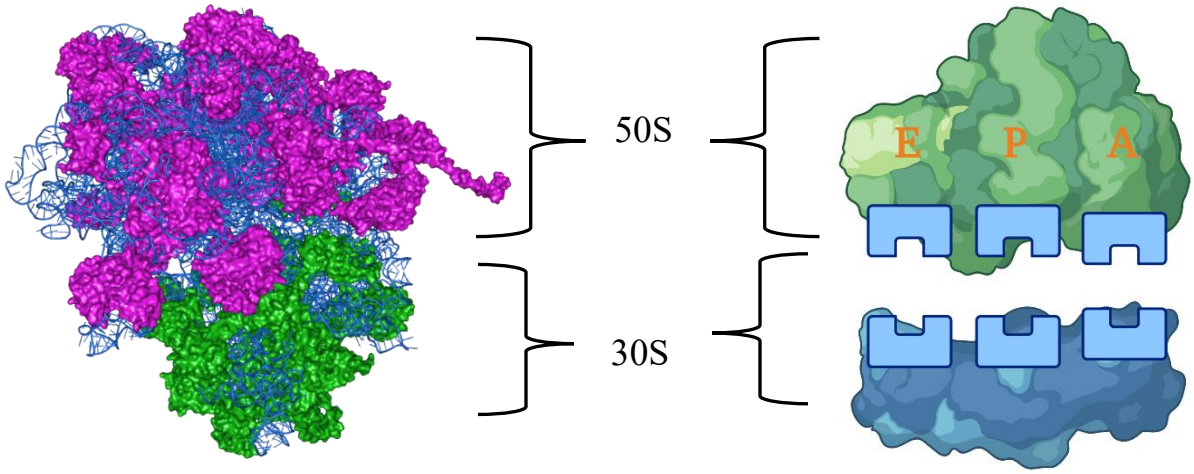

Figure 1-1. Structure of the bacterial ribosome. Left: Crystal Structure of *T. thermophilus* ribosome. Large Subunit proteins represented as pink, small subunit proteins represented in green, and rRNA shown in blue. (PDB: 4W29) Right: Cartoon representation of ribosome amino-acyl, peptidyl, and exit sites.

Initiation

The process of initiation is the first step of translation. Prior to the formation of the initiation complex, the ribosome is positioned via complimentary codon interactions between the Shine-Delgarno (SD) sequence and the 16S RNA of the small subunit. Following this positioning a 30S•mRNA complex binds a special initiator tRNA, N-formyl-Methionine tRNA (fMet-tRNA) at an AUG or similar start codon. Upon GTP hydrolysis by initiation factor 2 (IF2), the fMet-tRNA is moved into the peptidyl-transferase center, signaling the beginning of translation (Figure1-2).(Shine and Dalgarno, 1974; Schmeing and Ramakrishnan, 2009) There are various translation factors involved in this process, designated as initiation factor 1 (IF1), initiation factor 2, and initiation factor 3 (IF3) which all act to regulate the initiation process. IF1 binds to the A site potentially in order to prevent pre-mature association of non-fMet-tRNAs to the initiation complex. (Gualerzi and Pon, 1990; Simonetti *et al.,* 2009) Initiation factor 2 has recently emerged as the key GTPase involved in the formation of the initiation complex. IF2 functions as the sole initiation factor that can directly interact with both the small ribosomal subunit and fMet-tRNA; it has been shown the fMet-tRNA is the only tRNA identified by IF2. IF2 has been shown to structurally stabilize a semi-rotated conformational state of the ribosome.(Kozak, 1999; Ling & Ermolenko, 2015). The association of these translation factors and the initiator tRNA produces the Initiation Complex (Figure 1-2). Initiation Factor 3 functions differently than the other initiation factors; IF3 both operates on the 30S subunit post ribosome recycling by dissociating the deacylated tRNA from the stop codon in the former P site and inhibiting reassociation of the two ribosomal subunits. (Karimi *et al.*, 1999; Borg, Pavlov and Ehrenberg, 2016)

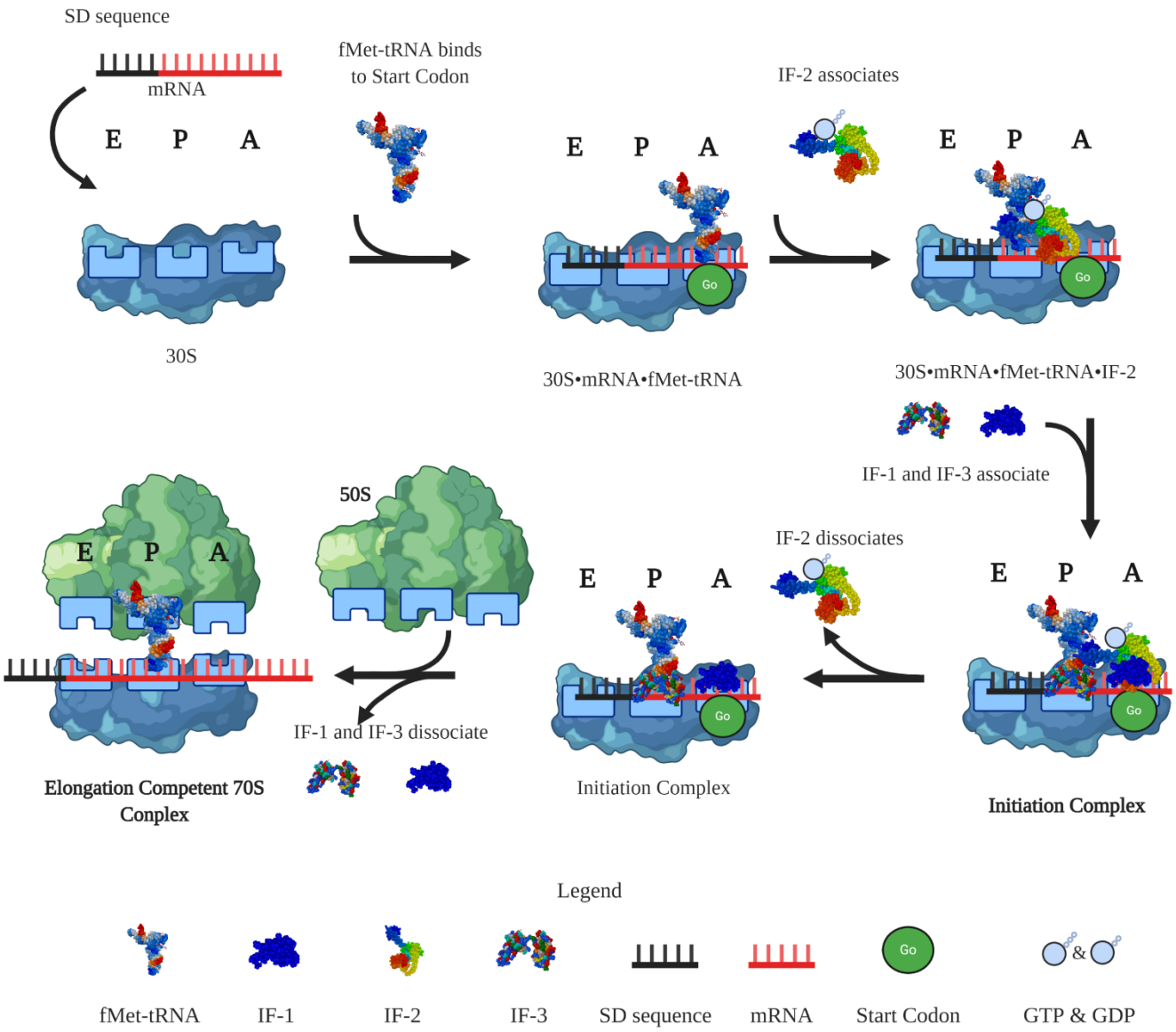

Figure 1-2. Schematic of Initiation. The mRNA base pairs with the 30S subunit through complementary interactions on the SD sequence. The fMet tRNA binds to the A site, and upon GTP hydrolysis is shifted to the P site by IF-2, IF1 binds the A sit after this shift preventing non fMet-tRNA association with the 30S. IF-3 maintains interactions with h44 of the 30S subunit preventing premature 70S association. The 50S joins with the 30S subunit after the fMet-tRNA has been shifted to the P site, and IF1-3 have dissociated. The order of events shown in the figure is for clarity, many interactions begin and end simultaneously.

Elongation

Elongation is the process of translation where the all of the protein backbone is synthesized. Like other stages of translation, elongation is a highly regulated and fundamentally conserved cycle. This process consists of 3 established steps decoding, peptidyl transfer, and translocation. There are two GTPases that cooperate to maintain the accuracy of the peptide strand: elongation factor Tu (EF-Tu), elongation factor G (EF-G). During elongation, EF-Tu maintains a key role in decoding and EF-G regulates the process of translocation. The sub-processes of elongation and the role of their regulatory enzymes will be discussed below.

Decoding

Decoding is the process where aminoacylated tRNA (aa-tRNA) is chaperoned to the 70S by elongation factor-Tu•GTP (EF-Tu). During this step the A site occupying mRNA codon will match the anti-codon of the aa-tRNA and the codon of the mRNA strand to be translated (Rodnina *et al.*, 1996). Through contacts with the GTPase-associated center on the 50S subunit via the L7/L12 stalk and the EF-Tu•GTP complex two events are enabled: the ribosome enters an "activated" state that facilitates the codon-anticodon interactions in the 30S•mRNA A site; and the EF-Tu complex can fulfill the pre- and post-GTP hydrolysis steps of initial selection and proofreading (Figure 1-3). These two sub-processes of elongation are to ensure that peptide bonds are formed with high fidelity. The initial selection of the correct aa-tRNA is coordinated by the EF-Tu•GTP•aa-tRNA complex and is dependent on the accuracy of Watson Crick pairing of the codon and anti-codon. The complex which is bound to the mRNA A site codon, experiences a rotation toward the P site that catalyzes GTP cleavage.(Mohr, Wintermeyer and Rodnina, 2002) During this rotation there are simultaneous interactions with the decoding center residues of the 16S rRNA that sterically accommodate the incoming aa-tRNA by interactions with key residues in the P site (Kimura and Suzuki, 2009). The rate of GTP hydrolysis induced

by these conformational changes varies depending on cognate, near cognate or non-cognate properties of the codon-anti-codon interactions, but GTP hydrolysis does not guarantee the acceptance of the tRNA. Proofreading is thought to proceed in two steps post GTP hydrolysis based on recent kinetic findings: an EF-Tu•GDP•aa-tRNA mediated step and an EF-Tu•GDP independent step, the end result of which is acceptance or rejection based on the steric requirements induced by ribosomal conformation. This sterically driven accommodation mechanism operates through the concerted cooperation of the 16S rRNA decoding center, the GAC, and ribosomal conformational change is a demonstration of the crucial, incremental processes required to create an accurately folded and functioning protein (Figure 1-3).

Furthermore, decoding primes the ribosome for peptidyl transfer through the distinct conformational adjustments required of tRNA association (Zhou *et al.*, 2014).

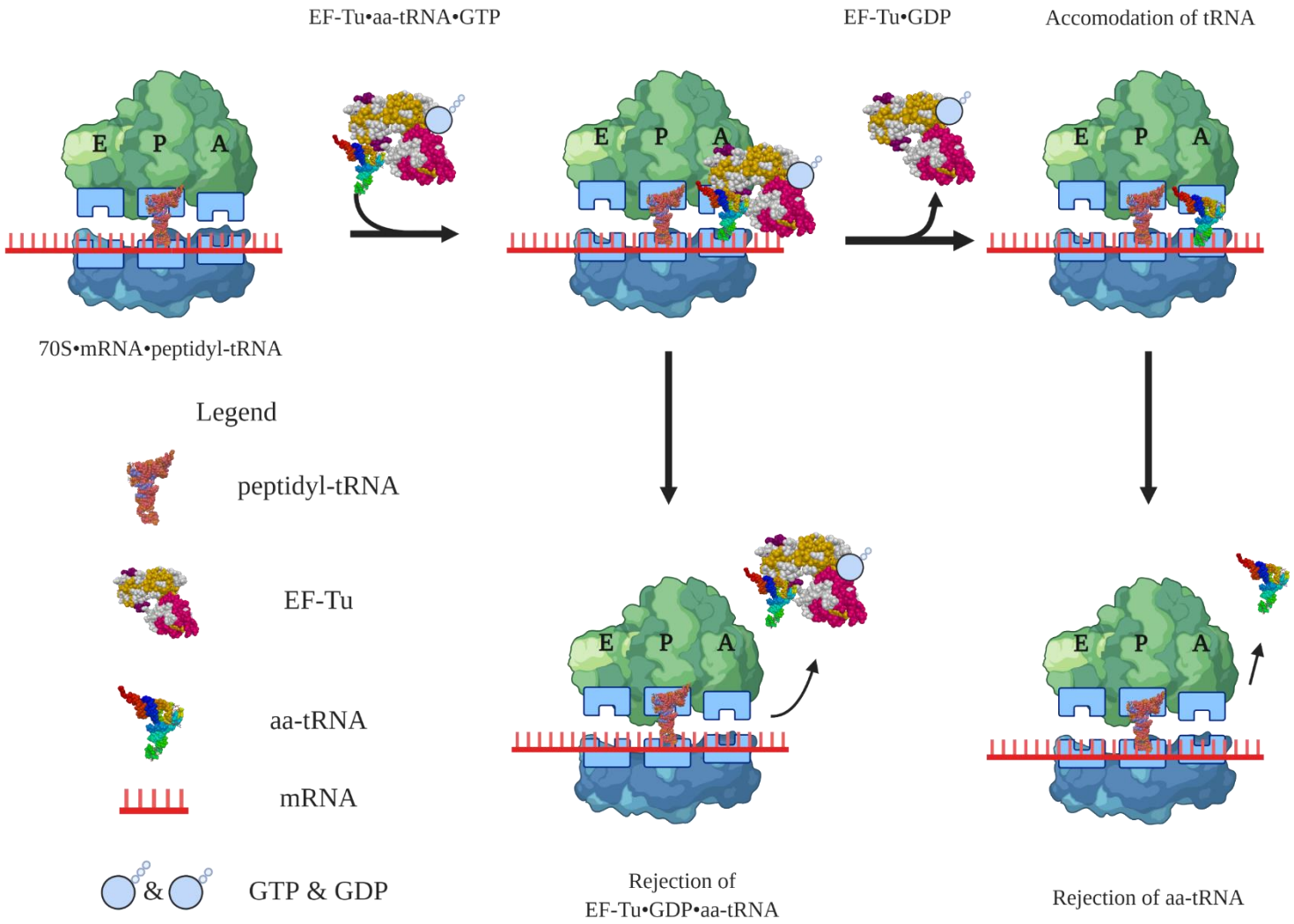

Figure 1-3. Schematic of the Decoding Process. EF-Tu delivers aa-tRNA to the 70S elongation complex via mRNA codon base pairing with the aa-tRNA anti-codon stem loop. EF-Tu hydrolyzes GTP, leading the elongation complex to Accomodation. This process has two proofreading steps for tRNA. EF-Tu•tRNA complex based rejection and aa-tRNA based rejection.

Peptidyl Transfer

Peptidyl transfer constitutes the reactions resulting in the formation of a new peptide bond. In order to facilitate this reaction, the P site tRNA, bound to the growing peptide chain, is sterically

situated in the peptidyl transferase center (PTC) to favor peptide bond formation (Nissen *et al.*, 2000). Peptide formation occurs via an induced fit mechanism involving a conformational change in the 23S rRNA, peptidyl-tRNA, and aa-tRNA residues. The α-amino group of the aa-tRNA in the A site attacks the ester group of the peptidyl tRNA to form a structural intermediate that facilitates peptide bond formation between the two tRNAs. The catalytic sites to form this intermediate are two different nucleotides: a ribose 2'-hydroxyl (-OH) at position A2451 on the 23S rRNA and the 2'-hydroxyl on the adenosine of the P site tRNA. The 2'-OH on the tRNA engages in substrate assisted catalysis, the rate of peptide bond formation is dependent on this hydroxyl group. (Weinger *et al.*, 2004). The A2451 2'-OH serves to deacylate the A site tRNA by functioning as a hydrogen donor and hydrogen acceptor. The aa-tRNA is eventually deacylated by the peptidyl transferase center through the process of proton shuttling. Proton shuttling involves the formation of a tetrahedral intermediate through direct hydrogen bonding of the A2451 hydroxyl group to the 2'-O of the A76 residue of the P site tRNA, which in turn is positioned to simultaneously donate its proton to the 3'-O and receive a proton from the positively charged nitrogen from the newly formed peptide backbone (Lang *et al.*, 2008). The passage of protons is what allows the PTC to pass the growing chain to the A site aa-tRNA. The deacylated P site tRNA is shunted into the E site via translocation by elongation factor G (EF-G).

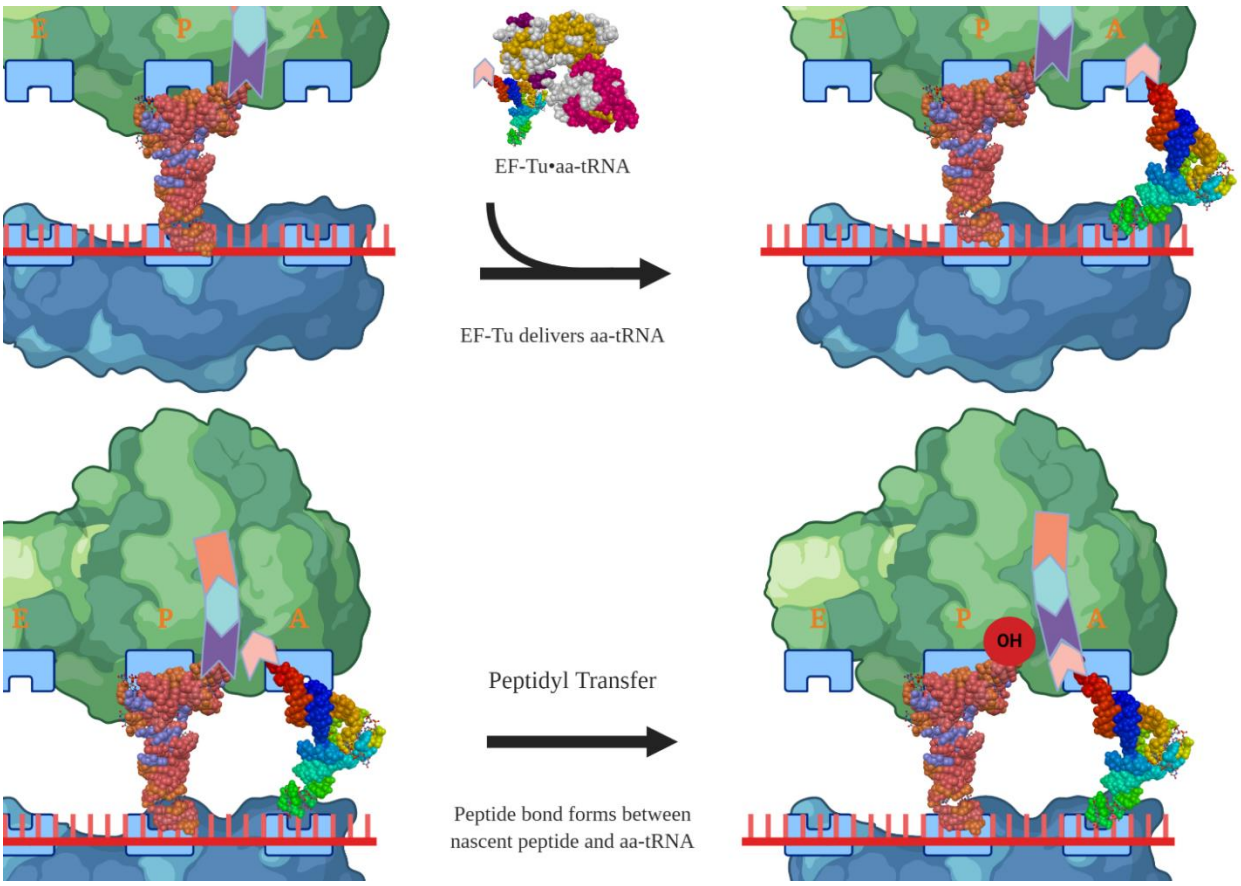

Figure 1-4. Schematic of the Peptidyl Transfer Process. Peptide bound tRNA occupies the P Site, upon EF-Tu facilitated aa-tRNA delivery and decoding, aa-tRNA binds to the A site. The nascent peptide strand then forms a peptide bond with the amino acid of the aa-tRNA, shifting the growing peptide into the A sit and priming the ribosome for translocation.

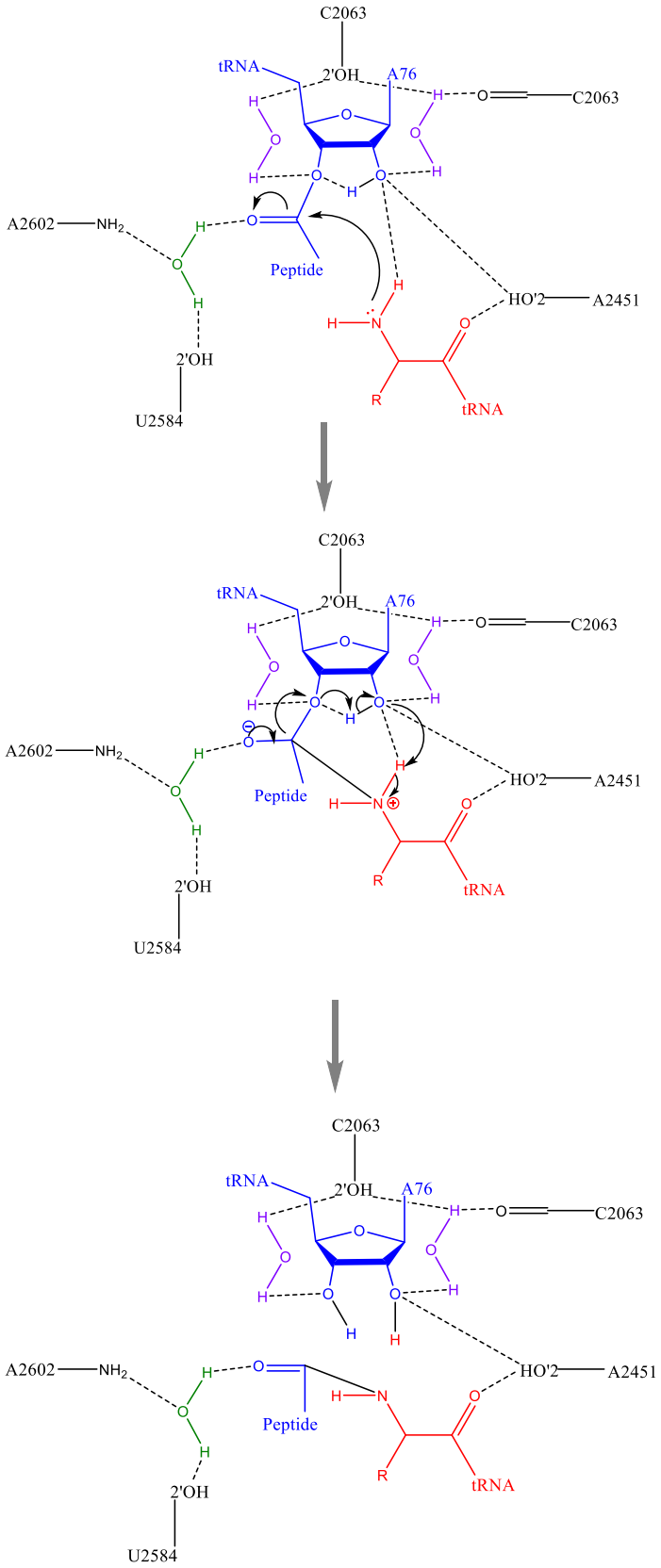

P site substrate

A site substrate

Ordered water molecules present in the PTC hydrogen bond network

Water molecule proposed to stabilize charge in the PTC

Ribosome

Figure 1-5. Proposed Molecular mechanism for PTC catalyzed proton shuttling to form a new peptide bond. The amine of the aa-tRNA attacks the carbonyl center of the nascent peptide, facilitating the proton shuttling via the 2'hydroxyl group of A76 of the 23S rRNA. (Leung et al. 2011).

Translocation

Translocation is the final action of the elongation cycle. Carried out by EF-G, the major result of this step is the movement of the aa-tRNA in the A site to the P site, which consequently moves the deacylated-tRNA in the P site to the E site where it exits the ribosome. The mRNA is moved by one codon in order to maintain the correct reading frame. (Schmeing and Ramakrishnan, 2009). Translocation occurs in two distinct steps, a reversible inter-subunit rotation and the EF-G catalyzed movement of the nucleotide complexes (Figure 1-5). The reversible rotation of the subunits allows a transition state after peptide bond formation so that the peptidyl ends of the tRNA in the P site and A site move corresponding to the 50S while the anticodon-codon binding stays unchanged. The result is tRNAs in p/e and a/p hybrid states and the binding of an EF-G•GTP complex. This complex binding catalyzes movement of the mRNA codons and tRNA anticodon stem loops prior to GTP cleavage (Spiegel, Ermolenko and Noller, 2007). This chimeric state has been characterized further by the Noller lab they showed the P site tRNA interacting with both the P and A site loops of the 50S subunit. They also demonstrated that the emergent mRNA curved upward relative the 30S subunit to bind ribosomal protein S3: this moved the mRNA strand one codon which would return tRNAs to normal P/P and E/E states(Zhou *et al.,* 2014). This movement is caused by domain IV of EF-G overriding the hydrogen bonds of the decoding center nucleotides A1492 and A1493 located in the A site (Liu *et al.,* 2014; Zhang *et al.,* 2015). EF-G then undergoes a conformational shift of 10 to 15 Å transforming EF-G from a PRE to a POST translocation conformation (Brilot *et al.,* 2013; Chen *et al.,* 2013). The subsequent cleavage of GTP is purportedly catalyzed by interactions with ribosomal proteins L1 and L11, the sarcin-ricin loop, Domain III of EF-G (Figure 3-1) and the conserved GTPase residue His84 or cognate His84 residues (Mohr, Wintermeyer and Rodnina,

2002; Wilden *et al.*, 2006; Schmeing and Ramakrishnan, 2009; Voorhees *et al.*, 2010; Ash *et al.*, 2011; Shi *et al.*, 2012; Brilot *et al.*, 2013; Koch *et al.*, 2015). Following GTP hydrolysis, the EF-G•GDP complex dissociates from the ribosome, allowing subsequent rounds of translocation to proceed until the termination stage of peptide synthesis.

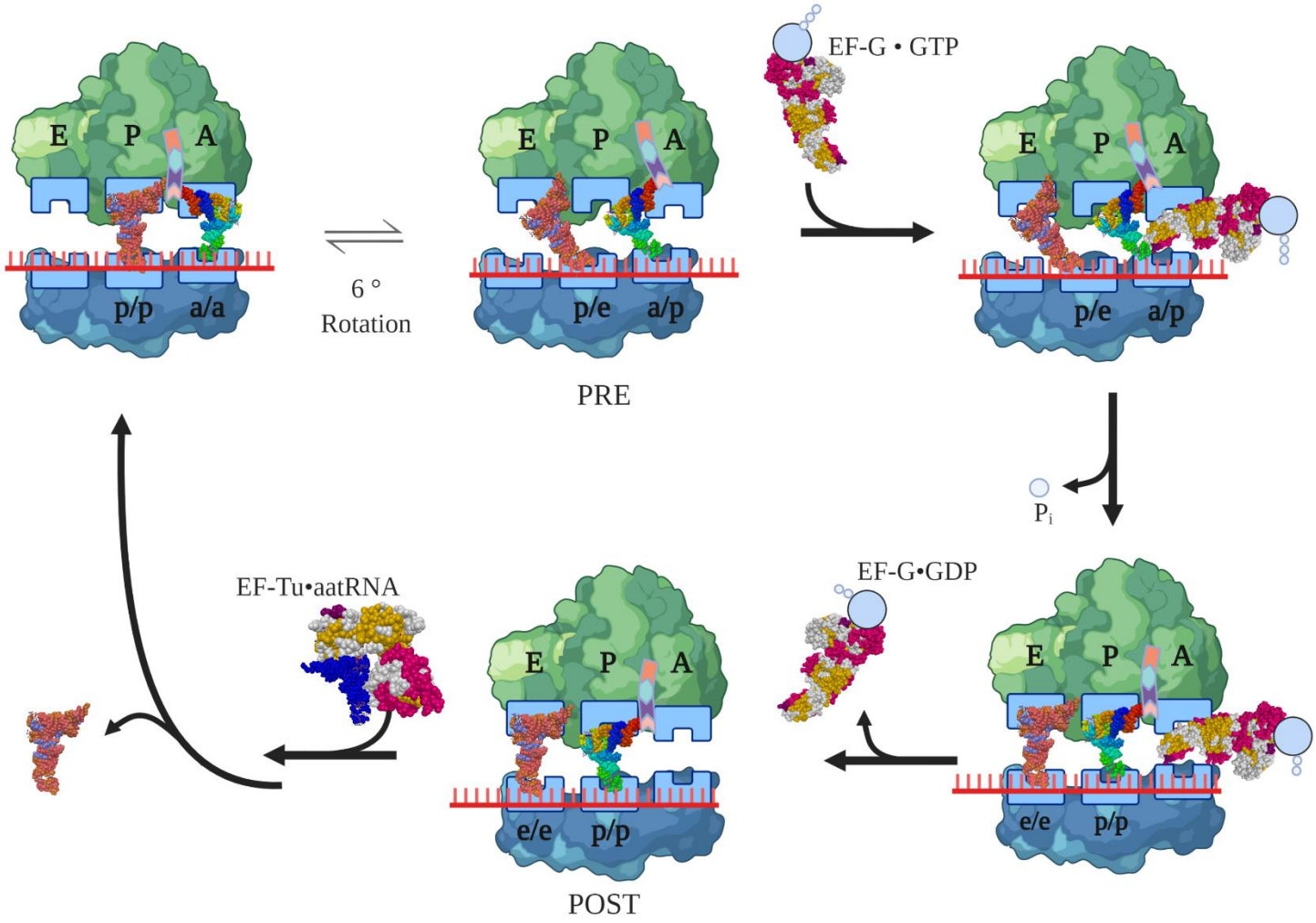

Figure 1-6. Schematic of Translocation. 50S and 30S subunits undergo a 6° rotation relative to each other causing tRNA in the A and P sites to adopt hybrid a/p and p/e hybrid states respectively. EF-G•GTP binds in the A site. GTP cleavage accelerates the subunit conformational shifts that facilitate mRNA movement by a single codon. EF-G•GDP dissociates forming POST translocation 70S complex. E site tRNA dissociates and EF-Tu escorts the next aa-tRNA to the A site for the next round of elongation.

Termination

The penultimate step of translation is the process of termination. Termination of translation signals the end of peptide polymerization, and the release of the nascent peptide chain. The conserved termination signal during translation is called the stop codon; identifiable by a UAG, UAA, or a UGA nucleotide sequence in mRNA. Stop codons do not code for any amino acids and were discovered by various mutation studies that lead to a unique nomenclature which designated UAG as “amber”, UAA as “ochre”, and UGA as “opal” stop codons. In bacteria two related class I release factors act to recognize the stop codons and hydrolyze the newly synthesized peptide: Release factor 1 (RF1) which specifies for UAG codons and Release factor 2 (RF2) which specifies for UGA codons, both are able to recognize the UAA codon (Koutmou *et al.*, 2014). These two proteins, though they serve the same rough purpose, produce distinct effects upon binding with the 70S complex. Both release factors bind to the ribosome such that they maintain interactions with L11 and L1 on the 50S subunit but they differ in their influence on subunit rotation: RF1 favors the non-rotated state of the ribosome more efficiently than RF2, with intersubunit rotation shifted toward a PRE translocation rotated state upon RF2 mediated peptide hydrolysis (Adio *et al.*, 2018). Class I release factors are regulated by the GTPase Release factor 3 (RF3), which is known as a class II release factor. RF3 is a non-essential GTPase in prokaryotes but its eukaryotic homolog eRF3 is required for proper translation. Unlike some other GTPases, RF3 binds to the ribosome when complexed with GDP, this binding allows for nucleotide exchange and GDP is replaced with GTP. The conformational change enacted by GTP binding results in the dissociation of RF1 or 2 from the ribosome. This dissociation is most effective at low concentrations of RF1/2, so the function of RF3 was viewed as an enzyme that would increase the relative concentration of free class I release factors

(Freistroffer *et al.*, 1997; Gao *et al.*, 2007). More recent developments indicate a nuanced role for RF3 in termination and indicate a far greater level of complexity for the entire process. For example, RF3 and RF2 have been implicated in quality control of peptide synthesis by facilitating early termination of peptide strands synthesized after an A site miscoding event. (Zaher and Green, 2009; Alejo and Blanchard, 2017). Structural data and various *in vitro* assays have indicated that the positioning of RF3 and RF1 to protein L11 on the ribosome play a greater role in RF3 mediated GTP hydrolysis than previously thought. The rotation of the ribosome, conformational changes in the release factors, peptide chain cleavage, and GTP hydrolysis all appear to play major roles in release factor dissociation and translational termination (Gao *et al.*, 2007; Peske *et al.*, 2014; Pierson *et al.*, 2016; Adio *et al.*, 2018). The efficiency of class I release factor dissociation is enhanced by almost 600 fold in the presence of RF3; RF1 dissociation increased from .005 s^{-1} without RF3 to .09 s^{-1} in the presence of RF3 (Freistroffer *et al.*, 1997; Koutmou *et al.*, 2014). RF3 is considered a non-essential translation factor because both RF2 and RF1 will dissociate without the presence of RF3. RF3 and RF2 have been implicated in quality control of peptide synthesis by early termination of peptide strands synthesized after miscoding events (O'Connor, 2015; Gibbs and Fredrick, 2018; Rodnina, 2018). The concerted interactions of the termination factors prime the 70S complex for the process of ribosome recycling.

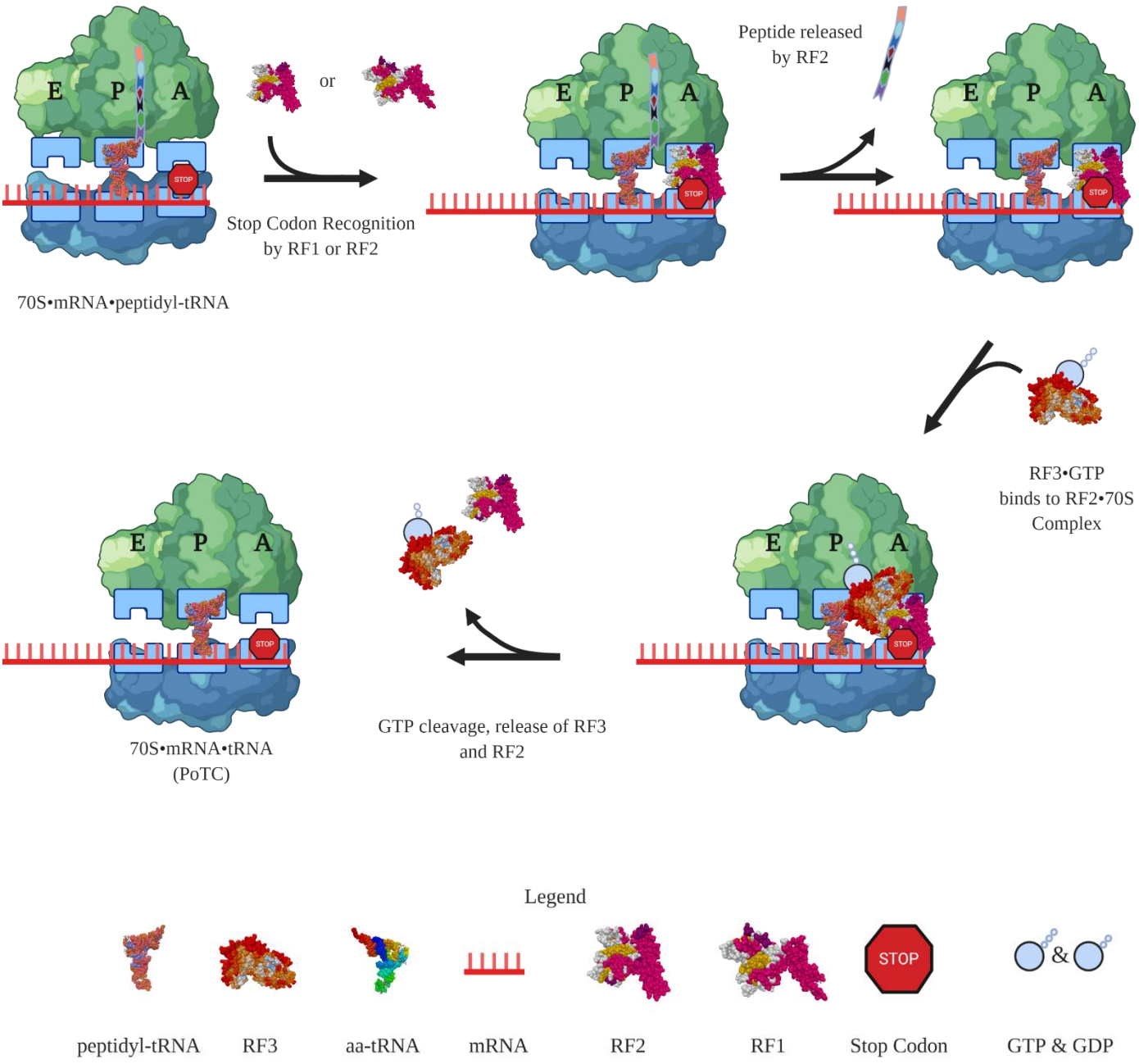

Figure 1-7. Schematic of Termination. Translating ribosome reaches a stop codon. This stop codon is recognized by either RF1 or RF2. Association of RF1 or 2 releases the nascent peptide. Release Factor 3 binds to Termination Complex, upon GTP cleavage RF2 and RF3 dissociate from the Termination complex, leaving only deacylated tRNA in the Post-Termination Complex.

Ribosome Recycling

Ribosomal recycling, formerly known as ribosome dissociation, is the final step before another round of translation commences. The key factors involved in ribosome recycling are EF-G, ribosome recycling factor (RRF), and IF-3. The recycling process occurs after RF-3 has dissociated RF-1 and RF-2, post stop-codon recognition leaving only the 50S subunit and a 30S•mRNA•tRNA complex, with the final tRNA deacylated in the P site. This state of the ribosome is referred to as the post-termination complex (PoTC), which is the state of the ribosome that initiates the process of ribosome recycling. The exact mechanism of ribosome recycling is currently unknown structurally, which has highlighted ribosome recycling as an important subject of research. There are two current hypotheses that argue the specific role of translation factors involved. One hypothesis has proposed that ribosome recycling occurs via the following pathway; RRF binds to the A site and is translocated to the P site via EF-G cleaving GTP, thus pushing the tRNA into the E site, while subsequently splitting the ribosome into its subunits. IF3 is then proposed to bind the now naked 30S•mRNA subunit to keep the 50S and 30S from re-associating. (Hirokawa et al., 2005; Inokuchi, Hirashima, Sekine, Janosi, & Kaji, 2000; Ito, Fujiwara, Toyoda, & Nakamura, 2002). The other hypothesis is that: RRF binds to the A site, followed by association of an EF-G•GTP complex to ribosome-bound RRF. After the cleavage of GTP the ribosome is dissociated into its 50S and 30S subunits. IF-3 then dissociates the deacylated tRNA from the 30S•mRNA complex and binds to prevent subunit reassociation. Therefore priming the 30S subunit for another round of translation (Karimi *et al.*, 1999; Zhang *et al.*, 2015; Borg, Pavlov and Ehrenberg, 2016; Chen *et al.*, 2017). The translocation-like aspects of the former mechanism have since been disproven, but a key source of conflict between the two hypotheses concerns the role of IF-3 and the nature of the PoTC's examined. Dissociation via RRF and EF-G has been shown to be dependent on the relative concentrations of EF-G and

RRF available; since EF-G and RRF compete for initial binding to the ribosome such that dissociation will progress only if RRF is the initial binding partner to the PoTC (Borg, Pavlov and Ehrenberg, 2016). Recently the presence of SD sequences in the synthetic mRNA sequences used to analyze ribosome recycling was shown to affect the kinetics of ribosome recycling significantly (Chen *et al.*, 2017). Where the two hypotheses agree is that there is a cooperative interruption of intersubunit bridge 2a (B2a) by domain IV of EF-G and RRF (Zhang *et al.*, 2015). B2a is formed by two helices on the large and small subunit labeled H69 and h44, respectively (Liu and Fredrick, 2016). Structural insights in the past often illuminated the specific mechanisms and interactions of the ribosome and translation factors. But due to the instability of the EF-G•RRF•70S transition state complex, the current structures lack the resolution required to provide concrete answers (Kiel *et al.*, 2003; Fu *et al.*, 2016; Ling and Ermolenko, 2016).

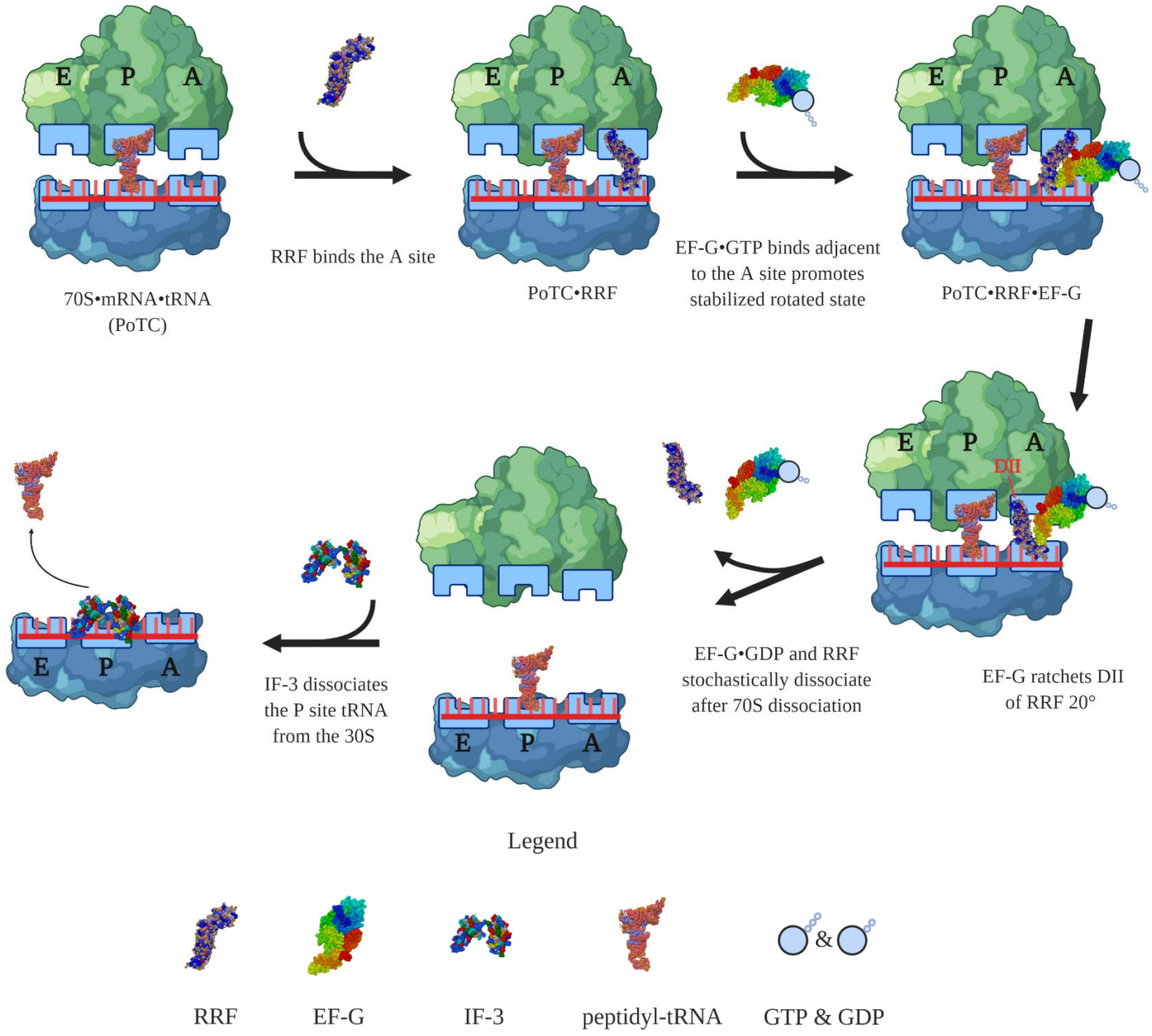

Figure 1-8. Schematic of Ribosome Recycling. The 50S and 30S of the PoTC rotate freely relative to each other until the rotated state is stabilized by RRF and EF-G•GTP binding. RRF binds to the A site where EF-G binds adjacently. EF-G further stabilizes the rotated state and ratchets domain II (DII) of RRF by 20 °. Hydrolysis of GTP by EF-G enables cooperative interruption of B2a by EF-G and RRF causing dissociation. IF-3 is then thought to dissociate the P site tRNA from the 30S complex.

Chapter 2. Bacterial Ribosome Structure

Bacterial ribosomes form hetero-dimeric structures *in vivo,* their basic structure is modeled off of *T. thermophilus* and *E. coli* as model organisms because these are the species for which the atomic resolution crystal structures of the ribosome were solved. These massive ribozymes consist of the 50S and 30S subunits. The 50S consists of two RNA strands the 23S and 5S, and 31 distinct ribosomal proteins denoted with the prefix "L-" for large subunit. The 23s rRNA strand has two conserved sequences that are required for substrate and factor binding, including the Sarcin-Ricin Loop (SRL) and the GTPase-associated center (GAC). The SRL is a constitution of 12 conserved bases that among other interactions maintains the fidelity of translation via EF-G interaction during translocation (Shi *et al.*, 2012). The GTPase associated center is made up of residues 1030-1124 of the 23S rRNA and large subunit proteins which will be detailed below. The 30S subunit contains the 16S RNA and 21 other protein domains labeled "S" for small subunit. The small subunit is primarily responsible for ensuring proper mRNA•tRNA codon-anticodon base pairing. The 16S rRNA recognizes the SD sequence of mRNA and the binding interaction between the two will dictate the efficiency of translation (Malys, 2012). The focus of this thesis will be on the GTPase Associated center; which presents an under-explored interface between subunit proteins and rRNA and the structural requirements to activate and induce the function of translational GTPases.

GTPase Associated Center

Every bacterial ribosome contains a catalytic GTPase activating center (GAC), located on the large subunit. Which consists of the ribosomal proteins L10, L11, the flexible L7/L12 (L12), and two conserved portions of 23S rRNA; one portion which is the SRL (Figure 2-1). The L10 and L7/L12 proteins form the ribosomal L12 stalk which facilitates acceleration of GTP hydrolysis on the ribosome through dimeric pairs of flexible L7/L12 protein complexes. It is established that the L7/L12 subunits form homo-dimers that branch off of the L10 protein from their N-terminus; depending on the organism anywhere from four, six, or eight sets of these dimers could be present on a ribosome (Diaconu *et al.*, 2005; Maracci and Rodnina, 2016). The L11 protein has also been demonstrated to allow for crucial ribosomal conformation changes that allow translocation or modulation of aa-tRNA kinetics. (Agrawal *et al.*, 2001; Yang, Noel and Whitford, 2017). The interactions between L11 and L7/L12 stalk are for the most part unexplored on a molecular level. L11 engages with the L12 carboxy-terminal domain (CTD) during GTPase associated steps of translation in multiple crystal structures (Gao *et al.*, 2009; Chen *et al.*, 2013; Zhou *et al.*, 2014). However, the disordered nature of the L12 stalk makes it hard to identify exact amino acid residues reliably with current levels of ribosome structural resolution. By employing site directed mutagenesis on the C -terminus of the L7/L12 stalk, our lab hopes to elucidate how L11 influences L7/12 in the catalysis of GTPase activity (Figure 2-3).

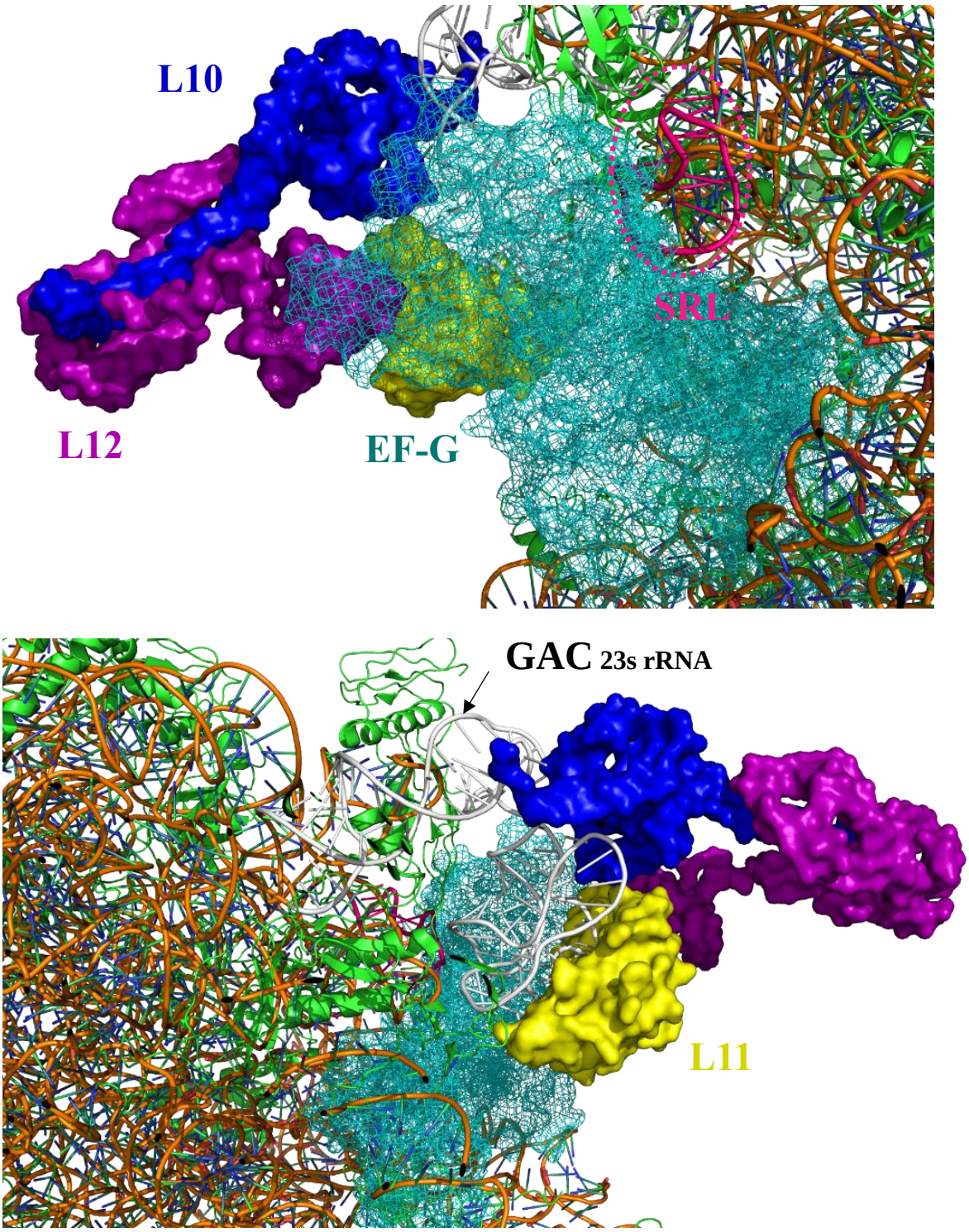

Figure 2-1. GTPase Associated Center of the Bacterial Ribosome. EF-G (Teal mesh) in association with the GAC. L12 (Purple) interacts with L11 (yellow) and EF-G via the CTD while bound to L10 (Blue). The SRL (Pink) makes contact with the G domain of EF-G. GAC 23s rRNA(White). (PDB ID: 4W29)

Structure and Interactions of the L7/L12 Stalk

L12 stalk complexes are highly conserved protein complexes on the 50S subunit of all ribosomes. The L12 stalk consists of a multiple dimer protein complex that branches off ribosomal protein L10. The CTD is a major point of interaction in catalysis of GTP cleavage, with a positively charged face. There is a disordered linker region that connects the NTD to the CTD of L12 which allows for the flexibility of the stalk. The G and G' domains of GTPases (Figure 3-2) have structural interactions with the SRL and the GAC at the base of the L12 stalk (Figure 2-1). One singular glutamine residue contained in a loop referred to as switch II has been shown to be required for certain GTPase's activity. (Schmeing and Ramakrishnan, 2009; Liljas and Sanyal, 2018). The L12 stalk plays a role in the activation of some GTPases, such as EF-G, but will has no stimulatory effect on IF2 activity (Huang, Mandava and Sanyal, 2010). Furthermore, structural analysis of GTPase-bound ribosomal transition states show low structural contact between L12 and the G and G' domains (Voorhees *et al.*, 2010; Chen *et al.*, 2013). The exact role L12 plays in GTPase activation is unclear, but it appears its presence and flexibility are essential to GTPase function. The L12 CTD is critical to normal GTPase function, and in mutants where the length of the flexible linker region was shortened GTPase function was severely impaired. (Bubunenko, Chuikov and Gudkov, 1992; Mohr, Wintermeyer and Rodnina, 2002; Diaconu *et al.*, 2005; Carlson *et al.*, 2017). Recent site directed mutagenesis studies have suggested that L12 and IF2 interact based on charge complementarity(Ge *et al.*, 2018). Previous work performed in our lab has shown that L12 is essential to GTPase binding and activity and was able to show the L12 CTD interacts with the G' domain of EF-G (Carlson *et al.*, 2017).

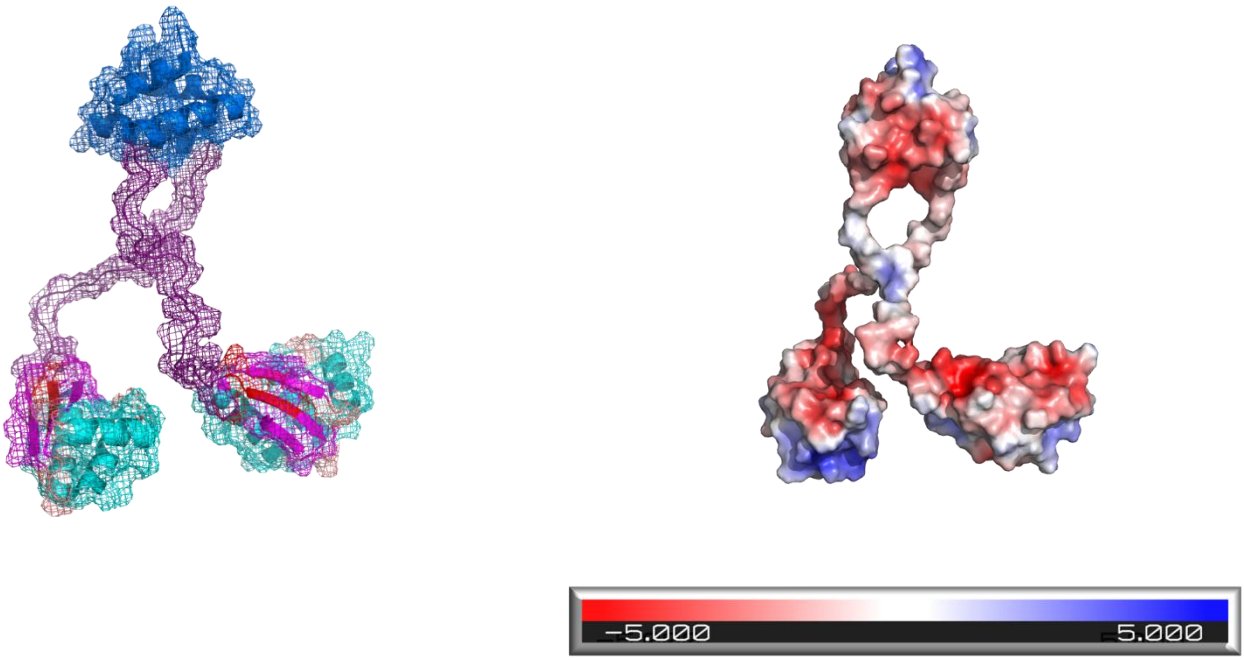

Figure 2-2. Structural and Electrostatic Properties of the L7/L12 Dimer. (PDB ID: 1RQU) Left: L7/L12 Dimer with NTD (blue), linker region (purple), and CTD highlighted (secondary structure coded: α-helices(cyan), β-sheets (magenta). Right: L12 Dimer overlayed with electrostatic map, negative charge (red) and positive charge (blue) measured on a gradient -5 being most negatively charged, 0 being uncharged(white), and 5 being most positively charged.

Structure and Interactions of the Ribosomal Protein L11

Similarly, to L7/L12, the L11 protein is a conserved portion of the GAC in all organisms. L11 has established roles in GTPase activation, and the GAC. The interactions between L11 and L12 during these processes has not been probed extensively. L11 consists of a C-terminal rRNA binding domain that aids stabilization of the 23S strand and rRNA induced GTPase activation. (Mitroshin, Garber and Gabdulkhakov, 2015) The N-terminal domain of L11 promotes the function of translation factors, as *E. coli* cells without L11 grow two times slower. (Dabbs *et al.*, 1981) The proximity of L11 and the L12 stalk proteins have been shown to increase L7/L12 affinity for rRNA by two degrees of magnitude (Iben and Draper, 2008). L11 has also been

implicated in affecting the thermodynamic and kinetic favorability of aa-tRNA accommodation on the ribosome (Yang, Noel and Whitford, 2017). Most pertinent to our research are the interactions between the L11 and L12 proteins; these interactions are chaperoned by the G-domain of GTPases to maintain stability of the L12 C-terminus.

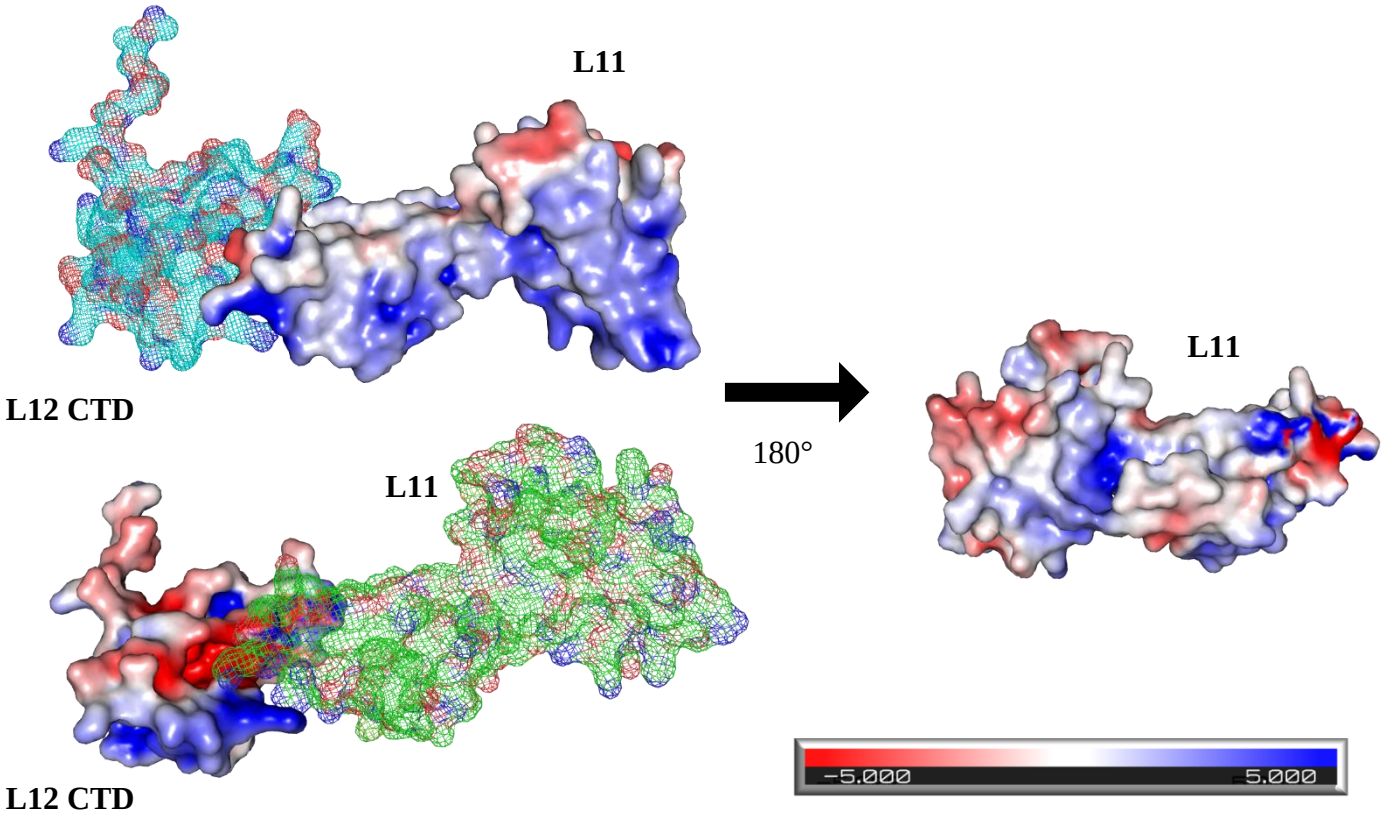

Figure 2-3. L11 to L12 Electrostatic and Structural Interactions. L12 CTD (Cyan mesh) and L11 (Green mesh) present a clear electrostatic interface. L11 is rotated 180° to present the charged residues closest to the L12 CTD. L11 overlayed with electrostatic map, negative charge (red) and positive charge (blue) measured on a gradient -5 being most negatively charged, 0 being uncharged(white), and 5 being most positively charged.

Chapter 3. Translational GTPases

GTPase Super Family

Fundamental processes require energy to progress; in most known life-forms this is achieved via the thermodynamic favorability provided by the hydrolytic cleavage of oligomeric phosphate bonds. These phosphatidyl- groups are generally bound to nucleotides like adenosine or guanosine. The end-goal of the numerous catabolic and anabolic processes of metabolism across all lifeforms can be linked to the maintenance of homeostatic concentrations of ATP and GTP alongside the factors that regulate them. These crucial regulators are cleavage enzymes generally referred to as ATPases or GTPases. GTPases for cellular processes require regulation in the form of two types of proteins: Guanine nucleotide exchange factors (GEFs) and GTPase activating proteins (GAPs) (Ero *et al.*, 2016; Gibbs and Fredrick, 2018; Rodnina, 2018). Regulation is especially evident in the process of translation; where the entire ribosome acts as a proverbial GAP for numerous GTPases, each of which facilitates a stage of protein synthesis. This superfamily of proteins known as GTPases are the engines driving each step in the production of polypeptides forward(Rodnina *et al.*, 2019). Like the requirement of energy for life, it is unsurprising that these enzymes are convergent and homologous in their structure and function.

EF-G

PDB ID: 4M1K

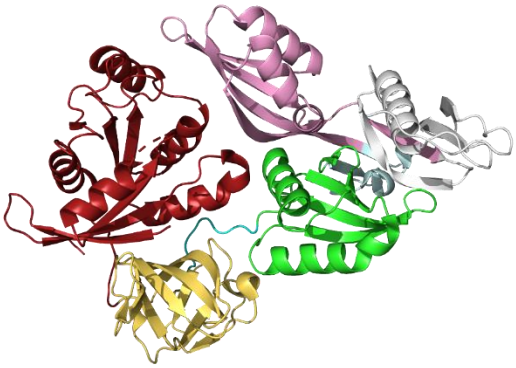

LepA

PDB ID: 3CB4

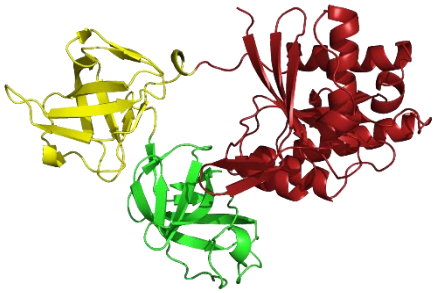

EF-Tu

PDB ID: 1EFC

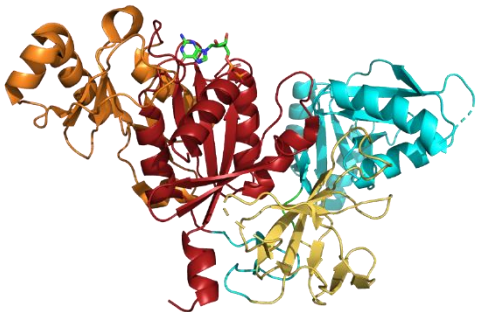

RF-3*

PDB ID: 2H5E

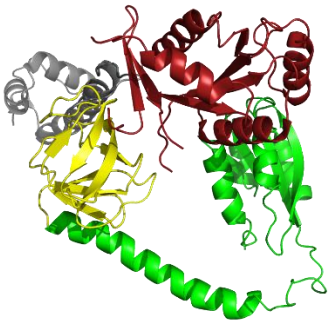

IF-2*

PDB ID: 4KJZ

Figure 3-1. Examples of Homologous Bacterial GTPases. The five represented GTPases, EF-G, LepA, EF-Tu, RF3, and IF-2 have a conserved structural homology highlighted by the color-coded sections above. G Domain (Red) G' Domain (Orange), Domain II (Yellow), Domain III (Green), Domain IV (White), and Domain V (Pink).

*Gray and Cyan regions are not highlighting structural homology

GTPases share the conserved structure of the GTP-binding domain or G-Domain. This active site is where GTP is bound and cleaved into GDP(Maracci and Rodnina, 2016). For example, within prokaryotic translation there are several fundamental GTPases: IF2, EF-Tu, EF-G, and RF3; all of which have structural homologs across the entire spectrum of life (Figure 3-1) (Hauryliuk, 2006; Leipe, Wolf, Koonin, & Aravind, 2002).

Homology of the G-Domain

The structural homology of the G-Domain is evident in all GTPases, (Figure 3-2) which consists of highly conserved structural motifs identified as G1 to G5. G1 also known as the P loop which interacts with the α and β phosphates of GTP. G2 and G3 are also identified as switch I and switch II respectively and perform a myriad of functions; they allow for conformational flexibility during nucleotide association and dissociation, G1 and G2 participate in the coordination sphere of a magnesium II (Mg^{2+}) ion that facilitates GTP/GDP binding, and facilitates amino acid interactions with the γ phosphate of the nucleotide. Switch II also contains a histidine residue that is crucial for GTPase activity that is conserved across all GTPase enzymes, recognized as His84 or a cognate amino acid that harbors and positions water molecule responsible for GTP hydrolysis (Maracci & Rodnina, 2016). The G4 and G5 domain ensure selectivity for guanine nucleotides as opposed to adenine, cytidine or uridine phosphorylated bases. (Vetter and Wittinghofer, 2001; Maracci and Rodnina, 2016) This G-Domain is followed by β-barrel domains that vary in location with respect to the type of nucleotide bound. The ribosome interacts with the G-Domain via the GTPase associated center and the His84 or a His84 cognate in switch II maintains interaction with a phosphate group of base A2662 of the 23S rRNA(Voorhees *et al.*, 2010; Tourigny *et al.*, 2013). Since the structure of catalytic sites in GTPases are fundamentally conserved, it appears the function derived from these interactions present the major point of divergence for GTPases.

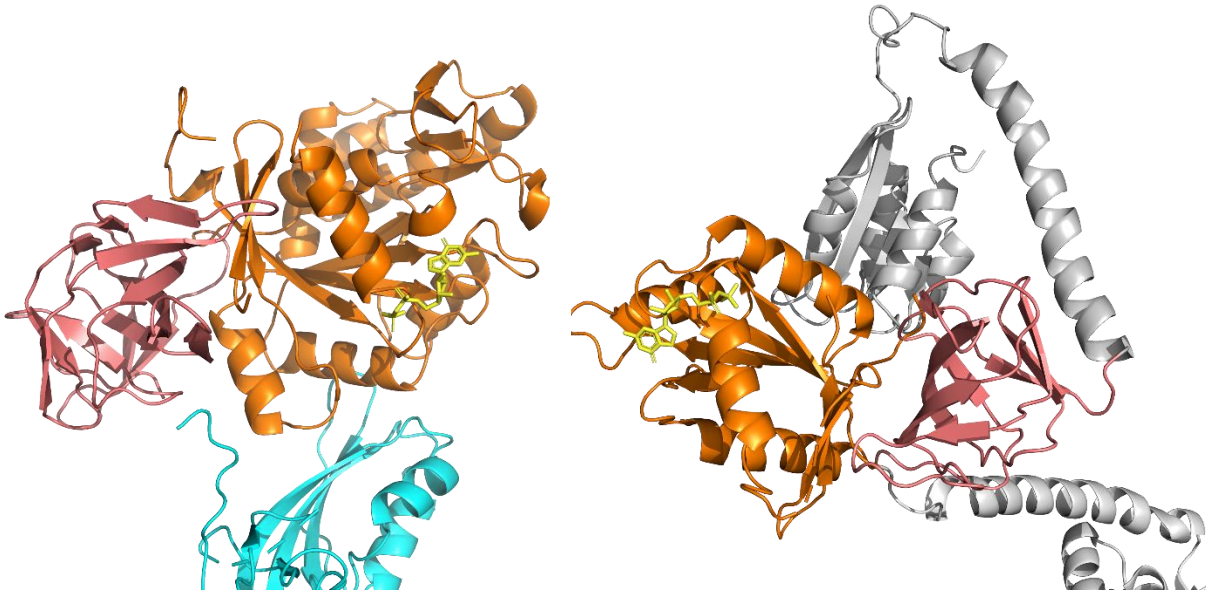

Figure 3-2. Comparison of GDP bound EF-G and IF2 G domains. The G domain of each GTPase is highlighted in orange, β-barrel structure of Domain II in pink. (PDB ID: 1DAR and 4KJZ)

Structural and Genetic Convergence of translational GTPases

The prokaryotic GTPases and their homologs, mentioned prior all present structural attributes that, the G-Domain notwithstanding, are homologous with respect to the interactions between the GTPase and the ribosome. Post G-Domain β-barrels further contribute to structural and functional similarities. For example, EF-G, Elongation Factor 4, and BPI-inducible protein A (BipA) all bind to the same binding site and share structural rigidity in domains I and II (Ero 2016). Due to the preponderance of genetic evidence and the relative universal evolutionary convergence of these enzymes it has been suggested that many translational GTPases (trGTPase) are all derived from a core set of essential translation regulating protein factors (Atkinson, 2015). One example of genetic structural convergence RF3 is a GTPase which facilitates the dissociation of class 1 release factors after complete peptide synthesis and greatly influences post-peptidyltransferase quality control (post-PT QC). However, where the knock down of RF1 or RF2 results in the compensatory action of the other, the genetic knock down of RF3 results

total abolition of post-PT QC; increasing aberrant and error prone protein production. (O'Connor 2015) RF3 shares many structural similarities to EF4, and unsurprisingly it has been suggested that both enzymes are descendant from the elongation factor sub-family (Leipe *et al.*, 2002). The two enzymes share influence in translational quality control, since EF4 has been suggested to behave as an important proofreading factor during the cycles of elongation. (Belardinelli *et al.*, 2016; Ero *et al.*, 2016; Gibbs and Fredrick, 2018). These two enzymes have presented an intriguing example of functional change over time, given a common evolutionary precursor. The diverse array of functions identified in GTPases; from cell signaling, to regulation of mitochondrial architecture, or the facilitation of translational processes has continued a demonstration that enzymatic structural homology provides crucial clues to first principles research in enzymatic function. (Smirnova *et al.*, 2001; Leipe *et al.*, 2002; Schmeing and Ramakrishnan, 2009). There is a GTPase associated with each step of translation, from initiation to recycling (Schmeing and Ramakrishnan, 2009; Goto, Muto and Himeno, 2013; Maracci and Rodnina, 2016). Though each task performed by a GTPase is different, many exact molecular mechanisms and the structures of the related transition states still remain elusive based on current methods. This has produced a perpetually amassing wealth of research on translation and related GTPases. EF-G is an example of a GTPase that is still yielding new findings as it has recently been implicated in 'sliding' of the ribosome across mRNA and preventing backslipping of mRNA (Rodnina *et al.*, 2019).

EF-G/EF-2

Elongation factor G and its various homologs are essential to the process of translation. EF-G performs enzymatic double-duty in prokaryotes as a tRNA translocase and a dissociative co-factor; in mitochondria two different forms of EF-G act in concert to enact the same functions, and finally eukaryotic elongation factor 2 (eEF2) only facilitates translocation. Until recently, EF-G was thought to be only involved in the translational processes of translocation and recycling; however, it has been shown to facilitate reading frame maintenance and allows the ribosome to slide over non-coding mRNA regions. EF-G consists of 5 distinct protein domains designated as domain I, II, III, IV, and V (DI-DV) (Figure 3-3). Domain I constitutes most of the G- and G'- Domains. The G'-domain directly engages with specific positively charged residues on the C terminal domain of the L12 stalk that are required to allow activation of EF-G and other GTPases hydrolytic function (Carlson *et al.*, 2017). Domains II and III are made up of the β barrel motifs present in all GTPases and form interfaces between S12 protein, 16S rRNA and the SRL of the 23S rRNA(Chen *et al.*, 2013; Maracci and Rodnina, 2016). Domains III and V lend conformational flexibility to EF-G, allowing the GTPase to extend and compress without significantly compromising activity (Lin, Gagnon, Bulkley, & Steitz, 2015). Domain IV of EF-G is the central point of interaction between the GTPase and the ribosome. EF-G interacts primarily with the A site. During translocation, EF-G catalyzes the transition between a rotated and non-rotated "PRE" and "POST" translocational state as discussed previously. However, the steric interactions of Domain IV differ between the PRE and POST translocational states; DIV makes contacts with the intersubunit bridge B2a in the PRE-state, and mRNA and P site tRNA in the POST-state. More recently research has showed that there are two distinct loops present in Domain IV: loop I and loop II which are highly conserved structurally. These loops insert into

the decoding center during translocation to interrupt hydrogen bonding between nucleotides A1492 and A1493. The role of these loops in ribosome recycling is unclear, but it is hypothesized that due to the proximity of DIV to bridge B2a, that these loop regions play some role in ribosome recycling. It has been shown via site-directed and truncation mutagenesis that loop II is an important effector of translocation activity (Zhang *et al.*, 2015). EF-G has shown interesting properties when bound to the ribosome with different substrates, when GTP is replaced with a non-hydrolysable analogue such as GDPNP, translocation continues but orders of magnitude more slowly. Conversely the presence of GDPNP in *in vitro* recycling assays does not allow ribosome recycling to progress. (Barat et al., 2007; Borg, Pavlov, & Ehrenberg, 2016; Hirokawa et al., 2005) Due to the different roles and interactions it is involved in, EF-G has become considered a non-canonical GTPase. Finally, because of EF-G's conserved role in translation it has become a viable target for antibiotics, from humans, fungus and competing bacteria alike. Examples of EF-G targeting antibiotics include fusidic acid, thiostrepton, and argyrin B which respectively function via: competitive binding with GTP, interference with proper ribosomal binding, and allosteric exertion of antibiotic activity through a currently unknown mechanism.

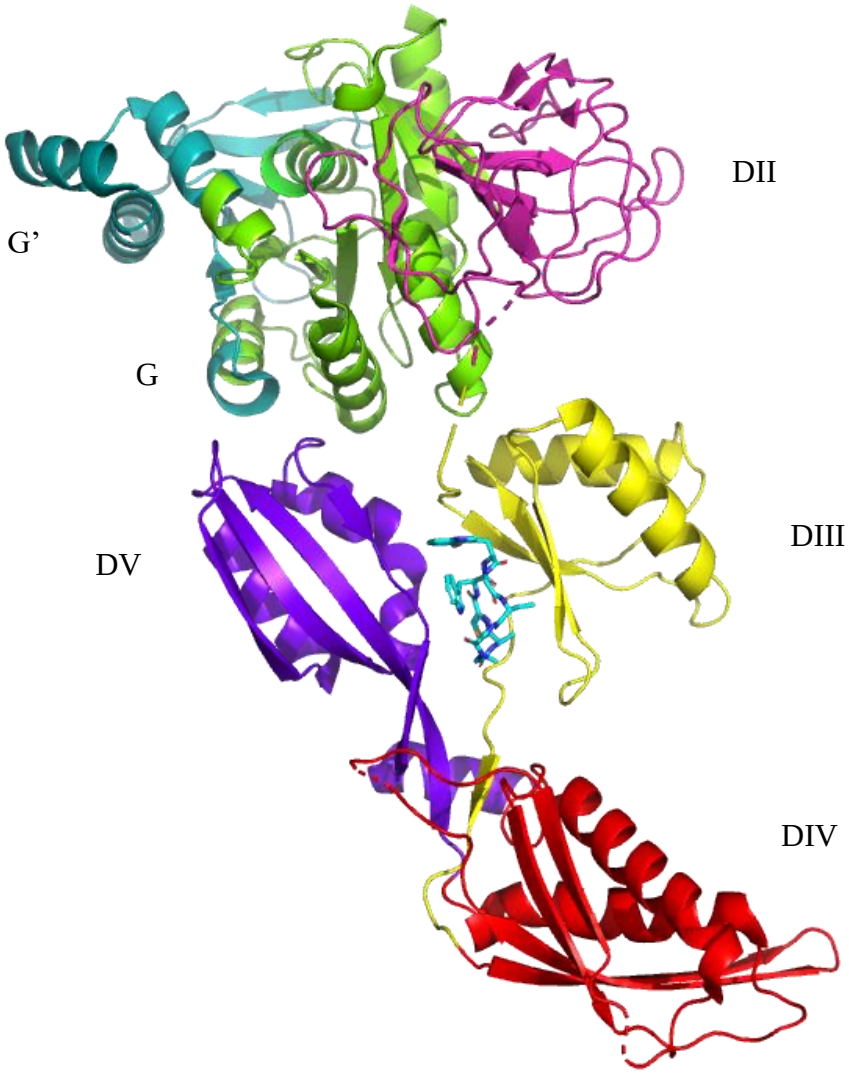

Figure 3-3. Crystal structure of *P. aeruginosa* EF-G with argyrin B bound. EF-G consists of 5 distinct domains. DI consists of G domain (Light Green) and G' Domain (Teal), DII (Pink), DIII (Yellow), DIV(Red), and DV (Purple). Argyrin B (Cyan) binds between DIII and DV. (PDB ID: 4FN5)

Relevance of argryin B

Bacterial antibiotic resistance is one of few preeminent threats to humankind. Natural products have been a consistent wellspring of new leads and drug candidates. Often these new antibiotics target the processes of translation or the membrane structure of the bacteria but are not viable as a therapeutic option in humans due to potential off target effects (Allardyce, Bell and Loizidou,

2019). One example of such a drug candidate is the cyclic heptapeptide argyrin B (ArgB). Argyrins are secondary metabolites of myxobacteria that have shown a promising spectrum of antibiotic and tumor inhibiting activity. The compound argyrin B targets elongation factor G in the bacterial strain *P. aeruginosa* and structural homologs in other bacterial strains. Furthermore, argyrin B has been demonstrated to exert cytotoxic effects on yeast cell, mouse cell, and human cancer cell lines. Argyrin B is not a viable antibiotic for therapeutic use because it is unable to penetrate the membrane of gram-negative bacteria other than *P. aeruginosa*. (Nyfeler et al., 2012), which also would constrain therapeutic potential. More recently a study was published that demonstrated an inhibitory effect on the human immune system proteome. (Allardyce, Bell and Loizidou, 2019). The complete synthesis of argyrin B was accomplished in 2001 with overall synthetic yields of 5.6 % (Ley 2001). The mechanism of action of argyrin B is currently unknown but was assumed to produce an inhibitory effect on the GTPase activity of EF-G and cognate EF-G enzymes in a cell (Nyfeler *et al.*, 2012). There is currently a 2.4 Å resolution crystal structure of *P. aeruginosa* derived EF-G that provides the allosteric binding site of argyrin B (Figure 3-4). This structure also presented an induced elongation of the protein by ratcheting domain IV approximately 45° (Nyfeler et al., 2012). We have surmised that this ratcheting has a distinct influence on the mechanism of action of argyrin B. Previous work performed by our lab suggested that argryin B is a unique translational inhibitor given the following observations; GTPase activity and binding is preserved but translation is abrogated completely. This work seeks to illuminate the full mechanism of action of argyrin B to provide insight into antibiotic resistance and regulation of the bacterial ribosome.

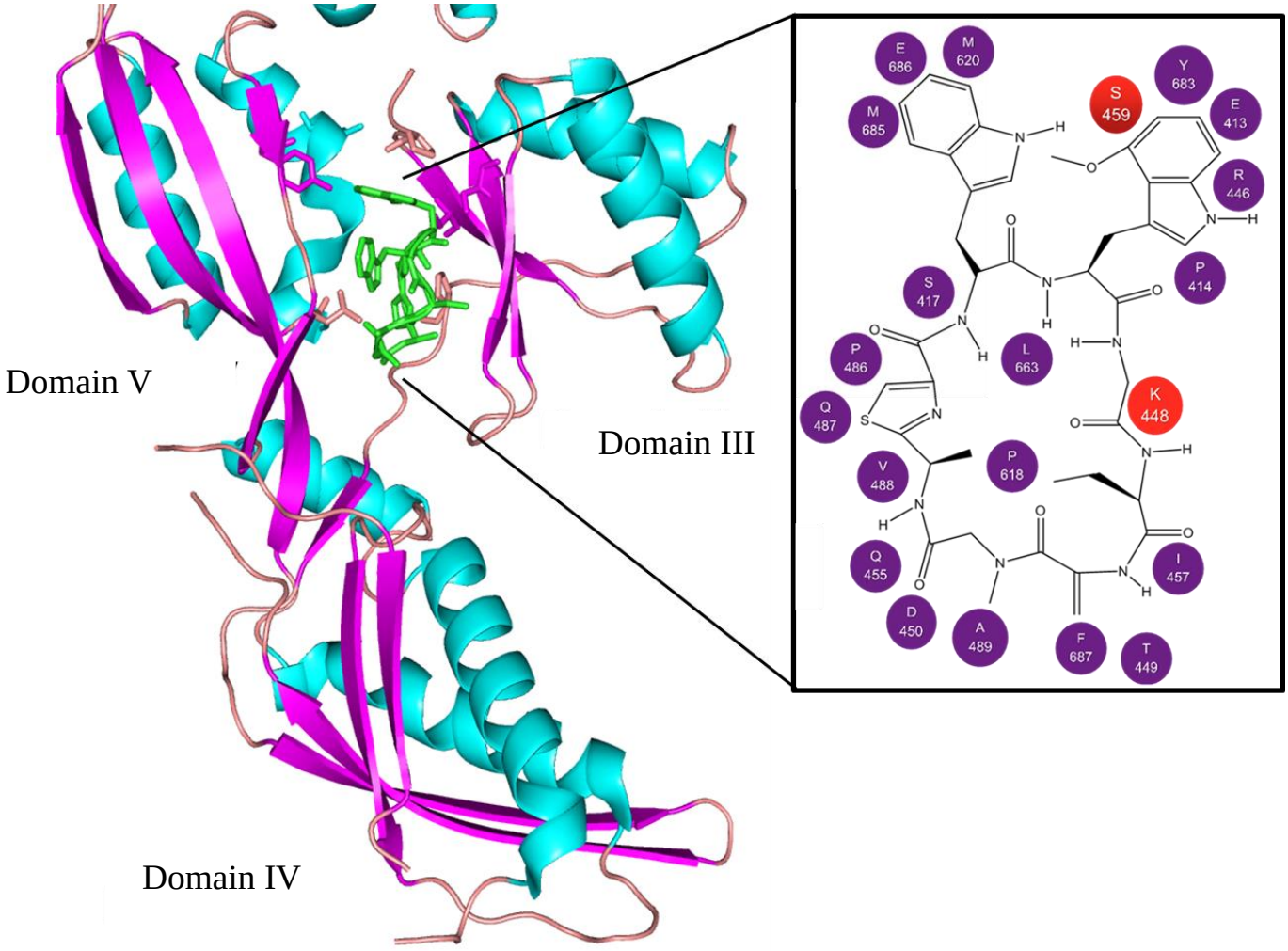

Figure 3-4. A.) *P. aeruginosa* derived EF-G with argyrin B (green) bound and structural activity relationship (SAR) of relevant amino acid residues the argyrin B binding site.. Red residues in the SAR indicate difference in binding site compared to *E. coli* EF-G. (PDB ID: 4FN5)

This work intends to elucidate the molecular mechanism of action of the antibiotic argyrin B and further study the protein-protein interactions of ribosomal proteins L7/L12 and L11 on the large ribosomal subunit. These aims will be accomplished by performing *in vitro*, structural and functional studies of the relevant biological processes of bacterial translation in question.

Chapter 4. Materials and Methods

Buffers

GTPase Lysis Buffer: 50 mM Tris-HCl pH 7.5, 7 mM $MgCl_2$, 60 mM NH_4Cl, 15 mM imidazole, 25% v/v glycerol,

GTPase Wash Buffer: 50 mM Tris-HCl pH 7.5, 7 mM $MgCl_2$, 60 mM NH_4Cl, 50 mM KCl, 15 mM imidazole, 25% v/v glycerol,

GTPase Elution Buffer: 50 mM Tris-HCl pH 7.5, 7 mM $MgCl_2$, 60 mM NH_4Cl, 250 mM imidazole, 25% v/v glycerol

GTPase Storage Buffer: 50 mM Tris-HCl pH 7.5, 7 mM $MgCl_2$, 60 mM NH_4Cl, 10% v/v glycerol

JE28 Lysis Buffer: 20 mM Tris-HCl pH 7.5, 20 mM $MgCl_2$, 150 mM KCl, 30 mM NH_4Cl, 5 mM imidazole

JE28 Wash Buffer: 20 mM Tris-HCl pH 7.5, 20 mM $MgCl_2$, 150 mM KCl, 500 mM NH_4Cl, 5 mM imidazole

JE28 Elution Buffer: 20 mM Tris-HCl pH 7.5, 20 mM $MgCl_2$, 150 mM KCl, 30 mM NH_4Cl, 150 mM imidazole

JE28 Salt Wash Buffer: 20 mM Tris-HCl pH 7.5, 20 mM $MgCl_2$, 150 mM KCl, 500 mM NH_4Cl

5X 100/10 Buffer: 100 mM Tris-HCl pH 7.5, 500 mM NH_4Cl, 52.5 mM $MgCl_2$, 2.5 mM EDTA pH 8.0

5X 500/10 Buffer: 100 mM Tris-HCl pH 7.5, 2.5 M NH_4Cl, 52.5 mM $MgCl_2$, 2.5 mM EDTA pH 8.0

5X 100/6 Buffer: 100 mM Tris-HCl pH 7.5, 500 mM NH_4Cl, 30 mM $MgCl_2$

Ribosome Storage Buffer: 20 mM Tris-HCl pH 7.5, 20 mM $MgCl_2$, 30 mM NH_4Cl, 25% v/v glycerol

L12 Initial Depletion Buffer: 20 mM Tris-HCl pH 7.5, 20 mM $MgCl_2$, 1 M NH_4Cl, 50% v/v glycerol, 5 mM β-mercaptoethanol

1X Tris-Glycine Buffer: 25 mM Trizma™ Base, 250 mM glycine, 0.1% w/v SDS

1X TAE Buffer: 40 mM Trizma™ Base pH 8.0, 0.1% v/v glacial acetic acid, 1 mM EDTA

5X GTPase Reaction Buffer: 400 mM Tris-HCL pH 7.5, 500 mM NH_4Cl, 100 mM $MgCl_2$

4X Protein load dye: 8% w/v SDS, 240 mM Tris-HCl pH 6.8, 40% v/v glycerol, 0.04% w/v bromophenol blue, 5% v/v β-mercaptoethanol

Rayleigh Light Scattering Buffer:

Coomassie gel stain: 0.3% w/v Coomassie Brilliant Blue G-250, 50% v/v methanol, 10% v/v glacial acetic acid

Gel destain solution: 30% v/v ethanol, 10% v/v glacial acetic acid, ddH_2O

Expression and Purification of 70S ribosomes from JE28 Cells:

Expression of JE28 Cells

JE28 *E. coli* cells contain a 3' genetically encoded hexa-histidine tag ($His_{(6)}$-tag) located on the gene rpIL, which encodes for ribosomal protein L12. Transferred from a glycerol stock JE28 cells were expressed in 10 mL of sterile Luria Broth (LB: 1% w/v Bacto™ Tryptone (BD Biosciences), 0.5% w/v Bacto™ yeast extract (BD Biosciences), 1% w/v sodium chloride) with a concentration of 35 µg/ml kanamycin (Kan^{35}) at 37 °C for 14 to 18 hours at 200 rpm at a 45° angle for aeration and proper growth. These inoculation cultures were then added to six 1 L flasks of sterile Kan^{35} LB. JE28 Cultures were then grown to mid log phase, indicated by optical density at 600 nm (OD_{600}) of 1.0. The 1 L flasks were then placed on ice for 1 hour to allow for run off ribosome growth. Post cooling, the JE28 cells were pelleted at 6000 rpm at 4 °C for 10 minutes in a 6 x 500 mL centrifuge rotor (Fiberlite™ fixed angle rotor from Thermo Scientific). Cell Pellets were either stored at -20 °C for future use or purified using the following procedure.

Immobilized Metal Affinity Chromatography Purification of 70S ribosomes:

Cell pellets were thawed on ice, then resuspended in 37.5 mL of JE28 Lysis buffer until solution was a homogenous mixture. Next 1 mM of phenylmethane sulfonyl fluoride (PMSF) and 1 mg/mL chicken egg lysozyme was added and allowed to mix gently at 4 °C for 10 to 15 minutes. The solutions were then sonicated in three 30 second intervals at 50% duty cycle and output level 5, which produced a consistent pulse approximately once every second. Cells were sonicated on ice at 4 °C to minimize thermal denaturation. If only one cell pellet was lysed, a 1-minute pause was incorporated into the sonication intervals. The lysate was then centrifuged in two stages at 4 °C; once at 16,000 rpm for 30 minutes, the high-speed supernatant (HSSN) from the first spin

was collected and centrifuged again at 16,000 rpm for 30 minutes. The clarified HSSN was then filtered through a 5 µm syringe filter, followed by a .45 µm syringe filter to remove small particle cellular debris not removed by centrifugation. The clarified lysate was then incubated with Nickel (II)- IDA resin pre-incubated with JE28 Lysis Buffer, Nickel (II)-NTA resin can be substituted for the same purpose. *

The ribosomes were then purified using immobilized metal affinity chromatography (IMAC), resin incubated lysate flowed through the column and was collected as waste or in a separate vessel. Following flow-through, the resin bound protein was washed with the following to remove remaining impurities: 5 column volumes (CV's) of JE28 Lysis Buffer, 10 CV's ofJE28 Wash Buffer, 5 CV's of JE28 Lysis buffer, each change of buffer required 5 minutes of incubation and resuspension of the resin. Following these wash steps, 3 to 5 CV's of JE28 Elution buffer was added to the resin and allowed to incubate for 15 minutes. To ensure protein was eluted off the column a qualitative assessment was performed using 195 µL of Bradford Reagent and 5 µL of eluent through the elution, this allowed us to determine when protein had completed flowing off the column. The elution was collected and placed in dialysis 12 kDa MWCO tubing and left in dialysis buffer.

*Lower ribosome purity was retrieved using Ni-NTA resin

Concentration and Quantification of IMAC Purified 70S Ribosomes

Post-dialysis, JE28 eluent was removed from dialysis tubing into clean sterile falcon tubes to allow for ease of transfer. All buffers and eluent were maintained at 4 °C to ensure protein stability. In order to concentrate the dialyzed 70S ribosomes, ultracentrifugation of the eluent was performed in high density poly-carbonate tubes with titanium centrifuge caps. These poly-carbonate tubes were balanced to within 2 decimal points on a top-loading balance prior to

centrifugation. The samples were then placed in a 70-Ti ultracentrifuge rotor and spun at 339,000xg for 4 hours at 4 °C. Supernatant was removed and ribosomal pellets were rinsed with 3-5 mL of 1x 50/100 buffer. ** The tubes were then placed upside down on a Kim-Wipe for 30 min at 4 °C to aid separation of a thin yellow film which covered the 70S pellet. The presence of this film indicated proper pelleting of the 30S subunit. If the slime did not fall off after 30 minutes, it was gently removed by rinsing the pellet with 1x 50/100 buffer. The pellet was resuspended overnight in 1 mL of 1x 50/100 buffer. These samples were pooled into a single PC centrifuge tube and centrifuge tube was filled with 1x 50/500 buffer and balanced with a counterbalance of identical mass. The sample was then spun at 339,000 x g for 4 hours at 4 °C. Following this spin the pellet was investigated a second time for yellow film: if the film was present the previous rinsing process using 1x 50/100 buffer was repeated; If the slime was not present it was resuspended in JE28 storage buffer with a 10 µL sample taken for SDS-PAGE and a preliminary check of 70S concentration. 70S concentration was accomplished by UV-Vis absorption at 260 nm and 280 nm on a Jasco or Agilent UV-Vis spectrophotometer. The micromolar concentration of the sample was found by multiply the 260 nm absorbance by a factor of 27. After the concentration was recorded of the pooled purified sample, the sample was aliquoted and flash frozen at -80 °C for long term storage.

** Supernatant was saved in a clean container, if ribosomes did not appear to pellet

Selective Depletion of Ribosomal Protein L12

70S proteins were selectively depleted by addition of $His_{(6)}$-tagged 70S to 250 µL of 2x L12 depletion buffer and a volume of water dependent on the concentration of 70S used in a 1 mL high density polycarbonate micro ultracentrifuge tube; the final concentration of 70S should be 450 pmol/mL 70S ribosome. This step was followed by mixture of 225 µL of 0 °C 100% ethanol

followed by shaking at 800 rpm for 5 minutes. This ethanol addition was repeated, the sample was immediately centrifuged in a Sorvall Micro Ultracentrifuge at 250,000 xg for 30 min at 4 °C in a S140 AT micro ultracentrifuge rotor (Sorvall). The resulting ribosome pellets were rinsed with 50 µL JE28 storage buffer, and then resuspended in 100 µL of JE28 storage buffer overnight. The resuspended depleted ribosomes were then loaded into a AKTAPrime FPLC pre equilibrated with JE28 Lysis buffer, and subsequently flowed over a 1 mL Ni-NTA IMAC column (GE Biosciences). The flow through was collected in 0.5 mL fractions using a fractionator. Collected fractions corresponding to the UV peak present on the FPLC chromatogram were spun at 250,000 xg for 1 hour at 4 °C. Final pellets were resuspended in 50 to 100 µL of JE28 Storage buffer overnight. Concentration was taken by UV-Vis spectroscopy at 260 nm and 280 nm, followed by flash freezing in liquid nitrogen for storage at -80 °C

Expression and Purification of trGTPases

GTPase Overexpression

Overexpression of GTPases followed a similar procedure to expression of JE28 ribosomes. BL21 cells are grown overnight in 10 mL of Kan^{35} LB, followed by inoculation of 6 x 1 L of Kan^{35} LB with the overnight 10 mL growths. When the OD_{600} reaches a range of 0.4 to 0.6 absorbance units, the incubator was set from 12.5 to 18 °C, and overexpression was induced with 400 µM isopropyl-β-D-thiogalactopyranoside (IPTG). Overexpression proceeded overnight, and the resulting cell pellets are harvested in an identical manner to JE28 cell cultures.

Immobilized Metal Affinity Chromatography Purification of GTPases

GTPase purification was a similar procedure to IMAC ribosome purification. GTPase lysis, wash, and elution buffers replace JE28 buffers of the same name. Cell lysis procedures were the same for JE28 lysis, although addition of DNase I is unnecessary. During IMAC, the GTPase

lysate was incubated with an IMAC resin (Ni-NTA or TALON) or allowed to flow over resin with intermittent resuspension to ensure proper mixing and binding of his-tagged proteins. Dialysis and storage buffers were equivalent for GTPase purification. Similar to JE28 purifications, SDS-PAGE samples were collected in 18 µL volumes at the lysed, clarified lysate, flow-through, wash, elution, and dialysis stages of column purification. The dialyzed eluent was placed in a Millipore Amicon Ultra spin concentrator of appropriate MWCO and concentrated to a concentration suitable for refinement purification or storage. Refinement purifications were performed using anion exchange column (AEC) chromatography on an AktaPrime FPLC. Concentration was observed using a Take3 plate on a BioTek Epoch spectrometer, using absorbances at 260 nm and 280 nm to obtain mg/ml protein concentrations. The final concentrated protein was aliquoted into sterile microcentrifuge tubes and flash frozen for storage at -80 °C.

Preparation of Ribosomal Protein L12 C-Terminal Domain Mutants

Site Directed Mutagenesis of L12

Based on previous work completed by Amanda Weis, site-directed mutagenesis (SDM) of the L12 C-terminal domain were made to full WT L12 Plasmid with oligonucleotide primers designed via the Agilent Technologies website and purchased from Integrated DNA technologies. Mutagenesis was performed with a QuikChange Lighting Site-Directed Mutagenesis Kit (Agilent Technologies). SDM reactions contained ddH_2O, 125 ng of both the forward and reverse primer, 50 ng of the double stranded template WT L12 plasmid, 1 µL of dNTP, 5 µL of 10X Quick Change Lightning Buffer, 1.5 µL of Quick solution reagent, and 1 µL of Quik Change Lightning Enzyme added immediately before polymerase chain reaction (PCR) cycles occurred. The PCR thermocycling process occurred as follows: 95 °C for 2 minutes to

allow for denaturation of the template DNA strand, followed by 18 cycles of denaturation at 95 °C for 20 seconds, annealing at 60 °C for 10 seconds, extension at 68 °C for 3.5 minutes. After the final cycle's extension step Dpn I restriction enzyme was added to digest methylated DNA from the template plasmid and allowed to incubate for 5 min at 37 °C. The DpnI treated reactions were then stored at -20 °C for future use.

L12 Mutant DNA Extraction for Sequencing

L12 Mutant extraction was performed via manufacturer's instructions with a Qiagen QIAprep® MiniPrep Kit. Cell stocks were prepared from the Xhol 10 Gold Ultra competent cells for DNA extraction, these cell stocks were spun into 2 mL pellets and in a microfuge tube. Pelleted cells were resuspended in Buffer P1. 250 µL Buffer P2 was added to the cell mixture and mixed by inversion 5 times to lyse the given cell pellet, Lyseblue reagent had been added to Buffer P2, so lysate appeared blue in color. Then 350 µL Buffer N3 was added and mixed by inversion 5 times, this caused Lyseblue reagent to turn colorless. The lysate was then centrifuged at 17,000 x g in a table top microcentrifuge (Sorvall) for 10 minutes. Supernatant from this spin was transferred to QIAprep spin column and spun at 17,000 xg for 60 seconds. The column was then washed with 0.5 mL of Buffer PB and spun at 17000 xg for 60 seconds., the flowthrough was discarded. The spin column was then washed with .75 mL Buffer PE and centrifuged for another 60 seconds. The flowthrough was discarded and the spin column was spun again to remove residual Buffer PE. The spin column was transferred into a clean microcentrifuge tube and the DNA was eluted by addition of 50 µL of Buffer EB to the center of the column, after waiting 60 seconds, the column was spun for 60 seconds at 17,000 xg. The extracted DNA concentration was measured using a nanodrop (Take3), and was used for BL21 transformations and sent to Nevada Genomics Center for sequencing.

L12 Transformation and Overexpression

Transformation of mutated L12 plasmids was accomplished using BL21 competent cells. These cells were removed from -80 °C storage and allowed to thaw for 10 to 20 minutes on ice. The thawed BL21 cells were then aliquoted into pre-chilled 14 mL round bottom falcon tubes in 50 to 100 µL portions with 1 negative control for each aliquot of competent cells used. To ensure transformation, 250 ng of each mutant plasmid was added to non-control cell mixtures and the reactions were allowed to sit on ice for 30 minutes. The transformation reaction was heat shocked at 42 °C for 55 seconds and placed on ice for another 2 to 3 minutes. Sterile, untreated LB or SOC was added to the falcon tube for a final volume of 1 mL and grown at 37 °C for 1 hour. Sterilized LB agar culture plates treated with 35 mg/ml of Kanamycin were placed in an ethanol sterilized fumehood. Plates were labeled by volume and indicated as control or non-control. The outgrowth competent cells were added to the Kan^{35} LB agar plates in decreasing volumes (e.g. 400, 300, 200, and 100 µL increments.) that were spread with an ethanol sterilized glass spreader. Cells were placed in a 37 °C incubator and allowed to grow overnight. Single colonies were selected and placed into sterile Kan^{35} treated 10 mL LB tubes and grown to mid-log phase (an OD_{600} of 0.4 to 0.6). These colonies were then spun down at 4000xg in a microtube centrifuge for 5 minutes. This process was repeated until a considerable cell pellet formed at the bottom of the microcentrifuge tube. This cell pellet was resuspended in 1 mL of bacterial growth and mixed with 50% glycerol then flash frozen for future use. Overexpression of L12 mutants was performed identically to GTPase overexpression, with varied growth times.

L12 Purification

L12 Purification was completed using identical methodology to GTPase IMAC purification with an added denaturation step. During cell lysis GTPase buffers were prepared with 7M urea to ensure the denaturation of endogenous GTPases that interact with L12 in the cell.

Functional Assays of Protein-Protein interactions

PiColor Gold Phosphate Release Activity Assay

The PiColor Lock Gold Phosphate release detection system was utilized to assess the effects of argyrin B and L12 CTD mutants on GTPase activity. The assay was performed in 96 well plates with reaction volumes of 50 µL. The reaction solutions were prepared in by addition of 10 µL of 5X M20 or MG buffer to ddH_2O. Ribosomes, GTPases and other reagents were added and allowed to incubate for 10 to 15 minutes at room temperature. GTP was added to reaction mixtures to reach a final concentration of 25 µM and incubated for 10 minutes. Incubation time for GTP addition was optimized by Amanda Weis to be within the range of 8 to 12 minutes. After the GTP reacted 12.5 µL (or ¼ of the reaction volume) of PiColor Lock Reagent was added to quench the reaction. Reaction quencher was prepared per manufacturer's instructions with a ratio of 1:100 accelerant to PiColor Lock Reagent. Stabilizer was added 5 minutes after the reaction was quenched. The absorbance at 635 nm was collected on a Biotek Synergy Spectrometer after 1.5 hours. To ensure accurate absorbance values the reaction plates were gently shaken to allow precipitated dye to dissolve back into solution.

Gel Filtration Binding Assay

Binding Reactions were performed in final volumes of 50 µL and incubated for 10 minutes at 37 °C for 10 to 15 minutes. M20 Buffer was added to a pre-calculated volume of ddH_2O, followed by ribosomes, GTPases, and other reagents. Reactions incubated for 10 to 15 minutes at 37 °C

while final column prep occurred. The gel filtration binding assay was carried out using Sephadex 300 fast flow size exclusion resin. Resin was equilibrated in Pierce Centrifuge columns with a minimum of 3 column volumes of ddH_2O, 3 column volumes of 1x M20 Buffer, and a final 500 µL rinse of 1x M20 buffer with non-protein reagents present in the specific reaction. Following the final equilibration step, the columns were placed into clean sterile collection tubes and the 50 µL reaction mixture was pipetted directly onto the center of the resin bed and centrifuged at 2000x g for 2 minutes. Immediately following centrifugation, centrifuge columns were removed, and reaction eluent was transferred to labeled microcentrifuge tubes for acetone precipitation.

Sucrose Cushion Binding Assay

To corroborate binding effects observed in the Gel Filtration Binding assays, sucrose cushion binding assays were performed with a Sorvall Micro-Ultracentrifuge. Both an AT-140 and an ST-120 rotor were used with high density poly-carbonate (PC) tubes of 1 mL or 0.5 mL for each rotor. The 12.5% sucrose M20 solution was syringe filtered through a sterile 0.2 µm filter. Binding reactions were prepared identically to Gel Filtration assay. Volumes of 500 µL or 250 µL were added to the 1 ml or 0.5 ml PC tubes respectively. The 50 µL reactions were carefully pipetted on top of the sucrose solution. The tubes were then spun at 250,000xg for 12 minutes at 4 ℃. The centrifuged solution was separated into a “supernatant” and “pellet” portion, with the top 60% of the solution considered the supernatant and the bottom 40% considered the pellet. These two portions were added to microtubes for acetone precipitation.

Acetone Precipitation for SDS-PAGE analysis

Acetone precipitation was performed to prepare binding assay results for analysis by SDS-PAGE. The reaction samples had a 5X volume of -20 °C acetone added to each reaction tube. These were left at -20 °C for at least 1 hour and then spun down at 13000xg for 30 min at 4 °C. The acetone was carefully pipetted off the resulting pellet and remaining acetone evaporated from the denatured pellet at room temperature. These pellets were resuspended in 12 µL of water or buffer for 2 to 3 hours with gentle shaking or overnight without shaking. Resuspension was followed by addition of 4X SDS-PAGE Loading dye.

SDS-Polyacrylamide and Native Gel Electrophoresis

SDS-PAGE was used to verify protein purity and molecular weight. Gels were constructed using a 12.5% 19:1 Bis-acrylamide solution prepared with Tris-HCl pH 8.8. The 1.5X stacking solution was poured after resolving gel polymerization. 4X SDS PAGE Dye was added to SDS PAGE samples in labeled microcentrifuge tubes, followed by heat denaturation at 95 °C for 5 minutes. The gel was then placed in the electrophoresis chamber and the samples were loaded into the stacking layer lanes. Before running, 10 µL of Spectra Broad Range Molecular Weight Standards (ThermoFisher) were loaded into a single lane, and the gel was run at 90 to 110 V.

Native Gels were prepared by addition of agarose to the SDS-PAGE recipes. Gels were loaded and run without MW standards at 4 °C at 50 V.

Bio-Layer Interferometry Binding Assay

The Bio-Layer Interferometry binding assay was carried out on a BLItz (ForteBio) instrument using BLI tips coated with HIS2 $His_{(6)}$-tag affinity antibodies (ForteBio). All procedures were carried out using a 30 second initial baseline, followed by the 120 to 180 second loading phase of

the His-tagged protein, a secondary 30 second baseline allowed any unbound protein to dissociate, then a 120 to 180 second association phase which measured protein-protein interactions with the tip bound protein, and finally a dissociation phase allowed unbound protein to dissociate. All experiments were carried out in Rayleigh Light Scattering Buffer to minimize interference of small molecules with the light scattering properties required for accurate BLI measurements. DMSO background corrections were obtained at 1%, 3%, 5%, and 7% (v/v) concentrations.

Equilibrium Fluorescence Guanine Nucleotide Binding Assay

To assess the effects of argyrin B on the binding affinity of EF-G to GTP and GTP analogues steady state fluorimetry was performed using a PTI Fluorimeter. Fluorescence response was measured using an excitation wavelength of 280 nm to measure endogenous tryptophan fluorescence, emission fluorescence was measured by observing a wavelength range of 300-350 nm, with an expected peak intensity at 340 nm. The binding of GDPNP would result in the quenching of EF-G's 280 nm fluorescence via conformational rearrangement. Spectra were obtained at room temperature (20- 25 °C) in a 2 mL quartz cuvette with excitation slit widths and emission slit widths at 2 nm. In order to observe the effect of argyrin B on equilibrium binding, two solutions were prepared, Solution A and B. Solution A contained µM EF-G and µM argyrin B, Solution B contained µM EF-G µM argyrin B and 1000 µM GDPNP. In order to titrate increasing concentrations of GDPNP, an equivalent volume of solution B was removed from solution A prior to solution B addition. All control experiments were conducted without argyrin B present in solution.

Single Round Translocation Endpoint Fluorescence Assay

Work previously accomplished by Justin Walter, demonstrated that single round translocation can be reliably observed with use of a fluorescent tag on a short mRNA sequence. Our single round translocation assay utilized the fluorescence excitation and emission of a chemically appended 5-hydroxyfluoroscein to the 3' terminus of the nucleotide. Fluorescence after successful translocation was quenched due to steric obstruction of the fluorescent tag via movement toward the ribosome Figure 4-1. Reactions were made with a final volume of 100 µL to ensure signal accuracy. PRE and POST translocational complexes were prepared by dilution of ribosomes and each nucleotide to concentrations of 0.18 µM 70S ribosomes, 0.2 µM $tRNA^{fMet}$, 0.2 µM $tRNA^{Phe}$, and 0.2 µM fluorescent mRNA. PRE translocation ribosomes were incubated with fluorescent mRNA and $tRNA^{fMet}$ at 37 °C for 10 minutes, followed by a second 10-minute incubation with $tRNA^{Phe}$ at 37 °C. POST-translocation ribosomes were incubated with fluorescent mRNA and $tRNA^{Phe}$ for 10 minutes at 37 °C. After the complexes were formed, EF-G and GTP were added to both PRE and POST- translocation ribosomes to catalyze translocation. If argyrin B was added, the drug was incubated in the EF-G•GTP addition step. Translocation was observed by quenching of 5-hydroxyfluorescein fluorescence relative to a

untranslocated control and a 2-3 nm shift in peak emission fluorescence.

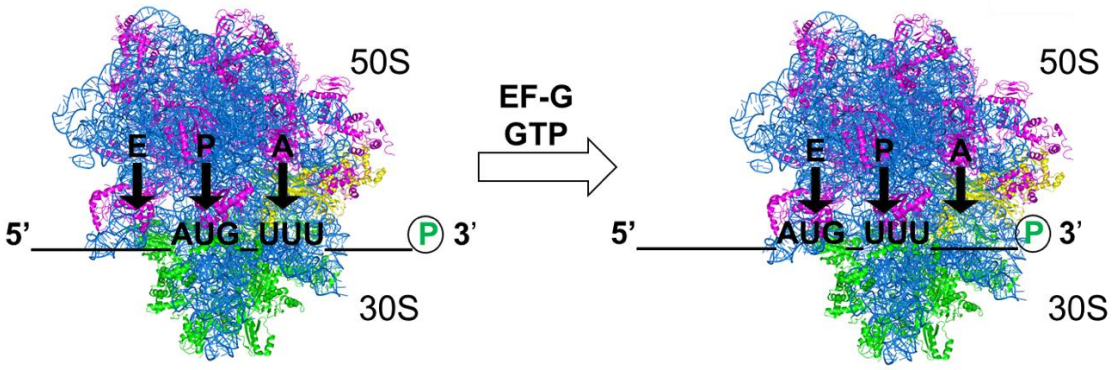

Figure 4-1. Single Round Translocation Assay Schematic. Fluorescence of the 5-hydroxyfluoroscein is quenched as the fluorescein-tagged nucleotide is translated by the ribosome. (PDB ID: 4W29)

Rayleigh Light Scattering

Rayleigh light scattering was employed to measure the extent of ribosome dissociation. Because of the ribosome's size when the two subunits dissociate there is a characteristic decrease in light scattering intensity. Rayleigh light scattering was observed over a 10-minute time course with a quartz 180 µL microcuvette and microcuvette adaptor in a PTI Fluorimeter. Excitation and emission wavelengths of 436 nm were utilized with uniform excitation and emission slit widths of 0.6 nm. To assess the extent of ribosomal dissociation in the presence of different translation factors 0.5 µM 70S ribosomes were added to solutions that contained 1 µM EF-G, 4.5 µM IF3, 250 µM GTP and concentrations of 1 µM, 3 µM, or 20 µM RRF to a final volume of 150 µL. The two solutions were prepared separately and incubated for 10 min at 37 °C in Rayleigh light scattering buffer in sterile microcentrifuge tubes, which were subsequently centrifuged at 17000 x g for 3 min to remove any free-floating small particles in solution. Following centrifugation, the solution containing the protein cofactors was placed into a clean cuvette. Relative controls of

1mM and 10mM Mg^{2+} Rayleigh Light Scattering buffers served as a measurement of full dissociation or association respectively.

In vitro Translation Assay

The effect of argyrin B on translation was assessed with the PURExpress *In vitro* Translation Assay (New England Biolabs). This assay was performed per manufacturer's instructions. 10 µL of Solution A and 7.5 µL of Solution B were pipetted into a 50 µL reaction tube. The following reactions were performed using two different plasmids, a control plasmid (DHFR) and a experimental Plasmid for Green Fluorescent Protein (GFP) added at 250 ng and 358 ng respectively. There were five reactions performed as follows: Without DNA added, DHFR control DNA added, DHFR control DNA and argyrin B added, GFP DNA added, and finally GFP DNA added with argyrin B. Reactions were filled to 25 µL with nuclease free water and incubated at 37 °C for 2 to 4 hours. The results were analyzed with non-denaturing Native PAGE and denaturing SDS-PAGE conditions.

Chapter 5. Results

EF-G Expression and Purification

EF-G was expressed and purified with BL21 *E. coli* cells, which are optimized for protein expression. *E. coli* EF-G was transformed by Amanda Weis. The IMAC and IEC purification of the EF-G derivatives were visualized via SDS-PAGE gel electrophoresis for purity. Their concentrations were ascertained via UV-Vis absorption at 280 and 260 nm with a reference wavelength of 495 nm on a BioTek Epoch Plate Reader.

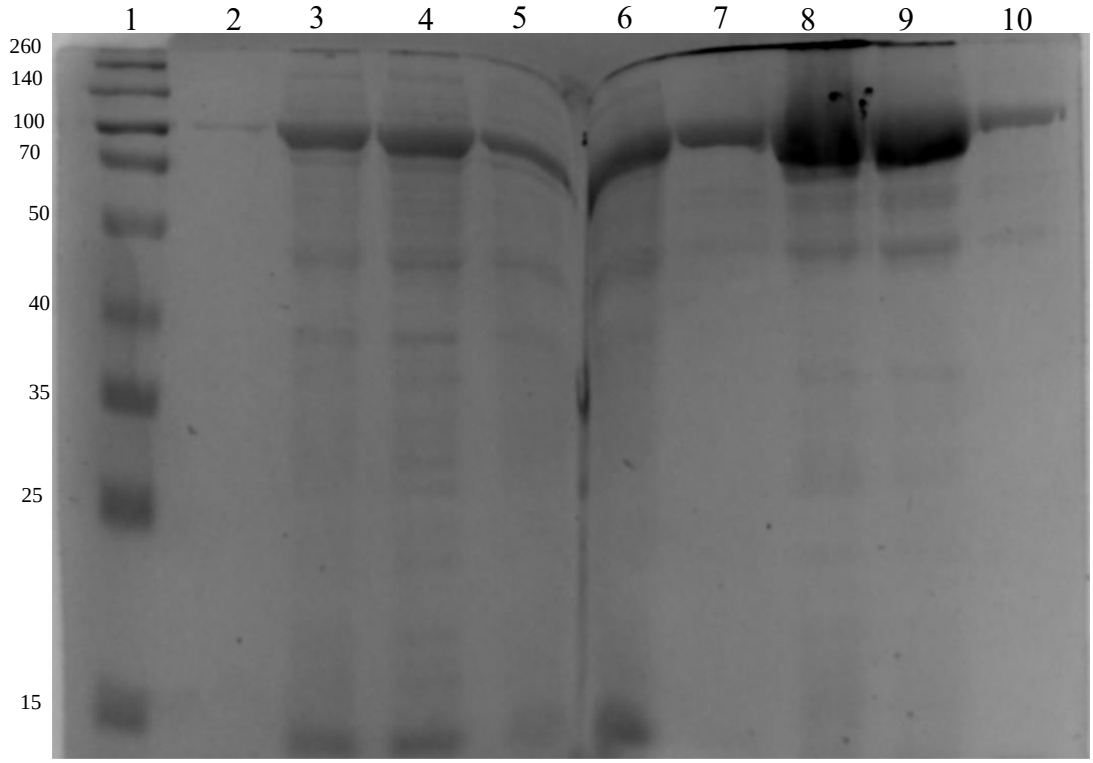

Figure 5-1. SDS-PAGE of IMAC and AEC EF-G Purification. Lane 1: Molecular Weight Standards, Lane 2: EF-G Standard, Lane 3: Cell Lysate, Lane 4: HSSN, Lane 5: IMAC Flowthrough, Lane 6: IMAC Wash, Lane 7: IMAC Wash 2, Lane 8: Dialyzed Eluent, Lane 9: Pre AEC, Lane 10: Post AEC

Purification of 70S Ribosomes

70S Ribosomes were purified successfully using a combination of IMAC Chromatography and ultracentrifugation. The 70S ribosomes were shown to pure via SDS-PAGE (Figure 5-2) and active within GTPase activity assays and binding assays with translational GTPases (Figure 5-4 and 5-6).

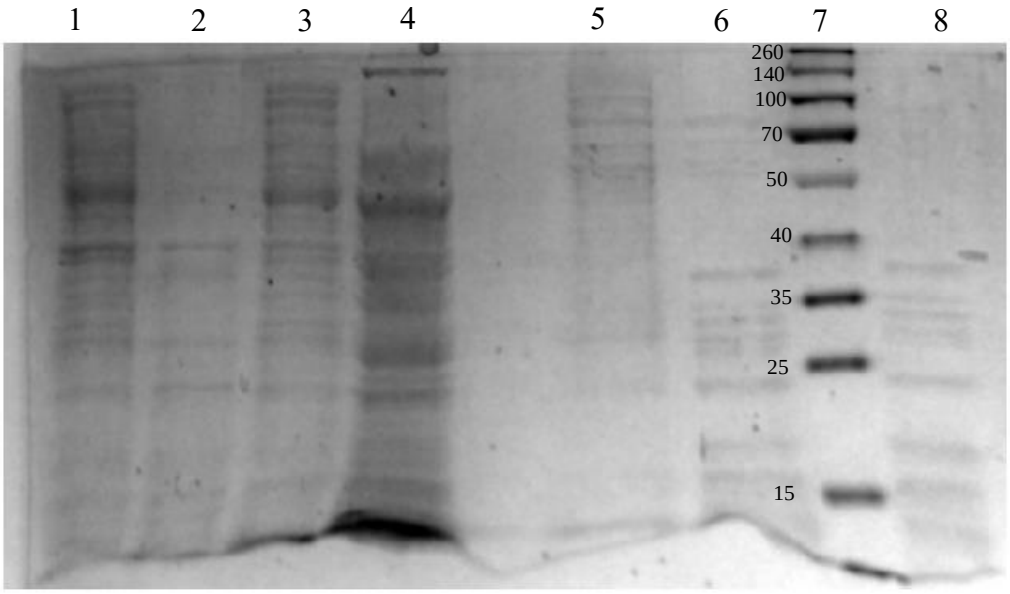

Figure 5-2. SDS-PAGE of IMAC Ribosome Purification. Lane 1: Cell lysate, Lane 2: HSSN, Lane 3: Filtered HSSN, Lane 4: IMAC Flowthrough, Lane 5: IMAC Wash, Lane 6: Dialyzed Eluent, Lane 7: Molecular Weight Standards, Lane 8: 70S ribosomes post-ultracentrifugation

The ribosome IMAC purification process showed that significant amounts of 70S were present at each stage prior to application to the IMAC column (Lanes 1-3, Figure 5-1). It is important to note that a significant concentration of 70S complexes or similar molecular weight proteins were present in the IMAC flowthrough but not the IMAC wash step (Lanes 4 and 5, Figure 5-1). This indicated that the $His_{(6)}$-tagged ribosomes successfully bound to the IMAC resin. Finally, a faint band was observed in the dialyzed eluent that indicated a ~100 kDa MW protein was present; which was presumed to be EF-G. Upon two rounds of ultracentrifugation and appropriate washing steps this faint band disappeared (Lanes 6 and 8, Figure 5-2)

Argyrin B inhibits translation

In order to verify that EF-G acts on translation as its mode of action as an antibiotic we performed an *In vitro* translation assay to observe argyrin B's effect on translation.

Reproduction of experiments performed by Amanda Weis have shown that argyrin B has an inhibitory effect on the overall process of translation. Previous SDS-PAGE results (Figure 5-3 A) showed no translation when no DNA was added. Translation occurred when the control plasmid for DHFR was added, however when argyrin B was added alongside the control plasmid translation was almost completely inhibited. GFP translation was unsuccessful in the represented figure but was successful in later trial. Argyrin B is not soluble in water and therefore was dissolved in DMSO. In order to ensure that the DMSO was not the cause of the inhibitory effect, the control plasmid was added to a translation reaction with 3% DMSO. The DMSO control showed that DMSO was not responsible for the inhibition of translation because DHFR was translated successfully. Repetitions of the GFP and DHFR trials plus and minus argyrin B demonstrated that the presence of argyrin B inhibited the translation of GFP in a Native PAGE gel (Figure 5-3 B). The GFP plasmid is present in Lane 5, argyrin B was added alongside the GFP plasmid in Lane 6. The Native PAGE gel was exposed to 395 nm light and the emission fluorescence at 509 nm.

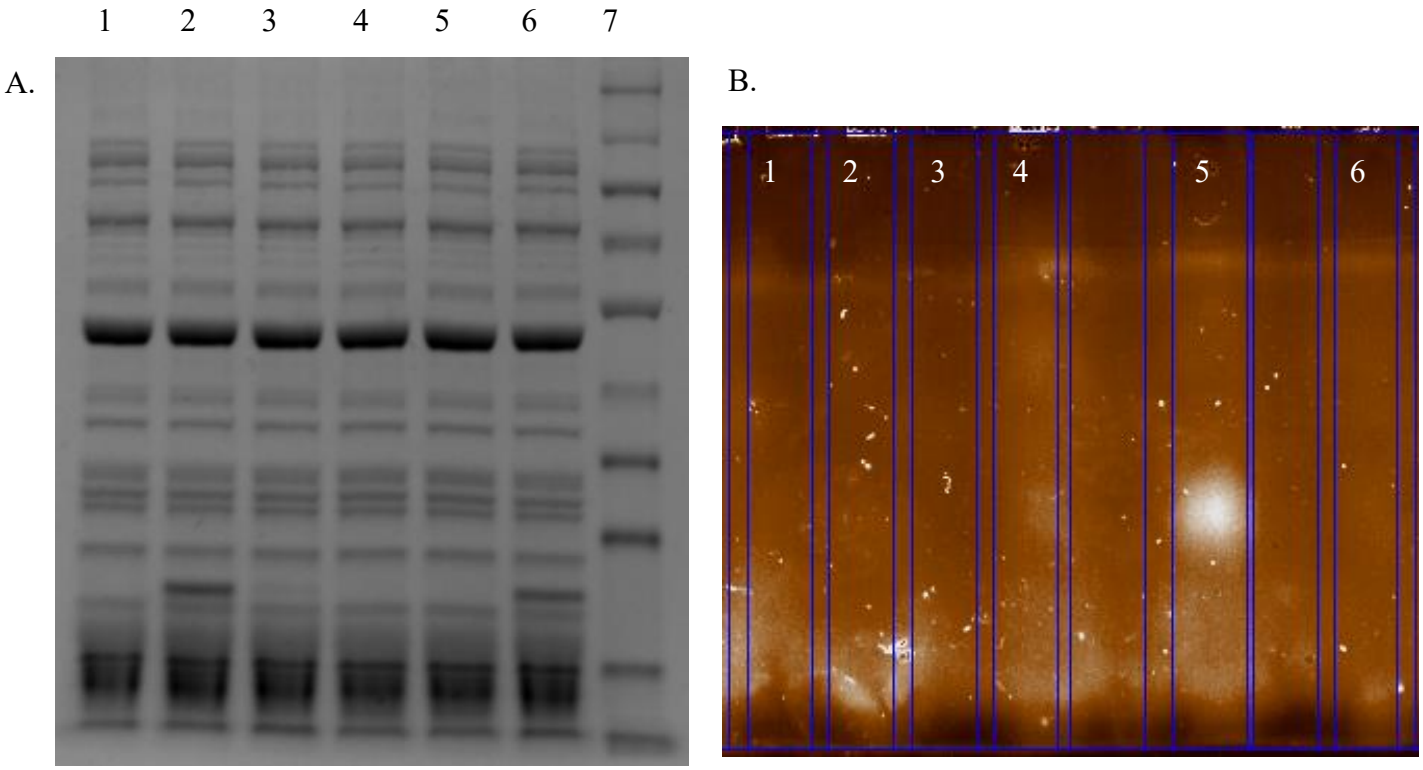

Figure 5-3. Inhibition of translation visualized via SDS and Native PAGE.

A.SDS PAGE of *In vitro* translation assay Lane 1: No DNA, Lane 2: DHFR Control, Lane 3:, DHFR + Arg B Lane 4: GFP plasmid, Lane 5: GFP + Arg B, Lane 6: DHFR + DMSO control Lane 7: Molecular Weight Standards

B. Native PAGE of *In vitro* translation assay Lane 1: No DNA Lane 2:, DHFR Control, Lane 3: DHFR + Arg B Lane 4: BSA Lane 5: GFP Lane 6: GFP + Arg B. Gel was exposed with an excitation wavelength of 390 nm and fluorescence emission of GFP was measured at 522 nm

Argyrin B decreases GTPase activity in EF-G in the presence of RRF

Argyrin B showed an almost uniform decrease in EF-G-catalyzed GTP cleavage. EF-G was exposed to both vacant 70S and post-termination complexes in the presence and absence of argyrin B to measure the inorganic phosphate release. These experiments were explored further by addition of increasing concentrations of RRF. When RRF was added to EF-G and 70S there was a decrease of 20% activity, however this decrease is within one standard deviation of error from the mean. The exposure of vacant 70S ribosomes to EF-G•ArgB complexes and increasing amounts of RRF, showed a decrease of about 40% activity compared to the control reaction of 70S, EF-G and GTP (Figure 5-4). These results were compared to the same reactions applied to PoTCs(Figure 5-5). The PoTC showed a sharper decrease in activity if EF-G•ArgB complexes were present with increasing concentrations of RRF. The error present in these measurements

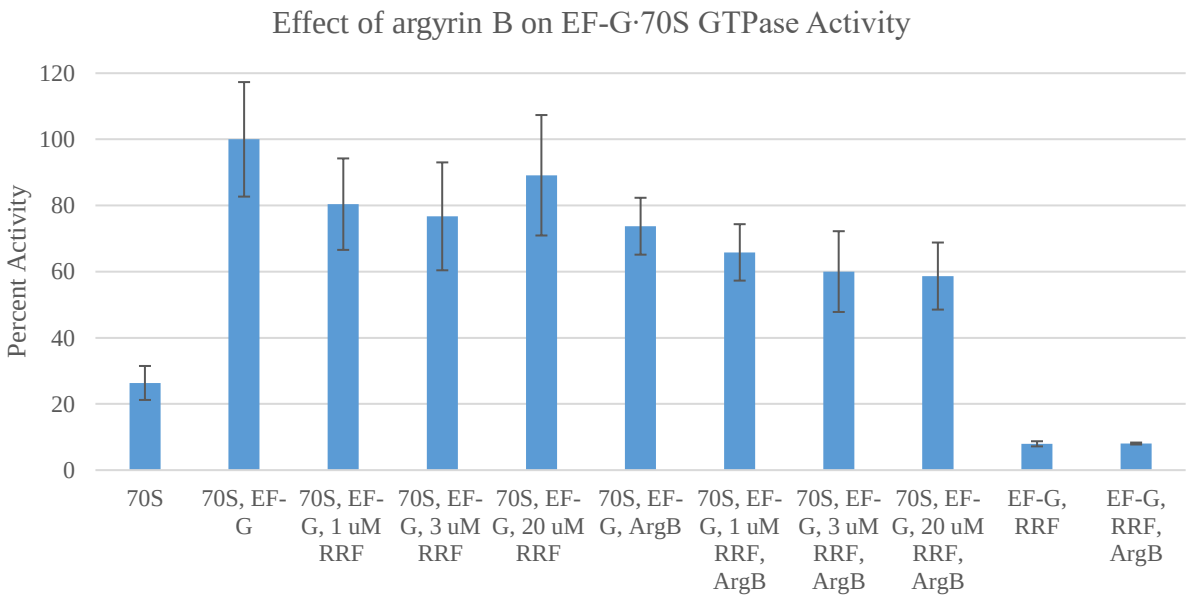

Figure 5-4. Effect of Argyrin B on EF-G to Vacant 70S GTPase Activity in the presence and absence of RRF. Experiments were performed in triplicate. All reactions contained 50 µM GTP. Error bars represent standard deviation from the mean.

were comparable to the vacant 70S trials. We also observed a similar 20% decrease when EF-G•Argyrin B complexes were exposed to the PoTC. When RRF was added in increasing concentration to the PoTCs exposed to EF-G•argyrin B complexes we observed a concentration dependent response leading to what could correspond to background levels of absorbance. This result implied that argyrin B's effect on EF-G is dependent on EF-G's GTPase activity and the presence of RRF.

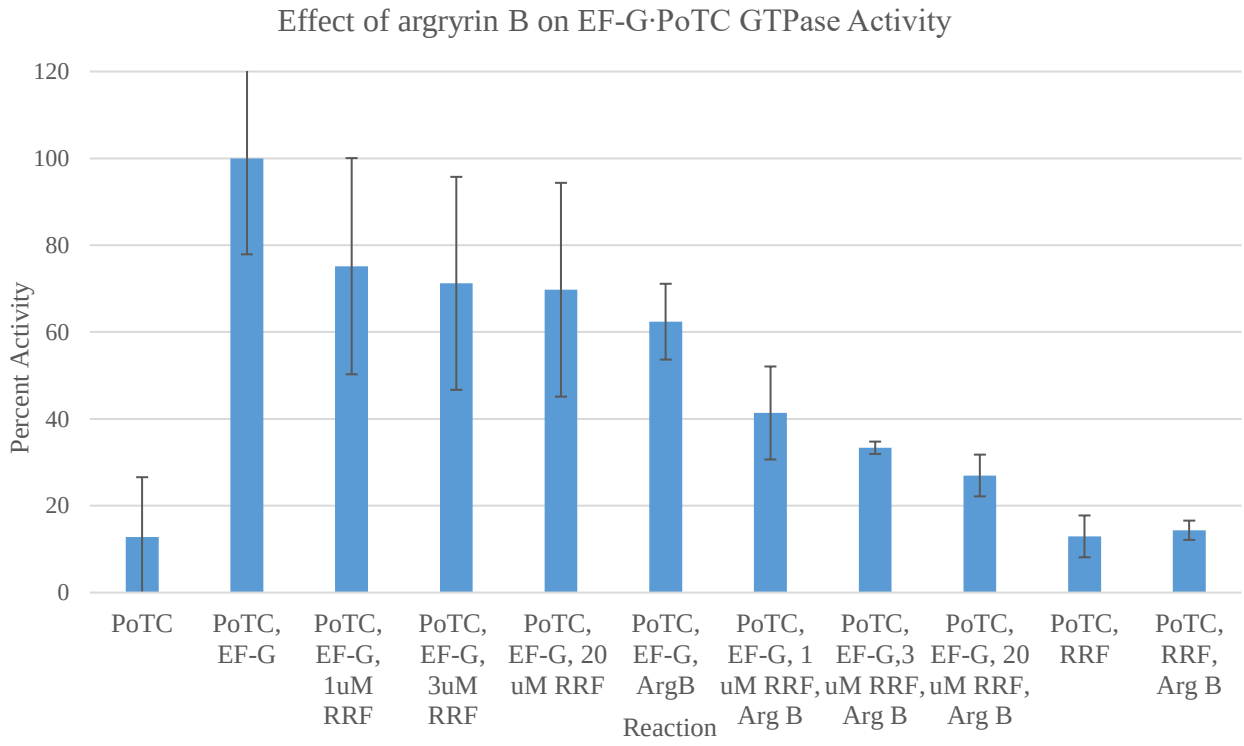

Figure 5-5. Effect of Argyrin B on EF-G to Post Termination Complex GTPase Activity in the presence and absence of RRF. All reactions contained 50 µM GTP All experiments were performed in triplicate. Error bars represent standard deviation from the mean.

Other translation factors that contained a G' domain, LepA and RF3 showed very little change in GTPase activity when exposed to argyrin B (Figure 5-6). Therefore EF-G was verified as the primary target of argyrin B in bacteria as referred to in literature (Nyfeler *et al.*, 2012).

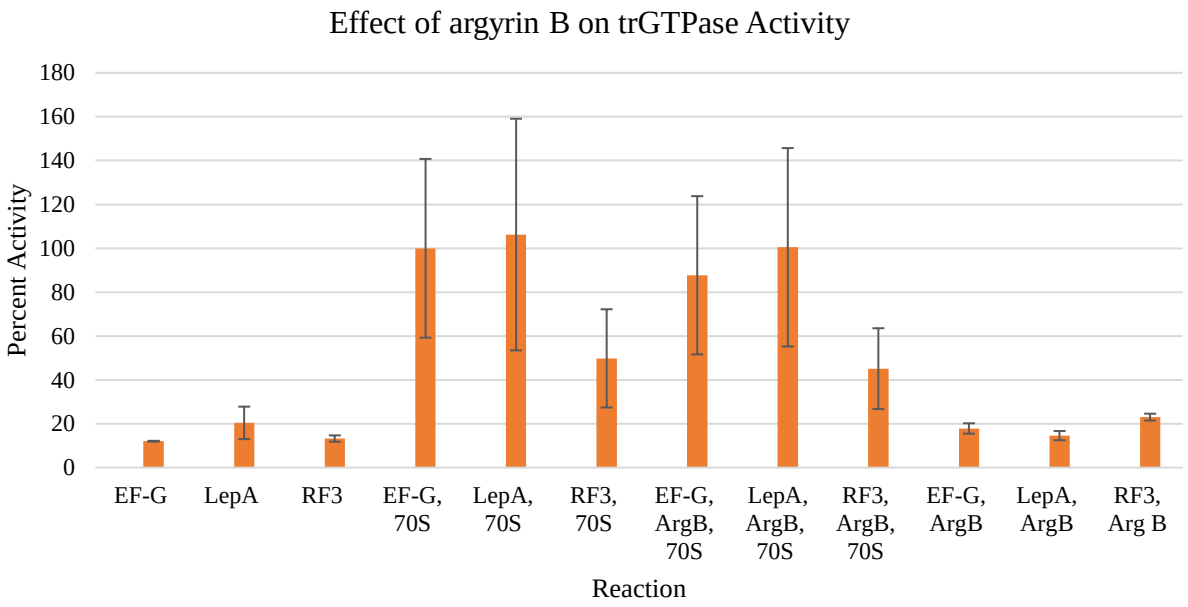

Figure 5-6. Effect of Argyrin B on Translational GTPases. Experiments were performed in triplicate, all reactions contained 50 µM GTP. Error bars represent 1 standard deviation from the mean.

Argyrin B does not stabilize binding to the 70S ribosome

Gel Filtration and sucrose cushion assays were performed to assess how EF-G's binding stability to the ribosome was influenced by argyrin B. We observed through these methods that the stability of EF-G binding was unchanged by the addition of argyrin B to vacant 70S ribosomes (Figure 5-7 and Figure 5-8).

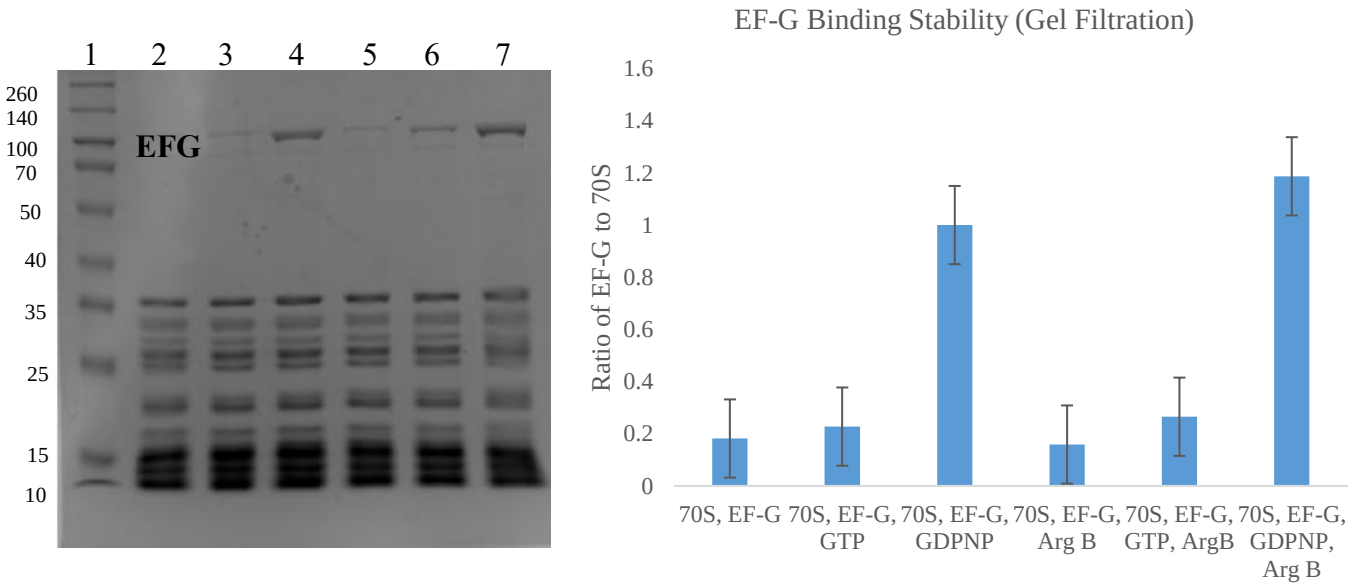

Figure 5-7. Effect of argyrin B on EF-G binding stability to Vacant 70S Complexes via Gel Filtration. Lane Assignments: Lane 1. Molecular Weight Standards; Lane 2. 70S, EF-G; Lane 3. 70S, EF-G, GTP; Lane 4. 70S, EF-G, GDPNP Lane 5. 70S, EF-G, Arg B; Lane 6. 70S, EF-G, GTP, Arg B; Lane 7. 70S, EF-G, GDPNP, Arg B. B. Binding stability of EF-G averages of four replicates, Error bars represent 1 standard deviation from the mean relative quantity of EF-G present on the gel.

The unaffected binding stability of EF-G to the ribosome agreed with prior work completed by our lab. WE observed that without a guanine nucleotide present there is a relative lack of stable binding of EF-G in absence of argyrin B, which was expected (Lane 2 and 5, Figure 5-6). When

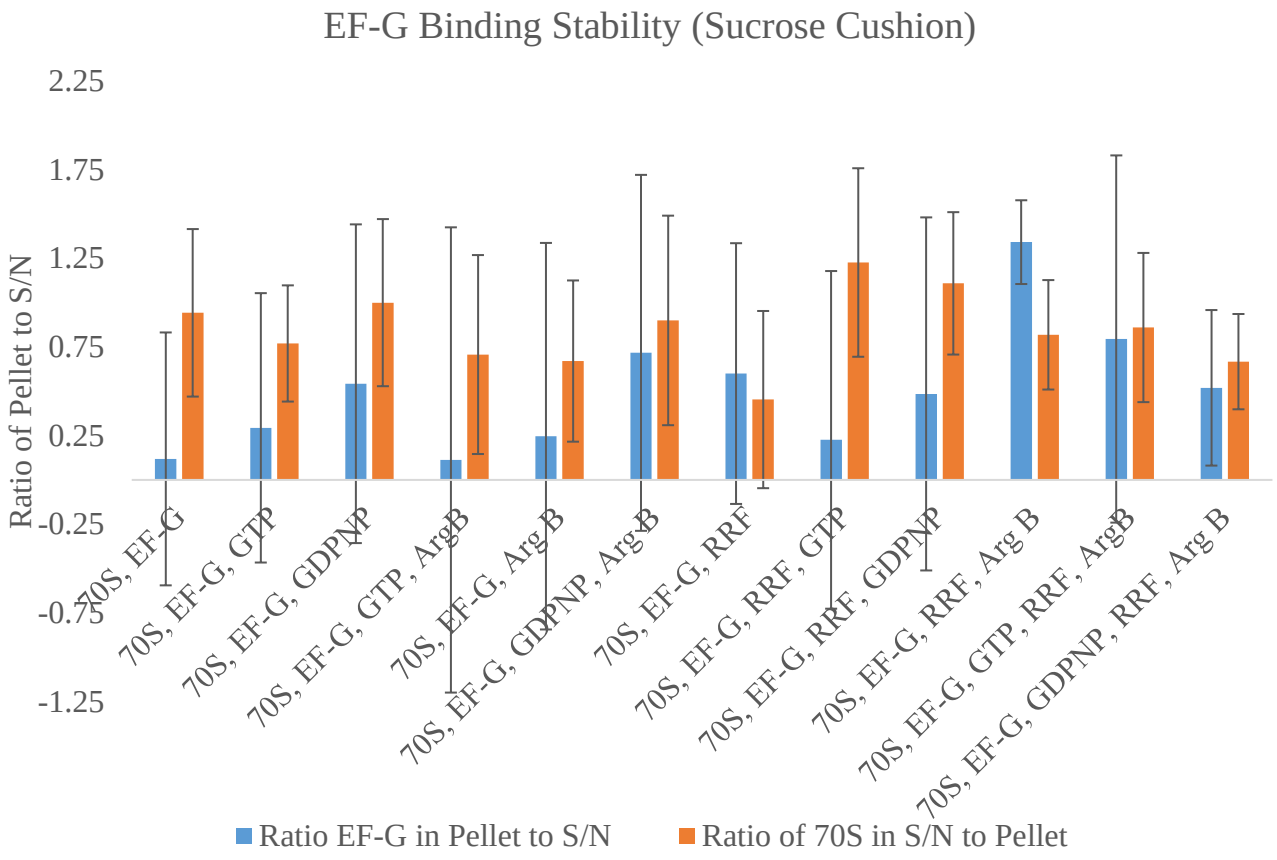

Figure 5-8. Effect of argyrin B on EF-G binding stability to Vacant 70S Complexes via Sucrose Cushion Assay. Binding stability of EF-G averages of three replicates, Error bars represent 1 standard deviation from the mean relative quantity of EF-G or 70S quantified on the gel with respect to 70S, EF-G, and GDPNP trials.

bind EF-G to the ribosome in a stable state because of the unhydrolyzable nitrogen-phosphate bond present between the β and γ phosphates. We observed a slight increase in binding when argyrin B was added (Lane 7, Figure 5-6). The results of our sucrose cushion assay showed high variability in the ratio of pellet bound EF-G to supernatant EF-G and the ratio of 70S in the supernatant to pelleted 70S (Figure 5-8).

We observed similar results to our gel filtration assay even with the high potential for error the observed EF-G ratios failed to demonstrate stable binding to 70S complexes with or without argyrin B (Reactions 1-6, Figure 5-8). We added stoichiometric equivalents of RRF to identical reaction conditions as reactions 1-6 to assess the effect of RRF on stable EF-G binding (Reactions 7-12 Figure 5-8). Reaction 10 showed relatively low error with respect to EF-G binding, however when subjected to a student's t-test against Reaction 7 it was shown to have a p-value of 0.301, indicative of a probability of 30% that the result occurred by chance.

Argyrin B inhibits Ribosome Dissociation in the presence of EF-G and RRF

Due to the major roles EF-G plays in ribosome recycling we performed Rayleigh light scattering experiments to probe the effects of argyrin B on ribosome recycling by observing the relative decrease intensity of the scattered light after the ribosome dissociated. Two positive controls were established for both full dissociation and association, based on previous work by Justin Walter. Ribosomes contain inter-subunit stabilizing interactions facilitated by Mg^{2+} ions: 70S ribosomes added to Rayleigh light scattering buffer that contained 10 mM Mg^{2+} remained fully associated, where 70S complexes exposed to buffer with only 1 mM Mg^{2+} have been shown to fully dissociate. This measure of dissociation was shown by a sharp exponential decrease in relative light scattering intensity. Full association was treated as a stable relative intensity with little change in signal. Upon addition of 70S ribosomes to EF-G, RRF, IF-3 and GTP, stable dissociation was consistently demonstrated. When argyrin B was present in an identical reaction solution there was an approximate 50% decrease in ribosome dissociation (Figure 5-7). This finding indicated that argyrin B inhibited EF-G facilitated ribosomal dissociation. The addition of GDPNP and GTP in equivalent amounts resulted in similar levels of dissociation of argyrin B.

When argyrin B is added in with equivalent concentrations GDPNP and GTP, the ribosomal complexes do not dissociate.

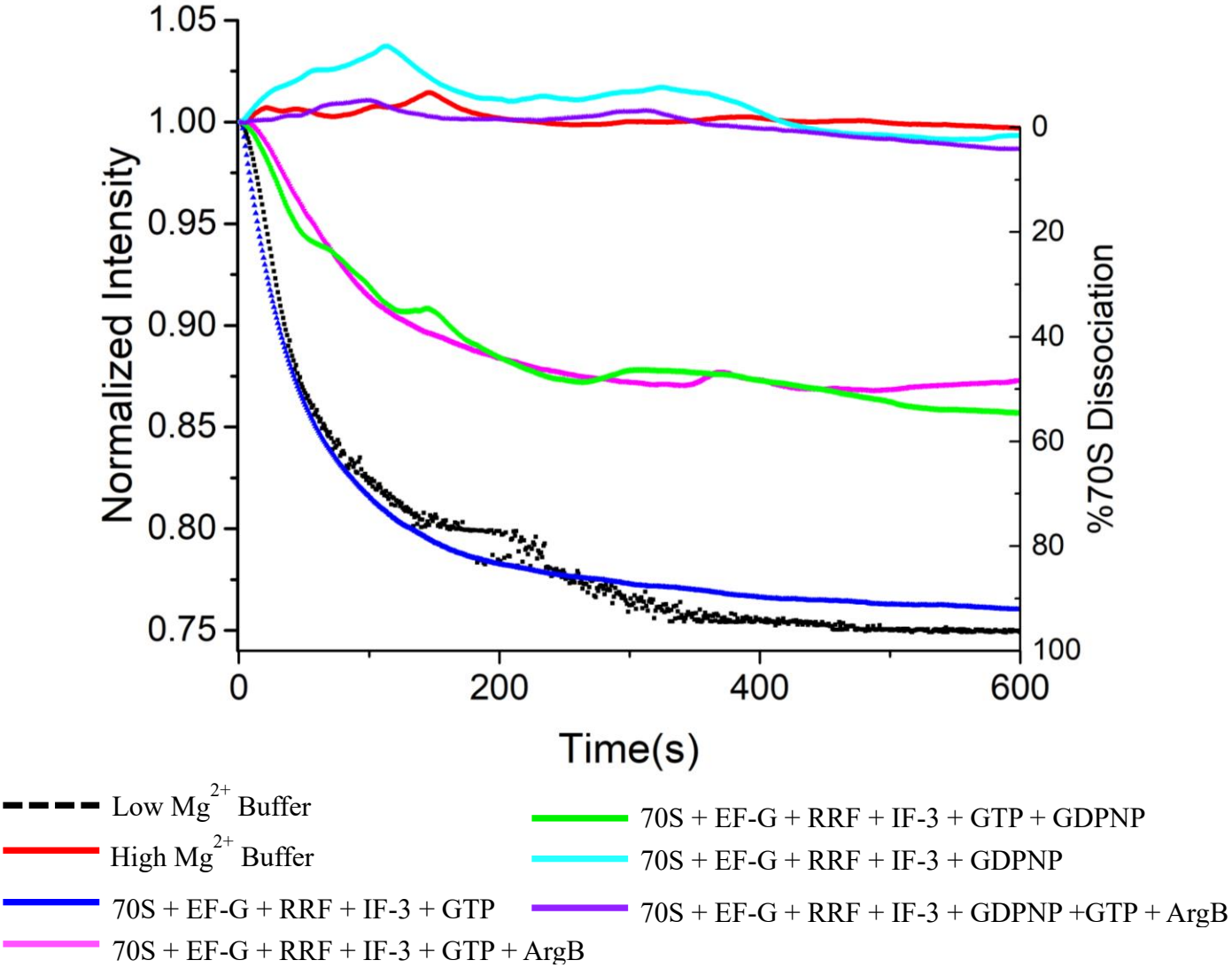

Figure 5-9. Effect of Argryrin B on Ribosome Recycling. Dissociation of 70S measured relative to dissociation of 70S in low Mg^{2+} buffer. 0.5 µM 70S was used with 1 µM EF-G and 1 µM RRF Intensity normalized to initial reading. 4.5 µM IF-3 was used to prevent 70S reassociation.

Translocation is not affected by argyrin B

In order to investigate the effect of argyrin B on EF-G's role in translocation, we employed a single round fluorescence assay (Figure 5-10). This assay was performed with a 5-hydroxyfluoroscein appended to the 3' end of a short mRNA sequence. This mRNA sequence contained a SD sequence followed by a codon for $tRNA^{Phe}$. EF-G allows for faster translocation of mRNA; on this principle we expected the fluorescence emission signal of PRE translocation complexes to be quenched relative to POST translocation complexes due to the movement of the fluorophore closer to the ribosome. From these measurements we determined that EF-G-catalyzed translocation was not changed by the presence of argyrin B. The PRE translocation complexes treated with only argyrin B showed similar fluorescence signal to the control PRE translocation complex. When argyrin B was incubated with EF-G•GTP prior to addition, the relative decrease in fluorescence that occurred demonstrated the formation of POST translocation complexes. To verify this finding, the addition of Phe-$tRNA^{Phe}$ without fMet-$tRNA^{fMet}$ was added to 70S and the fluorescent mRNA. Phe-$tRNA^{Phe}$ will bind to the P site of the ribosome in the absence of fMet-$tRNA^{fMet}$, which provided similar fluorescence signal to POST termination complexes Upon incubation of 70S with Phe-$tRNA^{Phe}$ we observed a relative decrease in fluorescence that indicated that the fluorophore was in the same position as a POST translocation, the addition of argyrin B decreased fluorescence further . Interestingly we did not observe an expected 2 nm blue shift in emission maxima. This evidence indicated that argyrin B does not have an observable effect on the process of translocation and therefore the mechanism of action of argyrin B is not directly connected to EF-G's role in translocation.

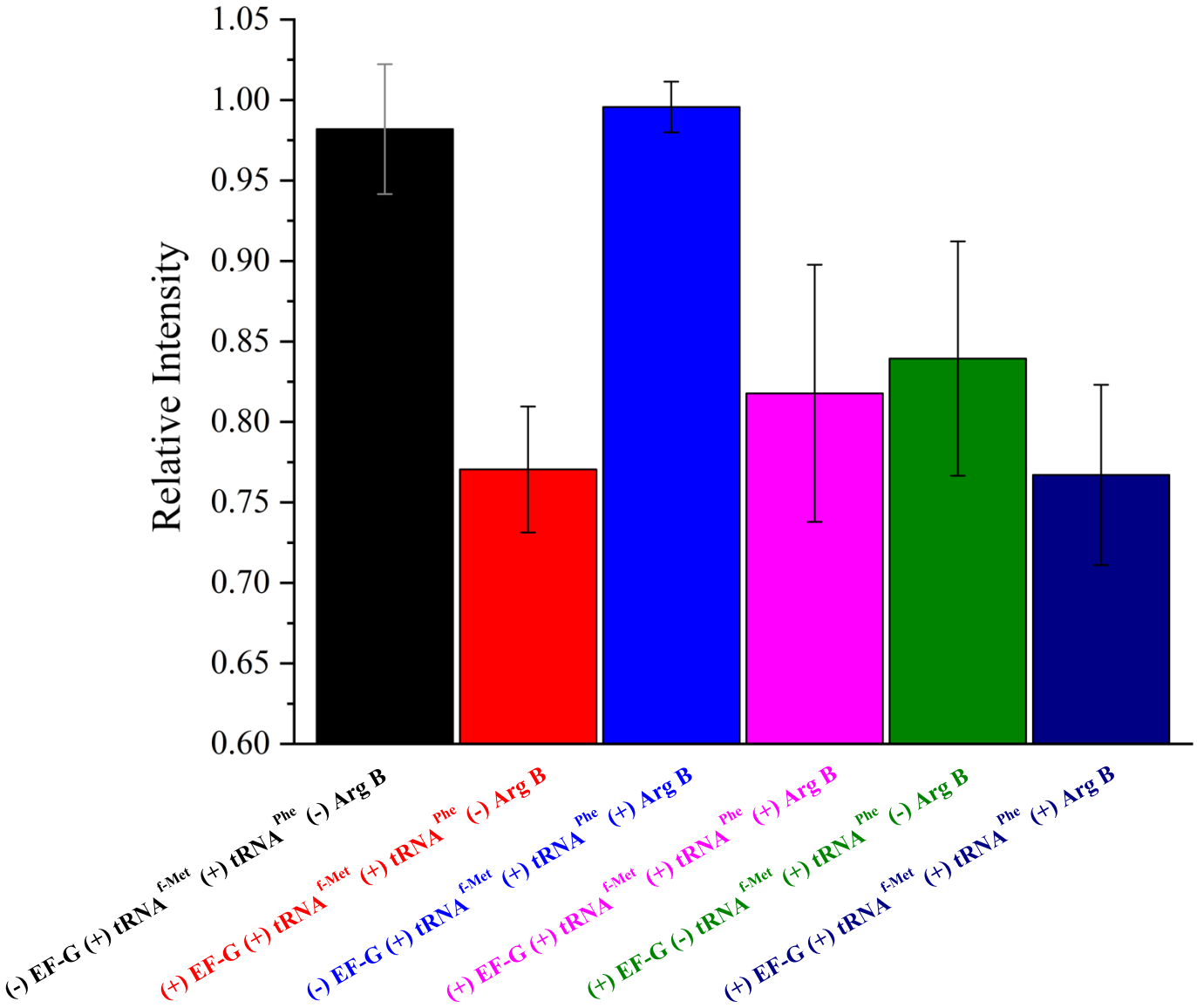

Figure 5-10. Effect of argyrin B on Single-round Translocation. Fluorescence emission intensity was obtained at 520 nm. Experiment was performed in triplicate. Average of Emission intensity was normalized to signal maximum. Error bars represent 1 standard deviation from the mean.

EF-G does not show increased affinity for GDPNP in the presence of argyrin B

Our fluorescence quenching experiments were performed to assess if argyrin B increases EF-G's affinity for GDPNP and by extension GTP (. When EF-G is binds GDPNP the natural tryptophan fluorescence emission at 340 nm is quenched. We observed that upon titration of GDPNP in the presence of argyrin B, a normal pattern of fluorescence quenching occurred. When a dissociation curve was made from our fluorescence maxima with a single binding site approximation, our data showed that argyrin B did not appear to increase affinity for GDPNP and therefore GTP. The binding affinity did not appear to produce a significant increase or decrease in binding affinity for GDPNP. Binding affinity was considered via dissociation constants K_D and $K_{D\ ArgB,}$ measured at 69 ± 30 μM and 92 ± 33 μM and compared to a literature value of 120 ± 24 μM. Binding affinities were calculated with fluorescence emission maxima using a single site binding model with Graphpad Prism 7 software.

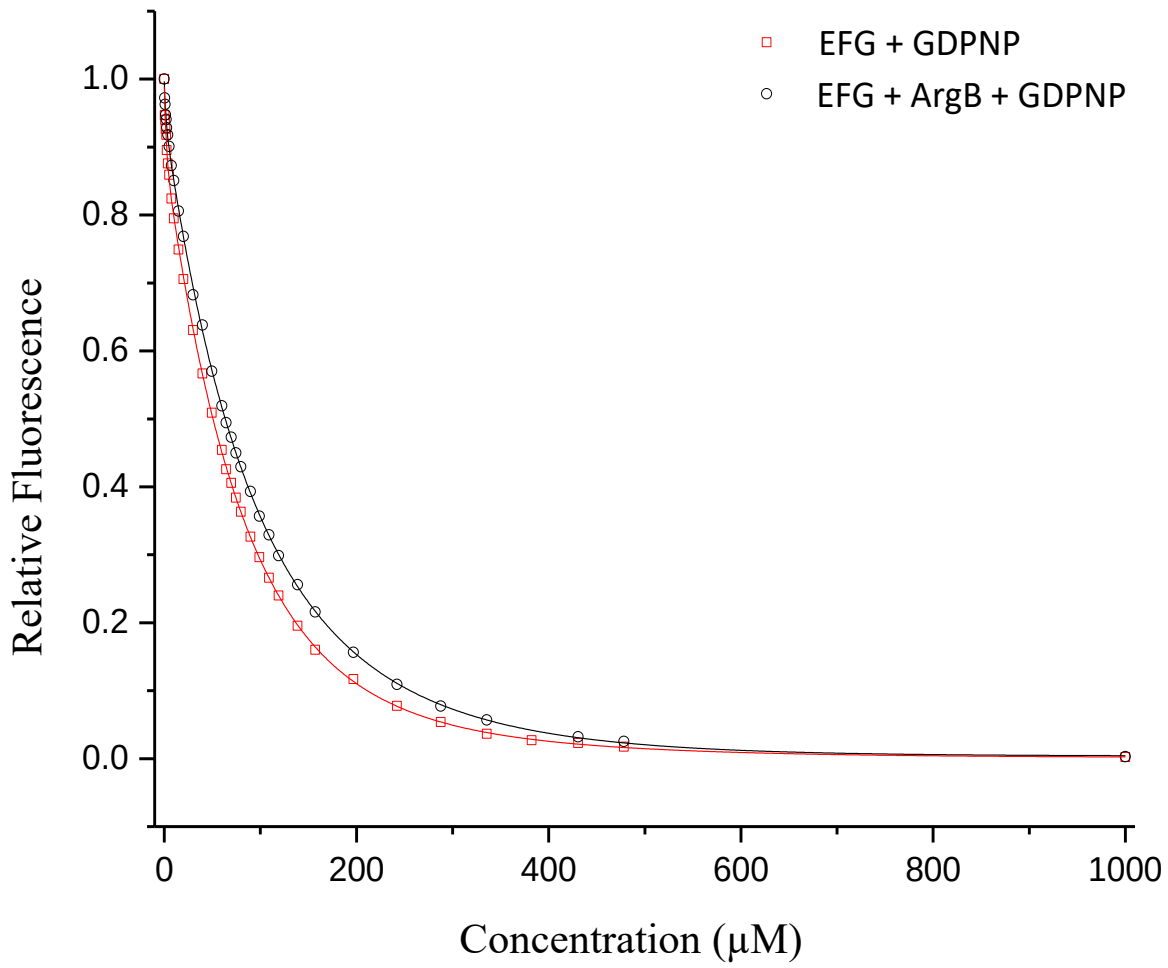

Figure 5-11. Fluorescence Titration of GDPNP in the presence of argyrin B. Excitation Wavelength: 280 nm, Emission Scanning Range: 290 – 380 nm. EF-G + GDPNP (Red), EF-G + GDPNP + argyrin B (Black) K_D = 69 ± 30 $K_{D\ Arg\ B}$ = 92 µM ± 33

Argyrin B increases EF-G association to the 70S ribosome

We employed BLI to observe the association of EF-G and RRF to the PoTC. The presence of argyrin B conferred increased association to the ribosome for EF-G (Figures 5-12)The presence of RRF also increased the association of EF-G•ArgB complexes to the PoTC (Figure 5-12). We ascertained EF-G's increased association to the PoTC from the binding saturation shown by each binding response curve.

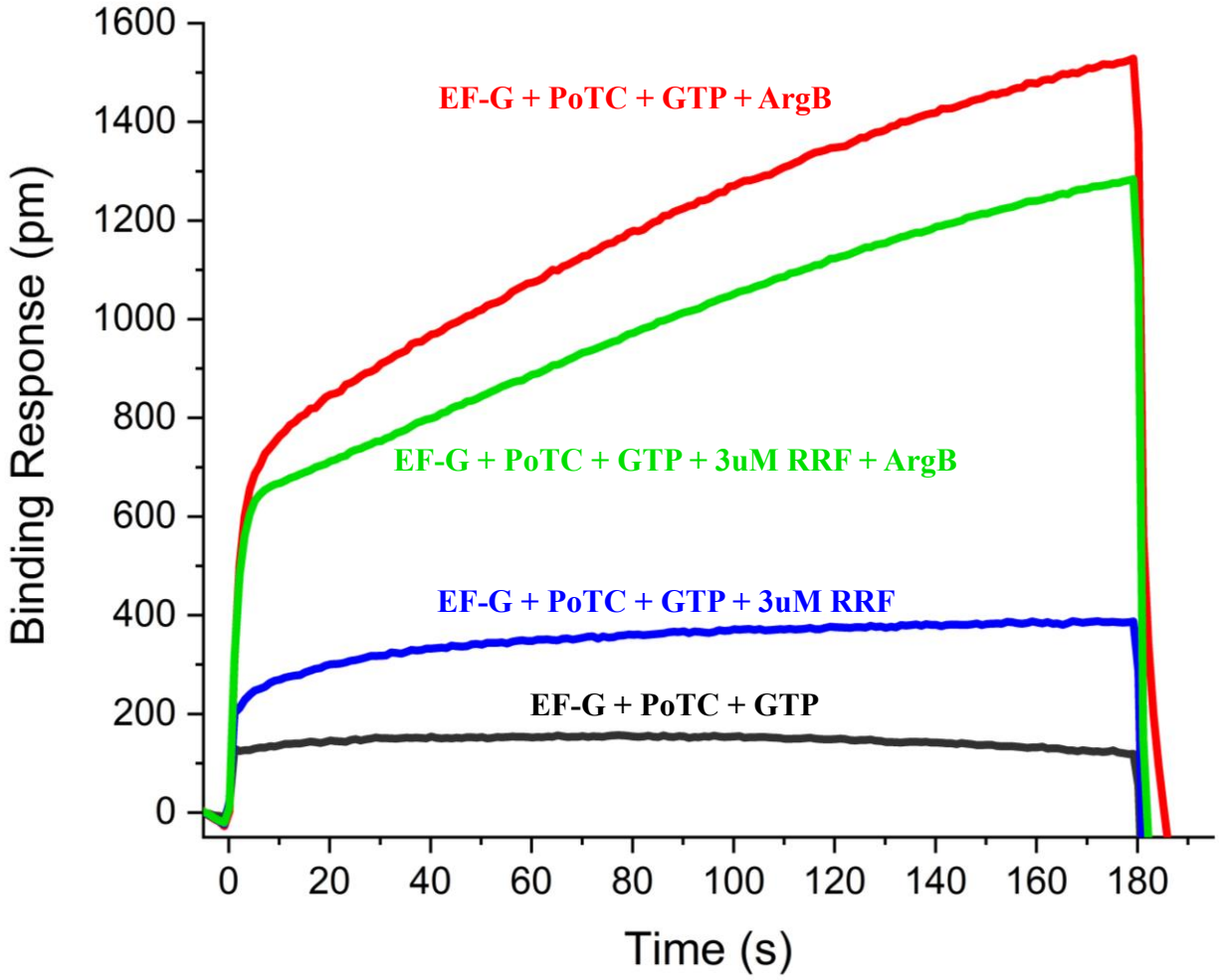

Figure 5-12. BLI binding response of tip bound EF-G associating with PoTC and RRF. 4 µL of 5 µM EF-G were loaded onto HIS2 tips prior

Experiments were performed in triplicate. PoTC was produced with non-$His_{(6)}$-tagged ribosomes, RRF was TEV cleaved to ensure signal fidelity.

This implied that EF-G is free to dissociate from the ribosome in either a GTP or GDP bound state, which indicated that a transition state of ribosome recycling could be stabilized due to the interaction of argyrin B.

Depletion of L12 from JE28 Ribosomes

The L12 protein of JE28 allows for selective depletion due to its chromosomally encoded $His_{(6)}$-tag. L12 Depletion was verified by comparison in activity and through FPLC (Figures 5-13 and 5-15). It has been well documented that the depletion of L12 form the 70S

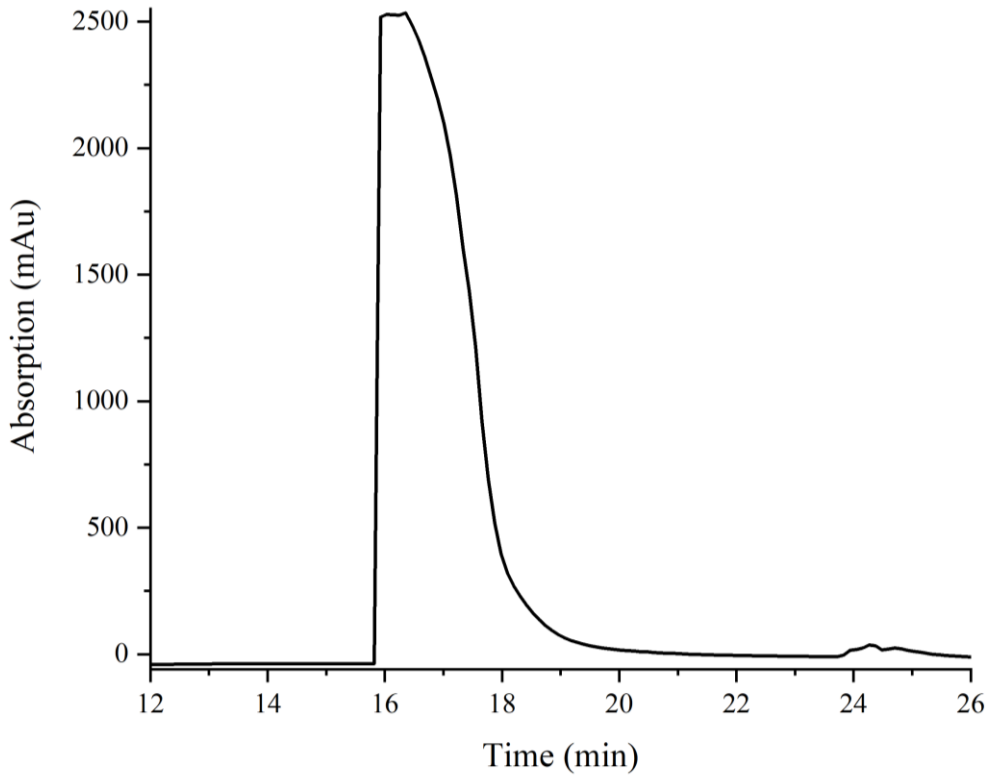

Figure 5-13. FPLC Chromatograph of L12 Depleted Ribosomes. Sharp increase in absorbance due to depleted ribosomes present in flow through of IMAC column. Sample was collected in 1 mL fractions at 1 mL /min.

ribosome abrogates GTPase activity. Due the dynamic nature of the protein the depletion of L12 allowed for the reconstitution of site directed mutants (Figure 5-15) to depleted ribosomes. This

allowed for a tangible preliminary probe on the specific molecular interactions between ribosomal protein L11 and L12 that facilitate GTP hydrolysis.

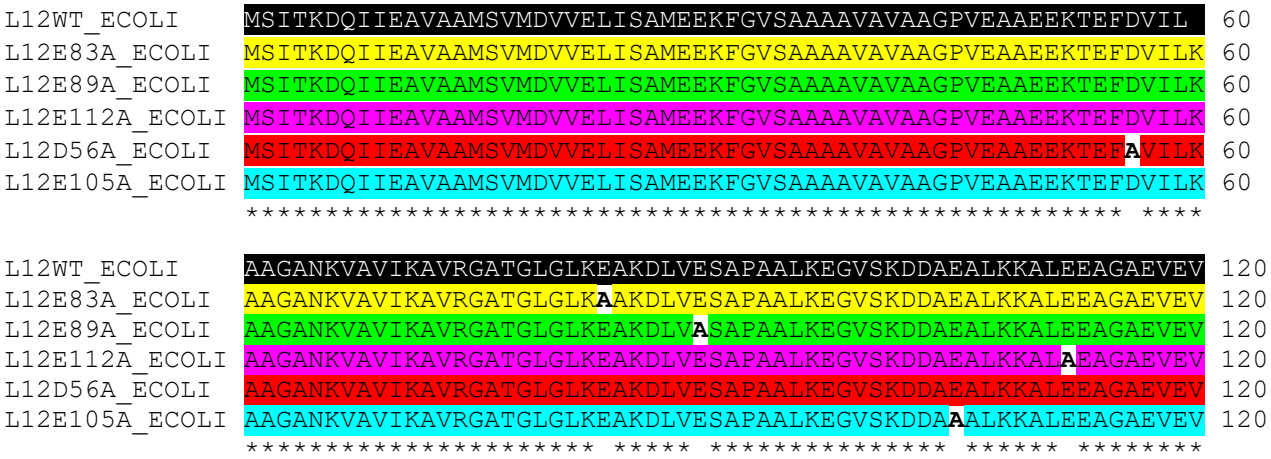

Figure 5-14. Visualization of L12 Amino Acid sequence with highlighted site mutations. L12 E83A (Yellow) L12 E89A (Green), L12 E112A (Magenta), L12D56A (Red), L12 E105A (Cyan) all were mutated an acidic residue to a hydrophobic alanine residue to probe amino acid residue function between L11 and the L12 CTD.

Preliminary Results on Effect of L12 mutagenesis on trGTPase Activity

The effect L12 of C-terminal mutations on GTP cleavage was analyzed by the absorption of the reaction mixture at 635 nm. These mutations were an extension of prior work performed by Amanda Weis, which examined lysine and arginine residues role in GTPase activity via alanine scanning mutations and mutations of opposite charge. In order to reconstitute the depleted ribosomes, 5-fold molar excess was incubated with depleted ribosomes for 20 minutes at 37 °C. The mutants were then incubated with EF-G, prior to addition of GTP. Upon quenching of the reaction, there were distinct changes in activity for four of the five mutants (Figure 5-16): two produced a significant increase in activity L12E103A and L12E898A, and L12E112A and L12D56A produced a sharp decrease in activity. The increase or decrease in GTPase activity

exhibited by each mutant is shown relative to the $70S_{WT}$ and EF-G. L12D56A (Red, Figure 5-16) and L12E105A (Cyan, Figure 5-16) show a sharp loss in activity by 48 and 56% respectively. The other three mutants presented little change in activity L12E83A showed a decrease in 16%, L12E89A an increase of 5%, and L12E112A a decrease of 9%.

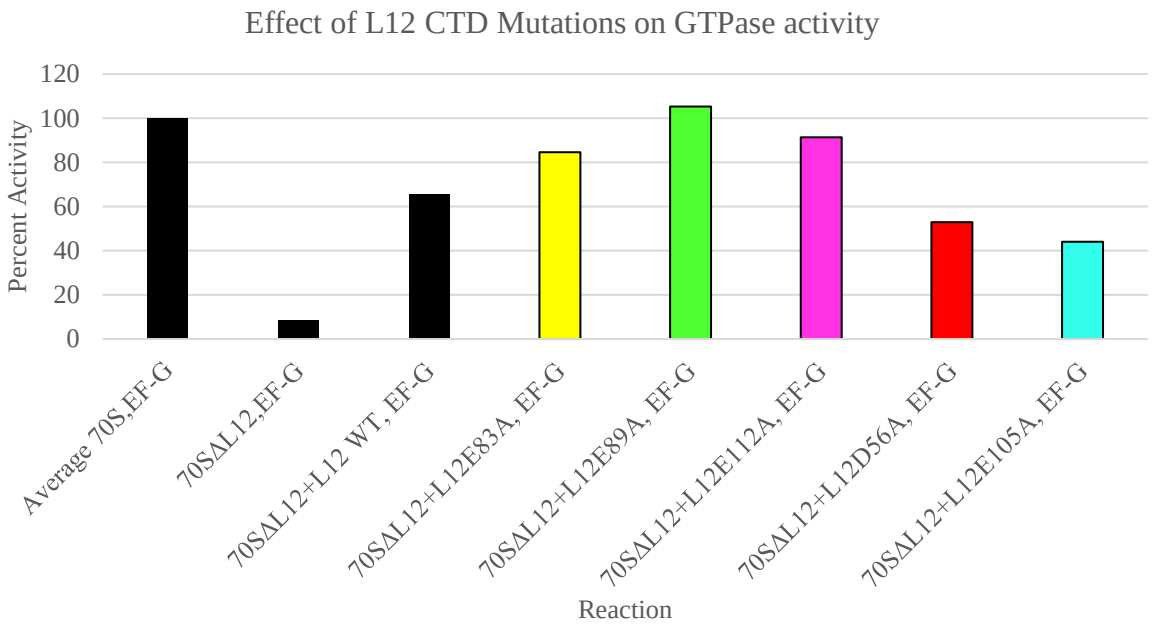

Figure 5-15. Effect of L12 CTD Mutations on EF-G Activity. Depleted ribosomes were incubated with 5x mutants for 30 minutes at 37 °C. Experiments were performed in triplicate. All reactions contained 50 µM GTP. An average of 9 prior 70S,EF-G experiments were used to represent positive control.

Effect of Acidic L12 mutations on L11 Binding

We employed an *in vitro* pull-down assay to determine the effects of our site L12 CTD site mutations on L11-L12 interactions. First L11 had its $His_{(6)}$-tag removed by a Super-TEV protease. In order to ensure the L11 protein was cleaved ran -TEV sample (Lane 1 A-C, Figure 5-18) within each resin washing step, we observed a loss in molecular weight relative to the other L11 bands present in the gels, including a TEV cleavage control (Lane 2, Figure 5-18 A-

C), which suggested that the TEV cleavage was successful. Furthermore the +TEV L11 band was present only in the flow-through step of the assay, which confirmed that L11 did not interact with the TALON resin used to stably bind the L12 mutants. Interestingly a ~50 kDa protein was present in the flow through and wash steps (circled, Figure 5-18 A and B), that was not present in the elution steps. This protein is likely a contaminating GTPase, since EF-Tu has a molecular weight of 43 kDa. Another explanation for the observed protein band is a L11-L12 complex, because L11 (14,875 Da) and dimeric L12 (~24 kDa) have a combined molecular weight of ~40,000, with the marginal increase above 40,000 kDa provided by the $His_{(6)}$-tag of L12 and L12 mutant monomers. Showed successful binding activity with L11 compared to $L12_{WT}$ (Lanes 3 and 5-9 Figure 5-18 C). $L12_{WT}$ and L12 mutants were successfully bound and eluted off the resin as demonstrated by the appearance of protein bands in the elution at 35 kDa, which is representative of the dimeric $His_{(6)}$-tagged L12 dimers. The mutant that appeared to bind the least L11 in the pull-down assay was L12E89A (Lane 5, Figure 5-18 C), since relatively little L11 eluted with the mutant. The other mutants appeared to bind L11 in comparable amount to $L12_{WT}$ (Lanes 3, 6, 7, 8, 9), this effect is potentially caused by a relative excess of L11 compared to L12. These results provide validation of the measurement of *in vitro* L11 to L12 binding via affinity based pull-down assay.

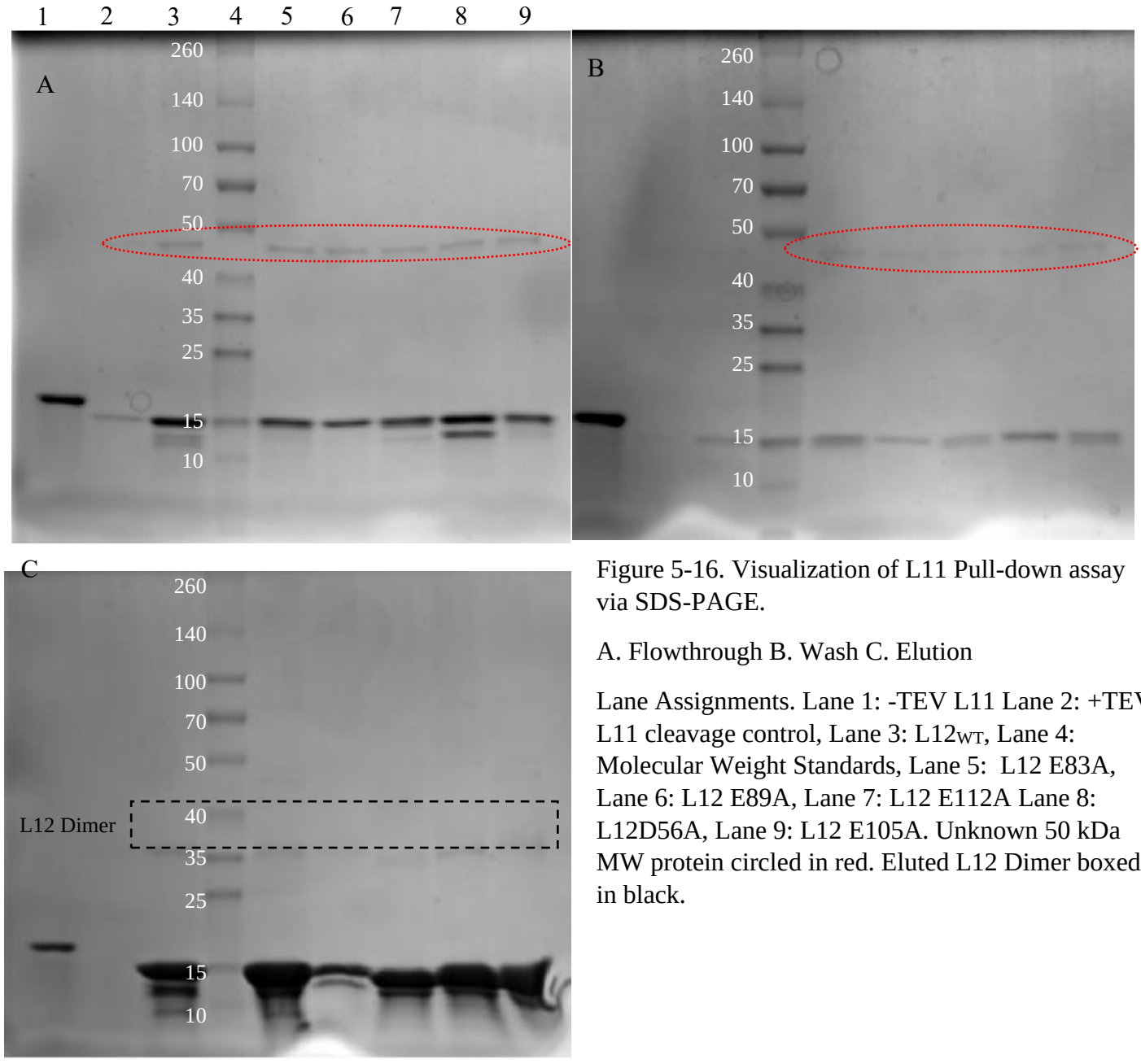

Figure 5-16. Visualization of L11 Pull-down assay via SDS-PAGE.

A. Flowthrough B. Wash C. Elution

Lane Assignments. Lane 1: -TEV L11 Lane 2: +TEV L11 cleavage control, Lane 3: $L12_{WT}$, Lane 4: Molecular Weight Standards, Lane 5: L12 E83A, Lane 6: L12 E89A, Lane 7: L12 E112A Lane 8: L12D56A, Lane 9: L12 E105A. Unknown 50 kDa MW protein circled in red. Eluted L12 Dimer boxed in black.

Chapter 6. Discussion

The effect of argyrin B on EF-G Ribosome Interactions.

One of the most important conclusions to draw from our studies of argyrin B is that as an antibiotic, the inhibition of translation via affecting EF-G is the mechanism by which argyrin B inhibits and kills bacteria. Work performed by Nyfeler et al showed argyrin B effected a distinct conformational change in EF-G. They observed that domain IV of EF-G is ratcheted ~45 degrees and adopts a slightly elongated conformation with respect to wild type EF-G based on their crystallographic model (Figure 6-1). They proposed that argyrin B inhibits GTPase activity as a potential mechanism of action but did not perform GTPase activity experiments. (Nyfeler *et al.*, 2012). This work has demonstrated that EF-G's GTPase activity is not inhibited in the presence of argyrin B unless RRF is present in significant quantities. The presence of GTPase activity is dissimilar to the mechanism of action of fusidic acid, which is a substrate level competitive inhibitor of EF-G activity. This type of inhibition was demonstrated to inhibit all GTPase related behavior of EF-G; namely translocation and ribosome recycling. The similarity between argyrin B and fusidic acid is that both antibiotics impede ribosome recycling. (Borg and Pavlov, 2016). The argyrin B induced elongation of EF-G is demonstrably similar to the conformations EF-G adopts when in complex with the ribosome, in contrast to the more compact conformations observed when the ribosome is not present (Lin *et al.*, 2015). This argyrin B induced elongated conformation would lend explanation to the observed increased association to the ribosome and RRF (Figure 5-12 and 5-13). This described conformation likely does not interfere with dissociation of EF-G from the ribosome, which explains the similar binding stabilities observed with EF-G•ArgB complexes to untreated EF-G in the gel filtration and sucrose cushion assays,

error withstanding. The process of ribosome recycling was clearly affected, as observed in our Rayleigh light scattering data (Figure 5-9), it is important to note that

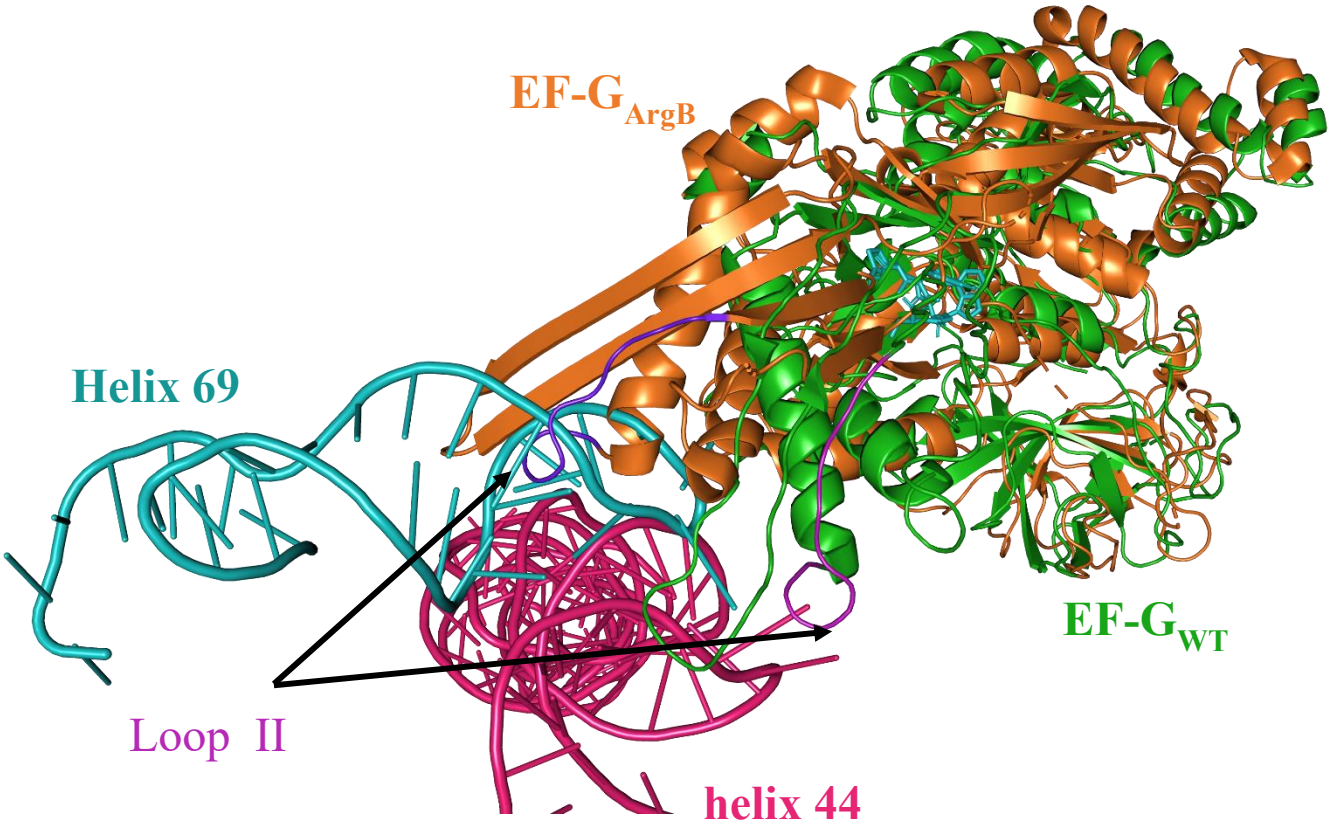

Figure 6-1. Ratcheting of EF-G by argyrin B. EF-G bound to argyrin B (Orange) was aligned with EF-G associated to the ribosome in a hybrid translocational state (Green). Ratcheting of 45° is shown. Loop II (Purple) of DIV is ratcheted deeper into the 70S complex. H69 (Cyan) and h44 (Magenta) are the helices that compose B2a the largest intersubunit bridge involved in subunit association. Note structure of H69 interferes with EF-G•ArgB complex in figure. (PDB ID: 4FN5 and 4W29)

equivalent concentrations of RRF and EF-G were used in this experiment, which could limit the extent of dissociation inhibited by argyrin B. There has been extensive and controversial research on the exact mechanism of ribosome recycling demonstrated by publications from Borg et al.

and Chen et al. The kinetic mechanism proposed by Borg and colleagues (adopted in Figure 6-2) presents a reaction intermediates that could provide clues to argyrin B's role in inhibiting ribosome recycling (Borg, Pavlov and Ehrenberg, 2016). The transition state highlighted in figure 6-3 shows the intermediate thought to be stabilized by argyrin B, therefore inhibiting EF-G and RRF facilitated ribosome dissociation. When compared to the proposed mechanism of Chen and colleagues, a similar transition state can be rationalized based on their kinetic mechanism (Chen *et al.,* 2017). This makes stabilization of the transition state highlighted in Figure 6-3 the most probable candidate for the mechanism by which argyrin B inhibits translation. Since our data suggested that argyrin B had no effect on translocation. We surmise that this is because GTP is still hydrolyzed and the elongated EF-G would still be able to stabilize the inter-subunit rotation of the ribosome while later dissociating, allowing further rounds of elongation. (Zhou *et al.*, 2014; Noller *et al.*, 2017; Rodnina *et al.*, 2019). These effects of argyrin B when compared to literature justified our proposed mechanism of action of argyrin B.

Proposed mechanism of action or argyrin B

Based on our observed results we propose that the mechanism of action of argyrin B is an inhibition of ribosome recycling via a steric hinderance that prevents the cooperative interruption of B2a by domain IV of EF-G and RRF due to the induced elongated conformation of EF-G when argyrin B is bound.

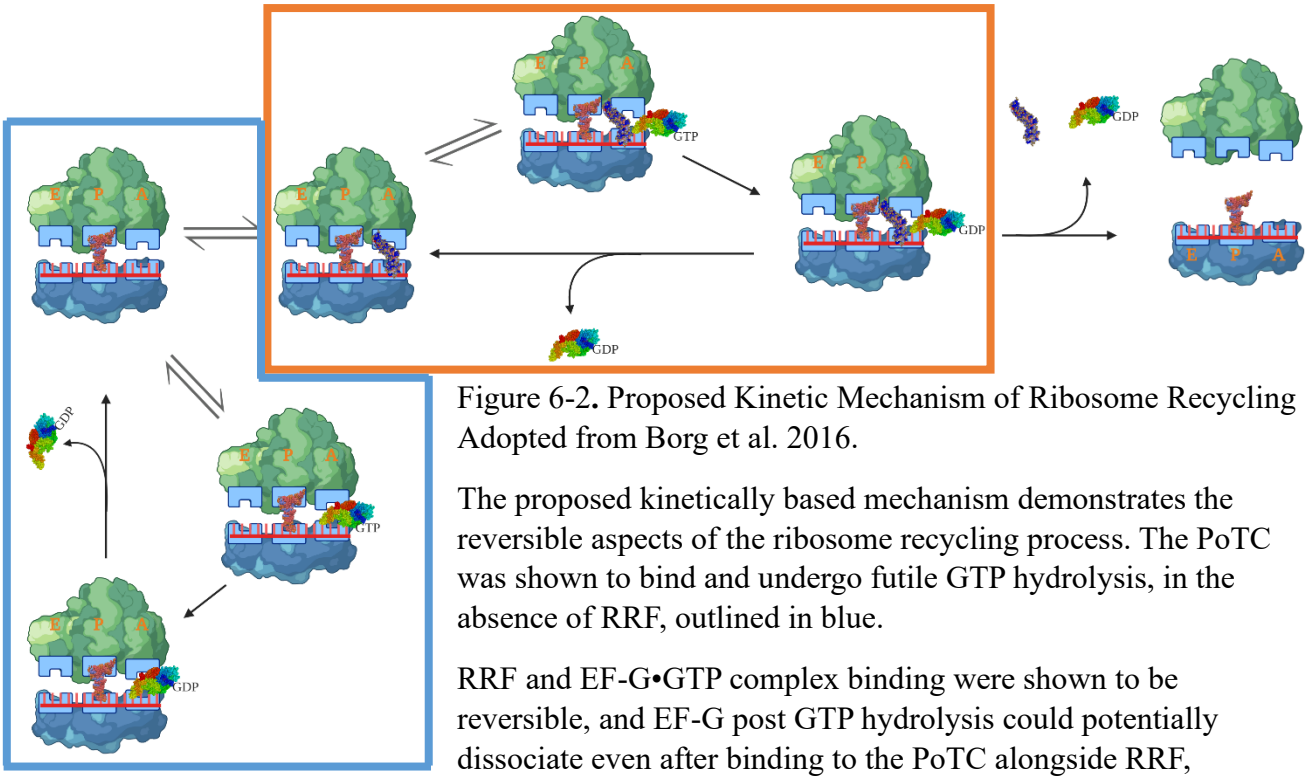

Figure 6-2**.** Proposed Kinetic Mechanism of Ribosome Recycling Adopted from Borg et al. 2016.

The proposed kinetically based mechanism demonstrates the reversible aspects of the ribosome recycling process. The PoTC was shown to bind and undergo futile GTP hydrolysis, in the absence of RRF, outlined in blue.

RRF and EF-G•GTP complex binding were shown to be reversible, and EF-G post GTP hydrolysis could potentially dissociate even after binding to the PoTC alongside RRF, reforming a PoTC•RRF complex, outlined in orange.

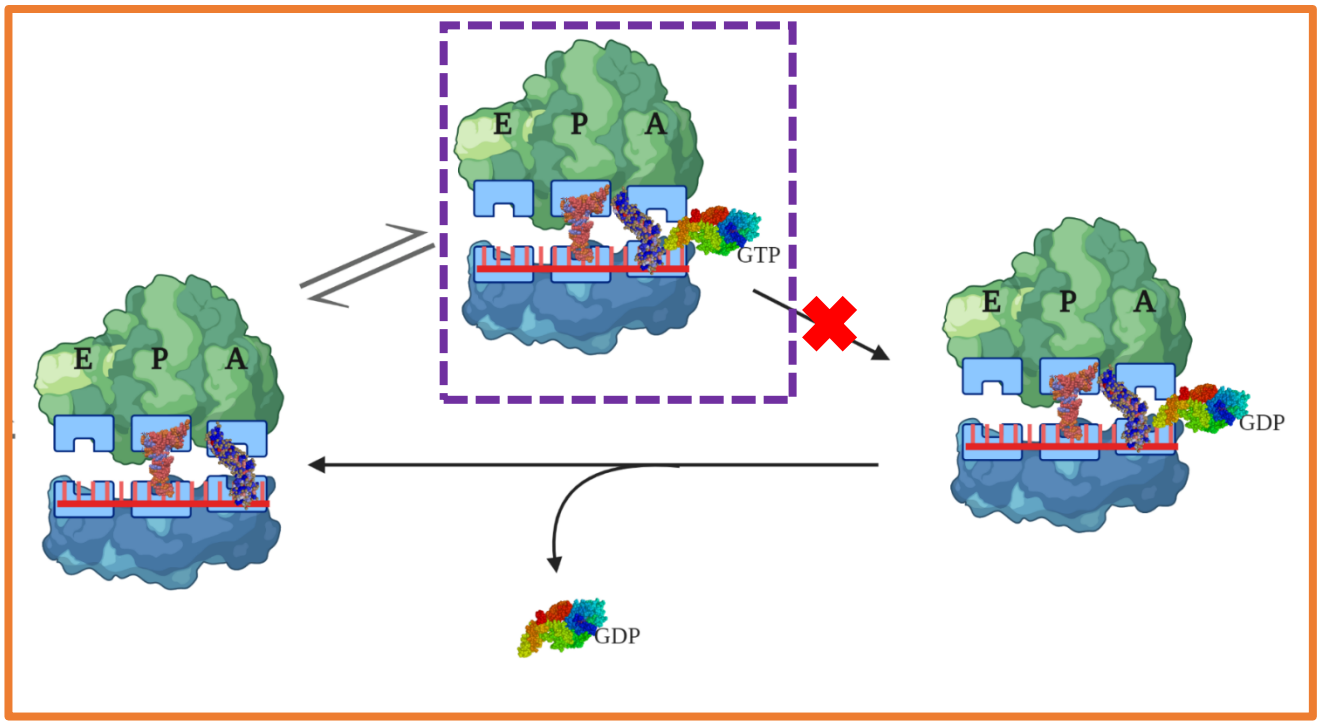

Figure 6-3**.** Proposed Transition State Stabilized by EF-G•ArgB from Borg et al. Kinetic Mechanism.

Argyrin B stabilizes a PoTC•RRF•EF-G•GTP transition state (Outlined in Purple) that does not allow GTP cleavage to occur and therefore inhibits formation of a pre-recycling PoTC•RRF•EF-G•GDP state and ribosome recycling. Because this transition state is in equilibrium, dissociation of EF-G is possible without GTP cleavage.

The observed 45° shift in EF-G's conformation (Figure 6-1) ratchets DIV of EF-G away from B2a, represented in Figure 6-1 by the H69(Cyan) and h44(Magenta). Disruption of EF-G's DIV was shown by Zhang et al. to alter ribosome recycling activity significantly(Zhang *et al.*, 2015). They proposed, by performing both truncation and site mutations that the distal loop II of DIV of EF-G was essential to stabilizing the rotated state of the PoTC and ribosome recycling. The rotated state of the PoTC is similar in nature to the hybrid translocational state where rotation has been stabilized by EF-G, by aligning the structure of EF-G bound with argyrin B to EF-G bound to the hybrid translocational ribosome at 3.4 Å resolution (Figure 6-1), insight could be drawn from the alignment of the two structural states. This alignment showed that loop II was rotated further into the ribosomal complex. When EF-G•ArgB was aligned in 9.9 Å structure of EF-G

bound to RRF and the 50S subunit (Figure 6-4) the rotation of loop II is evident but less pronounced. It has been observed that the interface of DIV and RRF is located far from loop II, this could imply that the ratcheting of EF-G by argyrin B fundamentally changes the structural characteristics of that interface and loop II position in dissociation catalysis (Karimi *et al.*, 1999; Zhang *et al.*, 2015; Fu *et al.*, 2016). The ratcheting present in Figure 6-4 intruigingly moves loop II closer to RRF, whicj This when paired with the kinetic mechanism proposed by Borg et al. justifies a reasonable hypothesis that the induced elongation of EF-G by argryin B changes the interface of RRF and the sterics of loop II of DIV such that dissociation of EF-G•GTP complexes is more favorable than facilitation of ribosome recycling by GTP hydrolysis.

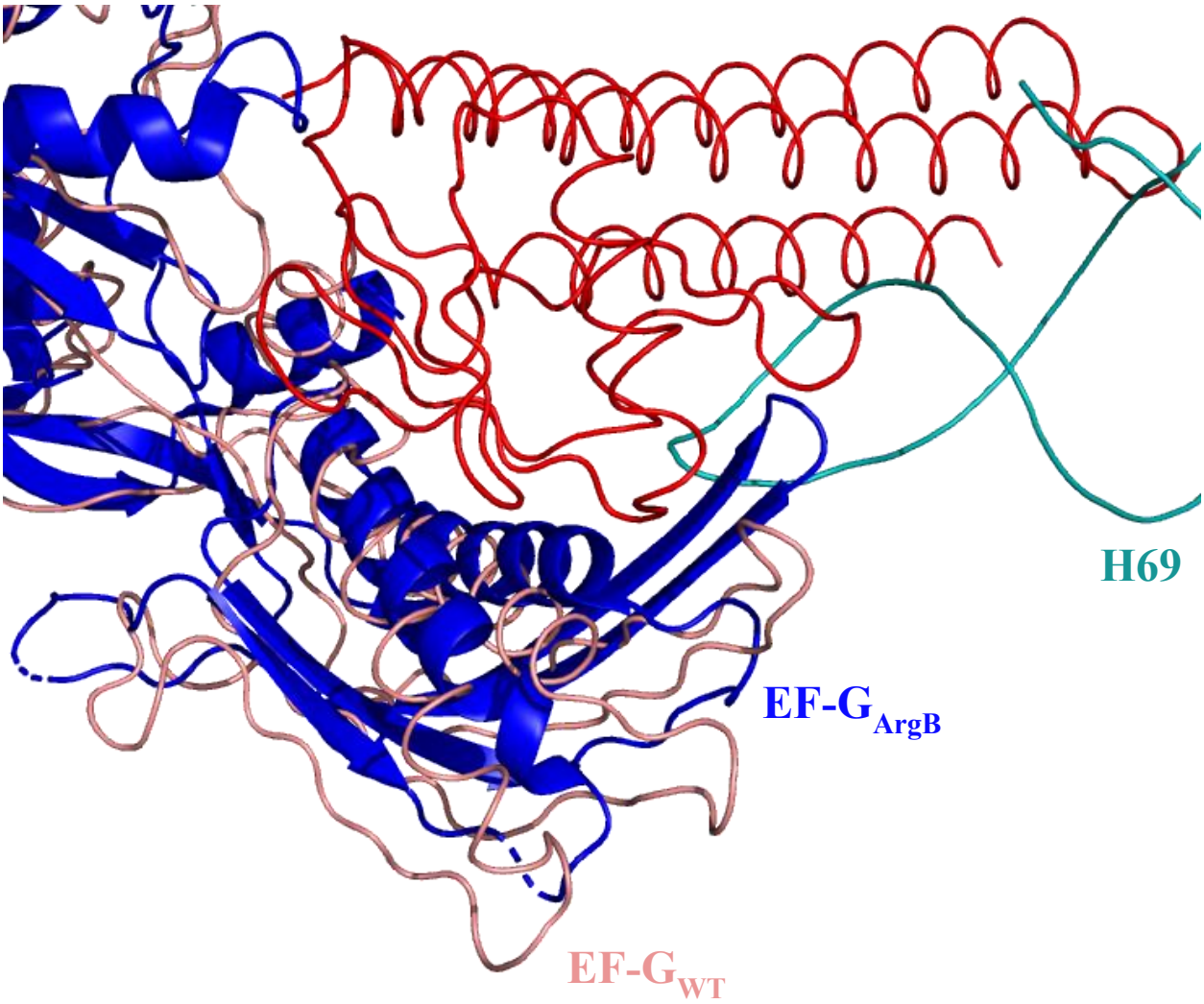

Figure 6-4. Alignment of EF-G$_{ArgB}$ to EF-G bound with RRF (Red) and the 50S subunit. EF-G$_{ArgB}$ (Blue) was aligned with EF-G$_{WT}$ (Tan). H69 (Cyan) of the 23S rRNA is visible. Ratcheting of EF-G is still apparent. Loop II of DIV is ratcheted towards H69 and RRF relative to EF-G$_{WT}$. Note structure of H69 interferes with EF-G$_{ArgB}$ complex in figure. (PDB ID: 4FN5 and 2RDO)

L12 Acidic residues are important for GTPase activation

Through preliminary results on the alanine scanning mutations of glutamic and aspartic acid residues of the L12 CTD we can speculate that the electrostatic interactions of L11 and L12 play a role in GTPase activation. L11 has been shown to play important roles GTPase activation through interactions with the L10 portion of the ribosomal stalk and 23S rRNA (Highland and Howard, 1975; Iben and Draper, 2008) The G domain of GTPases has been demonstrated to play a chaperone role of the L12 CTD, because during GTPase association, the hinge of L12 exposes the hydrophobic core, allowing L11 interactions to occur. (Zhang *et al.*, 2012). The interactions between the CTD of L11, L10, 23S rRNA has been well documented, as binding to residues 1051 to 1108 of the 23S rRNA with helix α2 and strand β2 of L10 contacting 2 C-terminal L11 helices(Agrawal *et al.*, 2001; Diaconu *et al.*, 2005). This documented interaction alone was shown to enhance $L10(L12)_4$ stalk binding by 100 times (Iben and Draper, 2008). The structural interactions between L11 and the L12 CTD, on the other hand remain enigmatic. The observed negatively charged electrostatic pocket observed in the L12 CTD (Figure 2-4 and 6-5) is most likely one the hydrophilic surfaces protecting the hydrophobic core of the L12 CTD from becoming solvent exposed. By probing the glutamic and aspartic acid residues that surround and make up this pocket, we were able to observe tangible decreases in activity and L11 binding due to single site mutations. Mutants E105A and D56A presented massive decreases in activity. Zhang et al. demonstrated that L11 affinity for purified and isolated L12 is a reliable measure of L12-L11 interaction via *in vitro* pull-down assay.

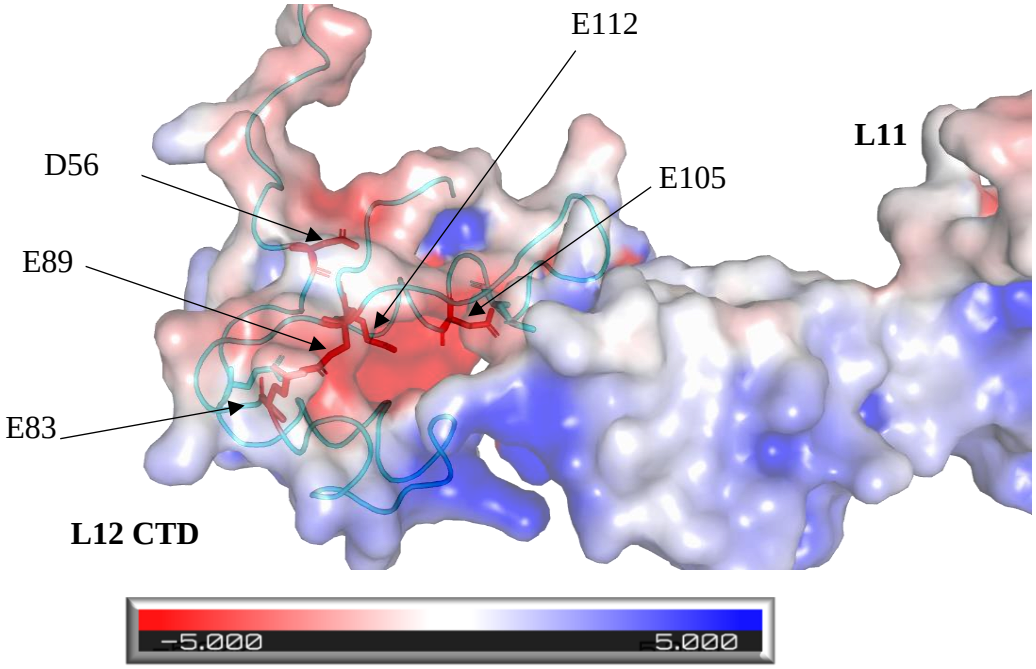

Figure 6-5. L11 electrostatic interactions with respect L12 CTD mutations. L12 mutation sites (Red sticks) are contrasted against other CTD residues(Cyan) L12 and L11 overlayed with electrostatic map, negative charge (Red) and positive charge (blue) measured on a gradient -5 being most negatively charged, 0 being uncharged(white), and 5 being most positively charged.

Zhang et al . observed that mutations to the hydrophobic core of the L12 CTD were intolerable to alanine scanning mutations. The results of our L11 pull down assay provided preliminary results showing that mutations to glutamic and aspartic acid residues do not inhibit L11 binding to the CTD of L12. These results suggest the conclusion that acidic residues on L12 are greater effectors of GTPase activation than L11 binding.

Chapter 7. Conclusions and Future Work

Conclusions

We have presented and justified a novel mechanism of action for a known antibiotic, argyrin B This allosteric inhibition of EF-G's function during ribosome recycling is significant when compared to other antibiotics like fusidic acid that inhibit EF-G via competitive inhibition (Borg and Pavlov, 2016). Furthermore, the potential ribosomal structural advances that would occur if the hypothetical transition state is indeed stabilized would provide insight on a controversial subject in ribosomal science. The understanding of this mechanism will afford valuable clues to how ribosome recycling functions structurally.

This work also holds promising preliminary results on the nature of L11 to L12 CTD electrostatic interactions and their effect on GTPase activity. Though further experimentation is required to determine the full effect of these acidic residues on L11 binding interactions.

Future Work

To confirm the ribosome recycling factor dependency of argyrin B, Rayleigh scattering experiments should be performed with increased RRF concentrations. With increased concentrations of ribosomes, RRF, and EF-G_{ArgB} complexes, Cryo-EM could be used to determine the exact structural interactions of EF-G_{ArgB} interactions with the ribosome and potentially provide high resolution models of a labile transition state.

L12 CTD mutations will be examined for their effect on GTPase binding to the ribosome, and their effect on the activity of other GTPases. L11 binding interactions will be probed further using the established pull-down assay and BLI.

Works Cited

Adio, S. *et al.* (2018) 'Dynamics of ribosomes and release factors during translation termination in E. coli.', *eLife*, 7, pp. 1–24. doi: 10.7554/eLife.34252.

Agrawal, R. K. *et al.* (2001) 'Localization of L11 protein on the ribosome and elucidation of its involvement in EF-G-dependent translocation', *Journal of Molecular Biology*, 311(4), pp. 777–787. doi: 10.1006/jmbi.2001.4907.

Alejo, J. L. and Blanchard, S. C. (2017) 'Miscoding-induced stalling of substrate translocation on the bacterial ribosome', (11). doi: 10.1073/pnas.1707539114.

Allardyce, D. J., Bell, C. M. and Loizidou, E. Z. (2019) 'Argyrin B a non-competitive inhibitor of the human immunoproteasome exhibiting preference for β1i', *Chemical Biology & Drug Design*, pp. 0–2. doi: 10.1111/cbdd.13539.

Ash, M. R. *et al.* (2011) 'The initiation of GTP hydrolysis by the G-domain of FeoB: Insights from a transition-state complex structure', *PLoS ONE*, 6(8). doi: 10.1371/journal.pone.0023355.

Atkinson, C. C. (2015) 'The evolutionary and functional diversity of classical and lesser-known cytoplasmic and organellar translational GTPases across the tree of life', *BMC Genomics*, 16(1), pp. 1–15. doi: 10.1186/s12864-015-1289-7.

Belardinelli, R. *et al.* (2016) 'Translocation as continuous movement through the ribosome', *RNA Biology*. Taylor & Francis, 13(12), pp. 1197–1203. doi: 10.1080/15476286.2016.1240140.

Borg, A. and Pavlov, M. (2016) 'Mechanism of fusidic acid inhibition of RRF- and EF-G-dependent splitting of the bacterial post-termination ribosome', 44(7), pp. 3264–3275. doi: 10.1093/nar/gkw178.

Borg, A., Pavlov, M. and Ehrenberg, M. (2016) 'Complete kinetic mechanism for recycling of the bacterial ribosome', *Rna*, 22(1), pp. 10–21. doi: 10.1261/rna.053157.115.

Brilot, A. F. *et al.* (2013) 'Structure of the ribosome with elongation factor G trapped in the pretranslocation state', *Proceedings of the National Academy of Sciences*, 110(52), pp. 20994–20999. doi: 10.1073/pnas.1311423110.

Bubunenko, M. G., Chuikov, S. V. and Gudkov, A. T. (1992) 'The length of the interdomain region of the L7/L12 protein is important for its function', *FEBS Letters*, 313(3), pp. 232–234. doi: 10.1016/0014-5793(92)81198-U.

Carlson, M. A. *et al.* (2017) 'Ribosomal Protein L7/L12 is Required for GTPase Translation Factors EF-G, RF3 and IF2 to Bind in their GTP State to 70S Ribosomes', *FEBS Journal*, 284(11), pp. 1631–1643. doi: 10.4172/2157-7633.1000305.Improved.

Chen, Y. *et al.* (2013) 'Structure of EF-G-ribosome complex in a pretranslocation state', *Nature Structural and Molecular Biology*, 20(9), pp. 1077–1084. doi: 10.1038/nsmb.2645.

Chen, Y. *et al.* (2017) 'The kinetic mechanism of bacterial ribosome recycling', *Nucleic Acids Research*. Oxford University Press, 45(17), pp. 10168–10177. doi: 10.1093/nar/gkx694.

Dabbs, E. R. *et al.* (1981) 'Mutants of Escherichia coli lacking ribosomal protein L1', *Journal of Molecular Biology*, 149(4), pp. 553–578. doi: 10.1016/0022-2836(81)90347-8.

Diaconu, M. *et al.* (2005) 'Structural basis for the function of the ribosomal L7/12 stalk in factor binding and GTpase activation', *Cell*, 121(7), pp. 991–1004. doi: 10.1016/j.cell.2005.04.015.

Ero, R. *et al.* (2016) 'Similarity and diversity of translational GTPase factors EF-G, EF4, and BipA: From structure to function', *RNA Biology*. Taylor & Francis, 13(12), pp. 1258–1273. doi: 10.1080/15476286.2016.1201627.

Freistroffer, D. V. *et al.* (1997) 'Release factor RF3 in E.coli accelerates the dissociation of release factors RF1 and RF2 from the ribosome in a GTP-dependent manner of RF3 on peptide release from the ribosome (Capecchi 1995). The expected stimulatory effect of GTP on poly', *The EMBO Journal*, 16(13), pp. 4126–4133. Available at: https://www.ncbi.nlm.nih.gov/pmc/articles/PMC1170035/pdf/004126.pdf.

Fu, Z. *et al.* (2016) 'Key Intermediates in Ribosome Recycling Visualized by Time-Resolved Cryoelectron Microscopy', *Structure*, 24(12), pp. 2092–2101. doi: 10.1016/j.str.2016.09.014.

Gao, H. *et al.* (2007) 'RF3 Induces Ribosomal Conformational Changes Responsible for Dissociation of Class I Release Factors', *Cell*, 129(5), pp. 929–941. doi: 10.1016/j.cell.2007.03.050.

Gao, Y. *et al.* (2009) 'The Structure of the Ribosome with', *Science*, (326), pp. 694–701. doi: 10.1126/science.1179709.

Ge, X. *et al.* (2018) 'Complementary charge-based interaction between the ribosomal-stalk protein L7/12 and IF2 is the key to rapid subunit association', *Proceedings of the National Academy of Sciences*, 115(18), pp. 4649–4654. doi: 10.1073/pnas.1802001115.

Gibbs, M. R. and Fredrick, K. (2018) 'Roles of elusive translational GTPases come to light and inform on the process of ribosome biogenesis in bacteria', *Molecular Microbiology*, 107(4), pp. 445–454. doi: 10.1111/mmi.13895.

Goto, S., Muto, A. and Himeno, H. (2013) 'GTPases involved in bacterial ribosome maturation', *Journal of Biochemistry*, 153(5), pp. 403–414. doi: 10.1093/jb/mvt022.

Gualerzi, C. O. and Pon, C. L. (1990) 'Initiation of mRNA translation in prokaryotes', *Biochemistry*, 29(25), pp. 5881–5889. doi: 10.1021/bi00477a001.

Highland, J. H. and Howard, G. A. (1975) 'Assembly of Ribosomal Proteins L7, L10, L11, L12 on the 50 S Subunit of Escherichia coli', *Journal of Biological Chemistry*, 250(3), pp. 831–834.

Huang, C., Mandava, C. S. and Sanyal, S. (2010) 'The ribosomal stalk plays a key role in IF2-mediated association of the ribosomal subunits', *Journal of Molecular Biology*. Elsevier Ltd, 399(1), pp. 145–153. doi: 10.1016/j.jmb.2010.04.009.

Iben, J. R. and Draper, D. E. (2008) 'Specific interactions of the L10(L12)4 ribosomal protein complex with mRNA, rRNA, and L11', *Biochemistry*, 47(9), pp. 2721–2731. doi:

10.1021/bi701838y.

Karimi, R. *et al.* (1999) 'Novel roles for classical factors at the interface between translation termination and initiation', *Molecular Cell*, 3(5), pp. 601–609. doi: 10.1016/S1097-2765(00)80353-6.

Kiel, M. C. *et al.* (2003) 'Release of Ribosome-bound Ribosome Recycling Factor by Elongation Factor G', *Journal of Biological Chemistry*, 278(48), pp. 48041–48050. doi: 10.1074/jbc.M304834200.

Kimura, S. and Suzuki, T. (2009) 'Fine-tuning of the ribosomal decoding center by conserved methyl-modifications in the Escherichia coli 16S rRNA', *Nucleic Acids Research*, 38(4), pp. 1341–1352. doi: 10.1093/nar/gkp1073.

Koch, M. *et al.* (2015) 'Role of a ribosomal RNA phosphate oxygen during the EF-G–triggered GTP hydrolysis', *Proceedings of the National Academy of Sciences*, 112(20), pp. E2561–E2568. doi: 10.1073/pnas.1505231112.

Koutmou, K. S. *et al.* (2014) 'RF3:GTP promotes rapid dissociation of the class 1 termination factor', *Rna*, 20(5), pp. 609–620. doi: 10.1261/rna.042523.113.

Lang, K. *et al.* (2008) 'The Role of 23S Ribosomal RNA Residue A2451 in Peptide Bond Synthesis Revealed by Atomic Mutagenesis', *Chemistry and Biology*, 15(5), pp. 485–492. doi: 10.1016/j.chembiol.2008.03.014.

Leipe, D. D. *et al.* (2002) 'Classification and evolution of P-loop GTPases and related ATPases.', *Journal of molecular biology*, 317(1), pp. 41–72. doi: 10.1006/jmbi.2001.5378.

Liljas, A. and Sanyal, S. (2018) 'The enigmatic ribosomal stalk', *Quarterly Reviews of Biophysics*, 51. doi: 10.1017/s0033583518000100.

Lin, J. *et al.* (2015) 'Conformational changes of elongation factor g on the ribosome during tRNA translocation', *Cell*. Elsevier Inc., 160(1–2), pp. 219–227. doi: 10.1016/j.cell.2014.11.049.

Ling, C. and Ermolenko, D. N. (2016) 'Caught on Camera: Intermediates of Ribosome Recycling', *Structure*. Elsevier Ltd, 24(12), pp. 2035–2036. doi: 10.1016/j.str.2016.11.009.

Liu, G. *et al.* (2014) 'EF-G catalyzes tRNA translocation by disrupting interactions between decoding center and codon-anticodon duplex', *Nature Structural and Molecular Biology*. Nature Publishing Group, 21(9), pp. 817–824. doi: 10.1038/nsmb.2869.

Liu, Q. and Fredrick, K. (2016) 'Intersubunit bridges of the bacterial ribosome Qi', *Journal of Molecular Biology*. Elsevier B.V. doi: 10.1016/j.jmb.2016.02.009.

Malys, N. (2012) 'Shine-Dalgarno sequence of bacteriophage T4: GAGG prevails in early genes', *Molecular Biology Reports*, 39(1), pp. 33–39. doi: 10.1007/s11033-011-0707-4.

Maracci, C. and Rodnina, M. V. (2016) 'Review: Translational GTPases', *Biopolymers*, 105(8), pp. 463–475. doi: 10.1002/bip.22832.

Mitroshin, I., Garber, M. and Gabdulkhakov, A. (2015) 'Crystallographic analysis of archaeal ribosomal protein L11', *Acta Crystallographica Section F Structural Biology Communications*. International Union of Crystallography, 71(8), pp. 1083–1087. doi:

10.1107/s2053230x15011395.

Mohr, D., Wintermeyer, W. and Rodnina, M. V (2002) ‘GTPase activation of elongation factors Tu and G on the ribosome.’, *Biochemistry*, 41(41), pp. 12520–8. Available at: http://www.ncbi.nlm.nih.gov/pubmed/12369843.

Nissen, P. *et al.* (2000) ‘The Structural Basis of Ribosome Activity in Peptide Bond Synthesis Published by : American Association for the Advancement of Science Stable URL : http://www.jstor.org/stable/3077318 REFERENCES Linked references are available on JSTOR for this article ’:, 289(5481), pp. 920–930.

Noller, H. F. *et al.* (2017) ‘Ribosome structural dynamics in translocation : yet another functional role for ribosomal RNA’. doi: 10.1017/S0033583517000117.

Nyfeler, B. *et al.* (2012) ‘Identification of elongation factor g as the conserved cellular target of argyrin B’, *PLoS ONE*, 7(9), pp. 1–12. doi: 10.1371/journal.pone.0042657.

O’Connor, M. (2015) ‘Interactions of release factor RF3 with the translation machinery’, *Molecular Genetics and Genomics*, 290(4), pp. 1335–1344. doi: 10.1007/s00438-015-0994-x.

Peske, F. *et al.* (2014) ‘Timing of GTP binding and hydrolysis by translation termination factor RF3’, *Nucleic Acids Research*. ElsevierCompany., 42(3), pp. 11–18. doi: 10.1093/nar/gkt1095.

Pierson, W. E. *et al.* (2016) ‘Uniformity of Peptide Release Is Maintained by Methylation of Release Factors’, *Cell Reports*. ElsevierCompany., 17(1), pp. 11–18. doi: 10.1016/j.celrep.2016.08.085.

Rheinberger, H. J., Sternbach, H. and Nierhaus, K. H. (1981) ‘Three tRNA binding sites on Escherichia coli ribosomes.’, *Proceedings of the National Academy of Sciences*, 78(9), pp. 5310–5314. doi: 10.1073/pnas.78.9.5310.

Rodnina, M. V. *et al.* (1996) ‘Initial binding of the elongation factor Tu-GTP-aminoacyl-tRNA complex preceding codon recognition on the ribosome’, *Journal of Biological Chemistry*, 271(2), pp. 646–652. doi: 10.1074/jbc.271.2.646.

Rodnina, M. V. (2018) ‘Translation in prokaryotes’, *Cold Spring Harbor Perspectives in Biology*, 10(9). doi: 10.1101/cshperspect.a032664.

Rodnina, M. V. *et al.* (2019) ‘Converting GTP hydrolysis into motion : versatile translational elongation factor G’, *Biological Chemistry Papers*. doi: 10.1515/hsz-2019-0313.

Schmeing, T. M. and Ramakrishnan, V. (2009) ‘What recent ribosome structures have revealed about the mechanism of translation’, *Nature*. Nature Publishing Group, 461(7268), pp. 1234–1242. doi: 10.1038/nature08403.

Shi, X. *et al.* (2012) ‘Functional role of the Sarcin-Ricin Loop of the 23S rRNA in the elongation cycle of proteins’, *Journal of Molecular Biology*, 419(858), pp. 125–138. doi: 10.1016/j.jmb.2012.03.016.Functional.

Shine, J. and Dalgarno, L. (1974) ‘The 3’-Terminal Sequence of Escherichia coli 16S Ribosomal RNA: Complementarity to Nonsense Triplets and Ribosome Binding Sites’, *Proceedings of the National Academy of Sciences*, 71(4), pp. 1342–1346. doi: 10.1073/pnas.71.4.1342.

Simonetti, A. *et al.* (2009) ‘A structural view of translation initiation in bacteria’, *Cellular and Molecular Life Sciences*, 66(3), pp. 423–436. doi: 10.1007/s00018-008-8416-4.

Smirnova, E. *et al.* (2001) ‘<Mol Biol Cell 2001 Smirnova.pdf>’, 12(August), pp. 2245–2256. doi: 10.1091/mbc.12.8.2245.

Spiegel, P. C., Ermolenko, D. N. and Noller, H. F. (2007) ‘Elongation factor G stabilizes the hybrid-state conformation of the 70S ribosome’, *Rna*, 13(9), pp. 1473–1482. doi: 10.1261/rna.601507.

Tourigny, D. S. *et al.* (2013) ‘Elongation factor G bound to the ribosome in an intermediate state of translocation’, *Science*, 340(6140), pp. 0–8. doi: 10.1126/science.1235490.

Vetter, I. R. and Wittinghofer, A. (2001) ‘The guanine nucleotide-binding switch in three dimensions’, *Science*, 294(5545), pp. 1299–1304. doi: 10.1126/science.1062023.

Voorhees, R. M. *et al.* (2010) ‘The Mechanism of Activation of GTP Hydrolysis on the Ribosome’, 330(November), pp. 835–839.

Weinger, J. S. *et al.* (2004) ‘Substrate-assisted catalysis of peptide bond formation by the ribosome’, *Nature Structural and Molecular Biology*, 11(11), pp. 1101–1106. doi: 10.1038/nsmb841.

Wilden, B. *et al.* (2006) ‘Role and timing of GTP binding and hydrolysis during EF-G-dependent tRNA translocation on the ribosome’, *Proceedings of the National Academy of Sciences*, 103(37), pp. 13670–13675. doi: 10.1073/pnas.0606099103.

Yang, H., Noel, J. K. and Whitford, P. C. (2017) ‘Anisotropic Fluctuations in the Ribosome Determine tRNA Kinetics’, *Journal of Physical Chemistry B*, 121(47), pp. 10593–10601. doi: 10.1021/acs.jpcb.7b06828.

Zaher, H. S. and Green, R. (2009) ‘Quality control by the ribosome following peptide bond formation’, *Nature*. Nature Publishing Group, 457(7226), pp. 161–166. doi: 10.1038/nature07582.

Zhang, D. *et al.* (2012) ‘Common chaperone activity in the G-domain of trGTPase protects L11-L12 interaction on the ribosome’, *Nucleic Acids Research*, 40(21), pp. 10851–10865. doi: 10.1093/nar/gks833.

Zhang, D. *et al.* (2015) ‘New insights into the enzymatic role of EF-G in ribosome recycling’, *Nucleic Acids Research*, 43(21), pp. 10525–10533. doi: 10.1093/nar/gkv995.

Zhou, J. *et al.* (2014) ‘How the Ribosome Hands the A-site tRNA to the P Site During EF-G-catalyzed Translocation Jie’, *Science*, 345(6201). doi: 10.1371/journal.pone.0178059.